

Martin Billinger, Dipl.-Ing.

# Single-Trial Estimation of Brain Connectivity

Feature Extraction, Classification, and Visualization  
for EEG-Based Brain-Computer Interfaces

## DISSERTATION

zur Erlangung des akademischen Grades  
Doktor der technischen Wissenschaften

eingereicht an der  
**Technischen Universität Graz**

Betreuer  
Univ.-Prof. Dipl.-Ing. Dr.techn. Gernot Müller-Putz

Mitbetreuer  
Dipl.-Ing. Dr.techn. Clemens Brunner

Institute of Knowledge Discovery  
Faculty of Computer Science and Biomedical Engineering

Graz, Dezember 2014

## EIDESSTÄTLICHE ERKLÄRUNG

### **AFFIDAVIT**

Ich erkläre an Eides statt, dass ich die vorliegende Arbeit selbstständig verfasst, andere als die angegebenen Quellen/Hilfsmittel nicht benutzt, und die den benutzten Quellen wörtlich und inhaltlich entnommenen Stellen als solche kenntlich gemacht habe. Das in TUGRAZonline hochgeladene Textdokument ist mit der vorliegenden Dissertation identisch.

*I declare that I have authored this thesis independently, that I have not used other than the declared sources/resources, and that I have explicitly indicated all material which has been quoted either literally or by content from the sources used. The text document uploaded to TUGRAZonline is identical to the present doctoral dissertation.*

9.7.2015

Datum / Date



Unterschrift / Signature

# Acknowledgements

At this place I want to express my gratitude to all the people who directly or indirectly made it possible for me to finish this thesis.

Thank you,

**Clemens**, for getting me started and supporting me throughout the thesis. If it was not for you, I would not even have considered doing a PhD.

**Christa Neuper**, for your supervision in the beginning of the thesis, until you were called to other duties.

**Gernot**, for taking over the role of supervisor and for guiding me to successfully finish the work.

Everyone working and studying at the BCI lab, for sharing a great time and many hours of fruitfully discussing each other's work.

**Mum, Dad, Eva**, and all my family, simply for being there. Although as a PhD candidate I was mostly living my own life, it is good to know that there is always a place you can go to.

**Christian**, for continuously reminding me what's important in life.

**Christian** again, **Matthias, Martin, Bernhard, Tobias, Artur, Philipp**, for the time spent outside University hiking in the mountains, climbing rock walls, drinking in bars, barbecuing on rooftops, and much more. You gave me the strength to keep going.

People in the Red Cross Graz Tuesday night shift, for giving me a different perspective on life and work. The time with you was synonymous for my time in Graz.

Dearest **Mareike**, for becoming part of my life, for your inspiration and support, for helping me endure, and for enduring me in some of the more difficult moments. You turned *me* into *us*.

This thesis was supported by the Austrian Science Foundation FWF project P20848 "Coupling Measures in BCIs", and by the FP7 Framework EU Research Project ABC (No. 287774).

## Abstract

The state of the art in motor imagery brain-computer interfaces (BCIs) is to use band power features along with optimized spatial filters such as common spatial patterns (CSP). However, this approach does not take information about causal connectivity within the brain into account for classification. The aim of the thesis is to use information about causal interactions and apply connectivity features to applications such as BCIs or functional brain monitoring. Such applications require single-trial features in order to operate online. Thus, a framework for single-trial connectivity estimation using vector autoregressive (VAR) models was implemented at the core of this thesis. The framework allows use of connectivity features in BCIs or online visualization systems.

Two key issues for single-trial connectivity estimation were identified: appropriate source selection and regularization of the VAR models. By taking these issues into consideration, single-trial connectivity estimation was successfully applied in motor imagery BCI simulations. In consequence, the connectivity measures full frequency directed transfer function (ffDTF) and direct directed transfer function (dDTF) achieved classification results similar to band power features. Furthermore, an online connectivity visualization system was implemented and successfully tested with motor execution and resting tasks. Only three other studies used effective connectivity measures in BCI related experiments, which is likely caused by the inherent difficulties of single-trial connectivity estimation. This thesis tackled these difficulties and demonstrated successful online application of the methods, which opens the door for future research in the direction of BCIs and other applications that utilize connectivity measures.

# Kurzfassung

Der aktuelle Stand der Technik bei Hirn-Computer-Schnittstellen (sogenannten brain-computer interfaces; BCIs) basiert auf der Analyse von Bandleistung der Hirnströme in Kombination mit optimierten räumlichen Filtern (z.B. common spatial patterns (CSP)). Veränderungen in den jeweiligen Frequenzbändern (zum Beispiel Alpha, 8-13 Hz) werden unter anderem durch Bewegungsvorstellung hervorgerufen. Aufgrund dieser Veränderungen können Steuersignale abgeleitet werden. Allerdings kann diese Herangehensweise Informationen über kausale Verbindungen (Konnektivität) zwischen Gehirnregionen nicht nutzen. Das Ziel dieser Dissertation ist es daher, Informationen über diese kausalen Verbindungen zugänglich zu machen, um sie für BCIs oder andere Echtzeitanwendungen zu nutzen.

Da diese Anwendungen „online“ funktionieren sollen, ist es erforderlich, dass die Berechnung von Merkmalen aus einzelnen und relativ kurzen Zeitfenstern (Single-Trial), erfolgen kann. Im Zuge dieser Dissertation wurde ein System entwickelt, das es ermöglicht Single-Trial-Konnektivität für BCIs zu nutzen oder diese online zu visualisieren.

Zwei grundlegende Probleme bei der Implementierung von Single-Trial-Konnektivität wurden behandelt. (1) Die Bestimmung von geeigneten Signalquellen im Gehirn, und (2) die Regularisierung der zugrundeliegenden mathematischen Modelle. Damit konnte Single-Trial-Konnektivität in BCI-Simulationen erfolgreich eingesetzt werden. Die Konnektivitätsmaße „full frequency directed transfer function“ (ffDTF) und „direct directed transfer function“ (dDTF) lieferten mit Bandleistung gleichwertige Klassifikationsgenauigkeit. Zudem wurden die entwickelten Methoden zur Onlinevisualisierung von Konnektivität während EEG-Messungen eingesetzt.

Bisher haben nur wenige Studien kausale Konnektivität in BCI-Experimenten eingesetzt. Dies liegt vermutlich an den Problemen die die Berechnung von Single-Trial-Konnektivität bereitet. In dieser Dissertation werden Lösungen für diese Probleme präsentiert und die erfolgreiche Onlineanwendung der Methoden demonstriert. Damit wird der Weg für zukünftige Forschung in Richtung Anwendung von Onlinekonnektivität geebnet.

# Contents

<b>Acknowledgements</b>	<b>iii</b>
<b>Abstract</b>	<b>iv</b>
<b>Acronyms</b>	<b>ix</b>
<b>1. Introduction</b>	<b>1</b>
1.1. Brain-Computer Interfaces . . . . .	1
1.1.1. Overview . . . . .	1
1.1.2. Definition of BCI . . . . .	1
1.1.3. Data Acquisition . . . . .	2
1.1.4. An Electrophysiological Model of the EEG . . . . .	3
1.1.5. Neurophysiological Phenomena . . . . .	3
1.1.6. Data Processing . . . . .	5
1.2. Connectivity . . . . .	6
1.2.1. Overview . . . . .	6
1.2.2. Categories of Brain Connectivity . . . . .	6
1.2.3. Connectivity Estimation . . . . .	7
1.2.4. Volume Conduction . . . . .	12
1.2.5. Dimensionality Reduction . . . . .	14
1.2.6. Relevance for Brain-Computer Interfaces . . . . .	15
1.3. Aim of this Thesis . . . . .	15
1.4. Organization of the Thesis . . . . .	16
<b>2. Materials and Methods</b>	<b>17</b>
2.1. Primary Publications . . . . .	17
2.1.1. A comparison of univariate, vector, bilinear autoregressive, and band power features for brain–computer interfaces . . . . .	17
2.1.2. Single-trial connectivity estimation for classification of motor imagery data . . . . .	18
2.1.3. SCoT: a Python toolbox for EEG source connectivity . . . . .	19
2.2. Online Visualization of Brain Connectivity . . . . .	21
2.2.1. Introduction . . . . .	21
2.2.2. Methods . . . . .	22
2.2.3. Results . . . . .	34
2.2.4. Discussion . . . . .	37
2.2.5. Conclusion . . . . .	39
2.3. Secondary Publications . . . . .	40

## Contents

<b>3. Discussion and Conclusions</b>	<b>41</b>
3.1. Overview	41
3.2. Model fitting	41
3.3. Source-Connectivity Framework	42
3.4. Connectivity	43
3.5. Relation to the State of the Art	44
3.6. Summary and Conclusions	44
3.7. Outlook	45
<b>Bibliography</b>	<b>46</b>
<b>A. Mathematical Derivations</b>	<b>58</b>
A.1. VAR Model Transformations	58
<b>B. Primary Publications</b>	<b>60</b>
B.1. Contributions	60
B.2. A comparison of univariate, vector, bilinear autoregressive, and band power features for brain–computer interfaces	61
B.3. Single-trial connectivity estimation for classification of motor imagery data	71
B.4. SCoT: a Python toolbox for EEG source connectivity	79

## List of Figures

1.1.	Dipolar model of the EEG . . . . .	3
1.2.	Event-related desynchronization . . . . .	4
1.3.	Typical processing loop of a BCI . . . . .	5
1.4.	Examples of connectivity categories . . . . .	6
1.5.	Autoregressive power spectrum estimation . . . . .	8
1.6.	Connectivity Measures . . . . .	11
1.7.	Volume Conduction Model . . . . .	12
2.1.	Single-Trial Connectivity BCI Framework . . . . .	19
2.2.	Benefits of CSPVARICA and Regularization . . . . .	20
2.3.	Multi-trial connectivity . . . . .	23
2.4.	Single-trial connectivity . . . . .	23
2.5.	Online connectivity . . . . .	25
2.6.	Paradigm timing . . . . .	26
2.7.	Paradigm visualization . . . . .	27
2.8.	Hardware infrastructure . . . . .	28
2.9.	Trial alignment . . . . .	30
2.10.	EEG sources . . . . .	31
2.11.	Online framework . . . . .	33
2.12.	Motor execution results . . . . .	36
2.13.	Rest-paradigm results . . . . .	37
2.14.	Signal processing delay . . . . .	38

## List of Tables

1.1.	Summary of connectivity measures. . . . .	10
2.1.	EEG layout . . . . .	26
2.2.	Participant-specific settings . . . . .	34

# Acronyms

<b>ALS</b>	amyotrophic lateral sclerosis
<b>AR</b>	autoregressive
<b>bAR</b>	bilinear autoregressive
<b>BCI</b>	brain-computer interface
<b>BP</b>	band power
<b>CNS</b>	central nervous system
<b>COH</b>	coherence
<b>CSD</b>	current source density
<b>CSP</b>	common spatial patterns
<b>dDTF</b>	direct directed transfer function
<b>DTF</b>	directed transfer function
<b>ECoG</b>	electrocorticogram
<b>EEG</b>	electroencephalogram
<b>EMG</b>	electromyogram
<b>EOG</b>	electrooculogram
<b>EP</b>	evoked potential
<b>ERD</b>	event-related desynchronization
<b>ERP</b>	event-related potential
<b>ERS</b>	event-related synchronization
<b>ffDTF</b>	full frequency directed transfer function
<b>FIR</b>	finite impulse response
<b>fMRI</b>	functional magnetic resonance imaging
<b>fNIRS</b>	functional near infrared spectroscopy
<b>GIL</b>	global interpreter lock
<b>IC</b>	independent component
<b>ICA</b>	independent component analysis
<b>IIR</b>	infinite impulse response
$\kappa$	Cohen's Kappa
<b>LDA</b>	linear discriminant analysis
<b>LFP</b>	local field potential
<b>MEG</b>	magnetoencephalogram
<b>MI</b>	motor imagery
<b>MRCP</b>	movement-related cortical potential
<b>NIRS</b>	near-infrared spectroscopy
<b>PCA</b>	principal component analysis
<b>pCOH</b>	partial coherence
<b>PDC</b>	partial directed coherence
<b>PET</b>	positron emission tomography
<b>PSD</b>	power spectral density

## Acronyms

**S** cross spectral density  
**SA** spiking activity  
**SCoT** source connectivity toolbox  
**SNR** signal-to-noise ratio  
**TiA** TOBI interface A  
**TSS** TOBI signal server  
**VAR** vector autoregressive  
**ØMQ** zero message queue

# 1. Introduction

## 1.1. Brain-Computer Interfaces

### 1.1.1. Overview

Human communication requires physical interaction with the environment in order to send messages to other individuals, who in turn need to be able to understand and interpret the messages. Such messages may take the form of short texts typed into a cell phone, or more traditionally, manifest as modulated pressure waves in air, commonly known as speech. Other forms of communication include body language or gestures. Different as they seem, these forms of communication have a common denominator: they rely on the ability to voluntarily or unconsciously control the motor system. A person's ability to do so can be impaired by disorders that affect the central nervous system (e.g. stroke [1], cerebral palsy [2], trauma [3]), the peripheral nervous system (e.g. amyotrophic lateral sclerosis (ALS) [4], trauma [5]), or the muscles themselves. People most severely affected, who have lost all possibilities of communication, are considered to be in a complete locked-in state [6]. Such patients could benefit from a device that provides a non-muscular channel for communicating or exerting control over the environment [7, 8]. If such a device relies on brain activity directly it is called a brain-computer interface (BCI) [9, 10].

Apart from the medical field, the gaming industry and the military are interested in the possibilities offered by BCIs [11, 12]. They explore new ways to control computer games and provide additional input sources such as brain switches. Other applications include passive monitoring of an operator's brain state for arousal or weariness [13] or utilizing the brain's contextual response for image search [14], where even a multi-brain BCI was recently developed for detecting targets in a stream of satellite images [15].

### 1.1.2. Definition of BCI

A BCI is a communication device that interprets brain activity and can be used to control other assistive devices such as spelling applications [16, 6], neuroprostheses [17, 18, 19], or wheelchairs [9, 20]. A decade ago BCIs were defined to use signals directly recorded from the brain, use goal-directed behavior (i.e. the user needs to actively seek an action), operate online, and provide feedback [9]. A more recent definition focuses on the application of BCIs. According to this definition a BCI must replace, restore, enhance, supplement, or improve central nervous system (CNS) output by measuring and converting CNS activity [10]. This definition does

## 1. Introduction

---

not require intentional control and therefore includes so-called passive BCIs [13]. Applications of passive BCIs include attention monitoring of drivers and pilots, or systems that react on the emotional state of their user [21]. A system that combines other assistive devices with a BCI or different types of BCI is a hybrid BCI [22, 23, 24]. Hybrid BCIs can combine multiple inputs or switch between inputs if they degrade. For example, a hybrid BCI could switch from joystick to BCI mode if muscles become fatigued in the user, and switch back to joystick if the user's concentration level required for BCI operation drops [25].

### 1.1.3. Data Acquisition

The brain signals typically used in BCI research are electroencephalogram (EEG), magnetoencephalogram (MEG), electrocorticogram (ECoG), local field potentials (LFPs), neuron spiking activity (SA), near-infrared spectroscopy (NIRS), and functional magnetic resonance imaging (fMRI). While EEG, ECoG, and MEG measure the electrical activity from large populations of neurons, NIRS, and fMRI measure the metabolic activity. Electrical activity measured by the aforementioned methods is thought to be primarily the result of ionic currents caused by synchronously occurring postsynaptic potentials [26, 27]. In contrast, metabolic activity measures local oxygen consumption of the CNS. Naturally, electrical activity occurs at faster time scales ( $\sim$ milliseconds) than metabolic activity ( $\sim$ seconds) [28].

From a practical point of view, MEG and fMRI belong to the more unwieldy data acquisition methods. Both require expensive and stationary machinery for conducting measurements, which makes them practically useless outside the lab. At the other end of the economic spectrum, EEG and NIRS require only light measurement equipment that is relatively portable and inexpensive. As invasive methods ECoG, LFP, and SA take a rather unique place among the acquisition methods. For ECoG an electrode grid is placed on the surface of the brain, which gives better spatial resolution than EEG but comes at a high risk for the patient. Such grids are rarely implanted for the purpose of BCI research. Instead, they are used in epilepsy treatment to find epileptogenic locations for surgery [29]. Thus, the grids are only implanted for a limited time and there is no guarantee that BCI relevant regions of the cortex are covered [30]. LFPs and SA can measure the activity of small groups or even single neurons by inserting micro electrodes into the neuronal tissue. Thus, these methods have excellent spatial and temporal resolution but are highly invasive. However, studies in monkeys [31, 32] and humans [33, 34] showed that BCI operation is possible with signals recorded from micro electrode arrays, even years after implantation [35].

EEG is the acquisition method most widely used in BCI related publications [36]. The EEG is well understood and exposes neurophysiological phenomena that are directly applicable to BCIs (see section 1.1.5). Therefore, the studies that comprise this thesis focuses on EEG.

## 1. Introduction

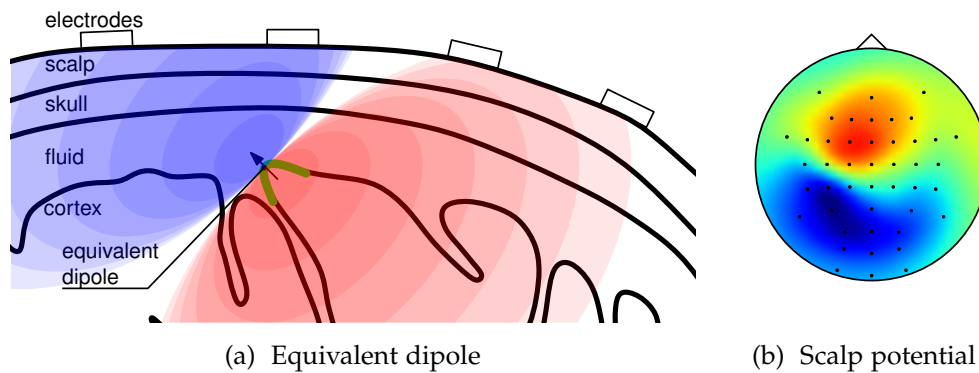


Figure 1.1.: Dipolar model of the EEG. (a) The EEG is modeled as a discrete set of cortical dipoles that correspond to ensembles of neurons. Inhomogeneities in the conductivity of tissues and irregular shape of source areas lead to smeared scalp potentials, but the dipolar distribution is still visible in the EEG component shown in (b).

### 1.1.4. An Electrophysiological Model of the EEG

The EEG is only measured at a considerable distance from where it is generated. Thus, activity of a neuron ensemble only contributes to the EEG if the responsible neurons are regularly arranged and activated more or less synchronously. A typical regular arrangement is found in the pyramidal neurons of the cortex, whose dendrites are arranged perpendicular to the cortical surface. Postsynaptic potentials in ensembles of those neurons result in a laminar net current along the dendrites. At a macroscopic level, the electrical field generated by this currents behaves roughly like a dipole layer [27]. However, the electrical field is distorted by inhomogeneities in the conductive media (cerebrospinal fluid, skull, and scalp).

For neuroimaging purposes the cortical surface is often modeled as a discretized dipole layer [37]. However, the number of dipoles typically exceeds the number of EEG electrodes. Thus, estimating the activity of these dipoles from the EEG is an ill-posed problem [38]. An even simpler model replaces the dipole layer of a neuron ensemble with one equivalent dipole [39]. This model assumes that the EEG is made of a discrete set of such dipoles (Figure 1.1). Most of the work in this thesis is based on this simplified model assumption.

### 1.1.5. Neurophysiological Phenomena

Two neurophysiological phenomena are commonly utilized in BCIs based on EEG: event-related potentials (ERPs) and spontaneous EEG. ERPs are associated with the brain's response to a variety of stimuli or events. An example of ERPs are movement-related cortical potentials (MRCPs) [40], which occur in relation to movement intention. Sensory evoked potentials (EPs) are a subset of ERPs that are caused by sensory (visual, auditory, somatosensory) stimuli [41]. These potentials often require multiple repetitions of a stimulus to become distinguished from the background activity in the brain. While EPs require external stimuli, oscillations

## 1. Introduction

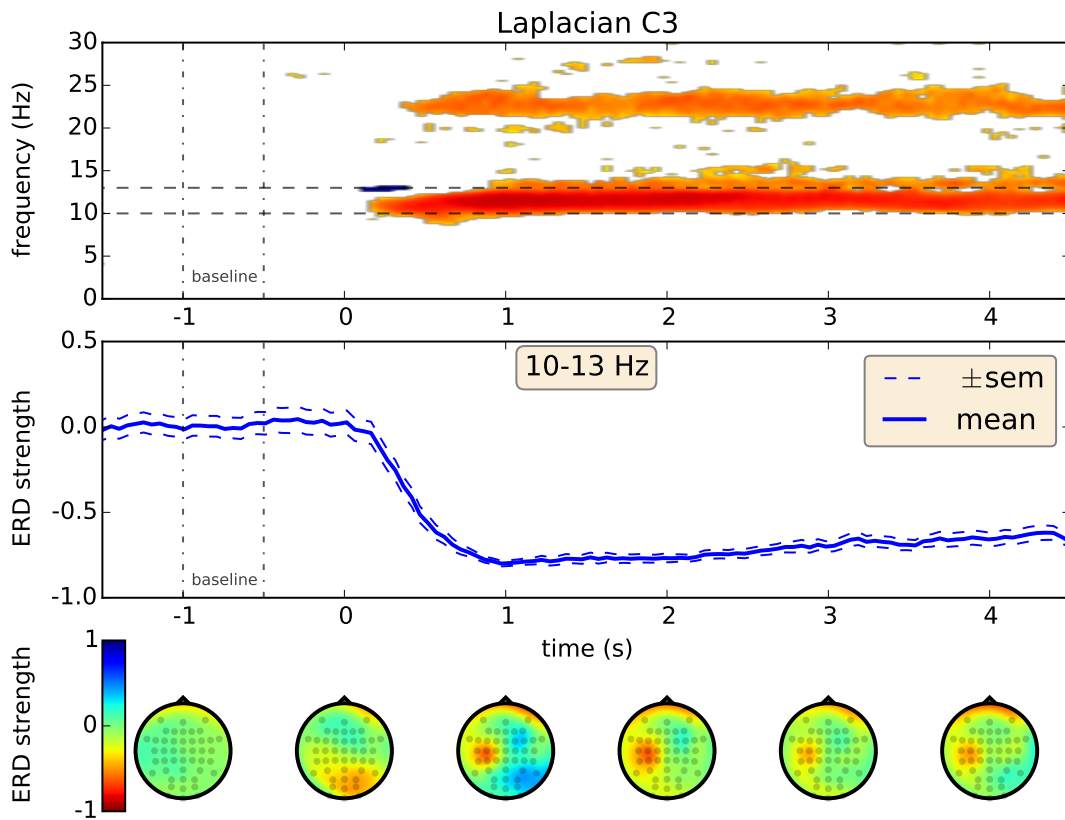


Figure 1.2.: Event-related desynchronization during right hand motor imagery (90 trials of one subject). See B.3 for a description of the measurement procedures. Top: ERD map of Laplacian channel C3 where only significant ( $p < 0.001$ ) deviations from the baseline are shown. Desynchronization is clearly visible in the mu and beta bands. Center: time course of ERD in the subject specific mu band (10-13 Hz) with mean and standard error of the mean (sem). Bottom: scalp distribution of ERD/ERS in the mu band over time.

occur naturally in the brain. The most prominent oscillations are the alpha (8-13 Hz), mu (8-12 Hz), and beta (14-30 Hz) rhythms [42, 43]. Distinguishing these rhythms by the frequency bands they occur in dates back to the early days of EEG research. However, the EEG rhythms turned out to be more complicated than this. For example the mu rhythm is different from the alpha despite being located in the same frequency band. Furthermore, the mu rhythm can be subdivided in a lower (8-10 Hz) and an upper (10-12 Hz) mu rhythm [44]. The alpha rhythm is generally associated with resting and eyes closed conditions. The mu rhythm is associated with the resting-state of motor areas and typically desynchronizes contralaterally during motor-related activity such as actively or passively executed movement and even expected, intended, attended or imagined movement. Similarly, the beta rhythm is known to synchronize shortly after a motor activity (post movement beta synchronization [45]). Additionally, harmonics of the alpha or mu rhythms can sometimes be observed that fall in the frequency range of the beta band.

## 1. Introduction

Desynchronization and synchronization of motor rhythms is known as event-related desynchronization (ERD) and event-related synchronization (ERS). These occur during executed or imagined movement for many people. Figure 1.2 shows a prime example of mu ERD during motor imagery [46]. A BCI can use these band power (BP) changes for control by distinguishing between two or more different imagined movements such as left hand, right hand, or feet [47].

### 1.1.6. Data Processing

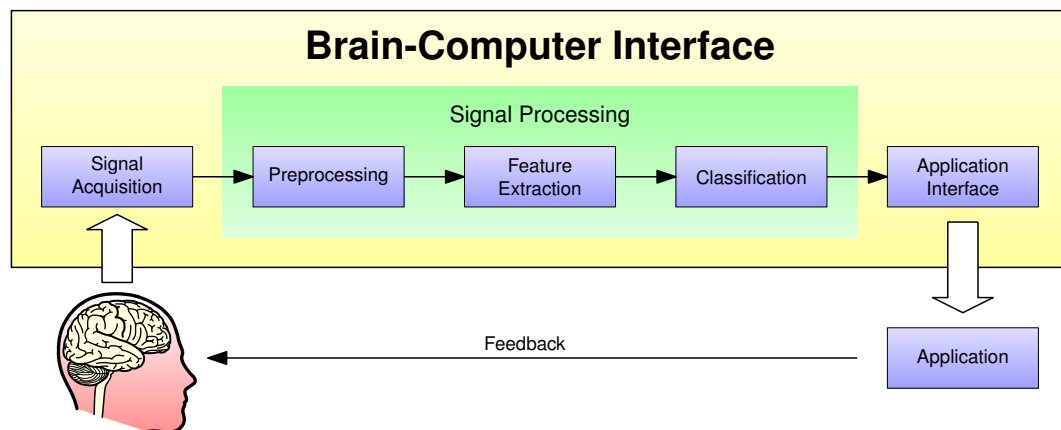


Figure 1.3.: Typical processing loop of a BCI.

A typical signal processing pipeline of BCIs comprises preprocessing, feature extraction, and classification stages (Figure 1.3). In the preprocessing stage, signals are filtered in the spatial and/or frequency domain. Spatial filters usually create a linear mixture of existing signal channels; popular techniques include bipolar and Laplace filters, or common spatial patterns (CSP) [48, 49]. After preprocessing, the data is further processed in the feature extraction stage. To date, most non-invasive BCIs use features derived from individual channels or linear combinations of channels [36]. Commonly used feature types include BP [50, 51, 52], autoregressive (AR) model coefficients [53, 54], and wavelets [55]. Using suitable classification algorithms in the next stage, these features allow BCIs to discriminate between different brain states or mental tasks. Commonly used classifiers include simple thresholds, linear discriminant analysis (LDA) [56, 57], support vector machines [58], and neural networks [59]. However, these features do not contain information about causal relationships between channels. This thesis shows that such information can provide useful features for BCIs. Although this has been studied before [60, 61, 62], these articles lack important details or are based only on artificial data, which makes their results neither reproducible nor very conclusive. In contrast, throughout this thesis a rigorous framework is developed that supports evaluation of causality features in BCIs.

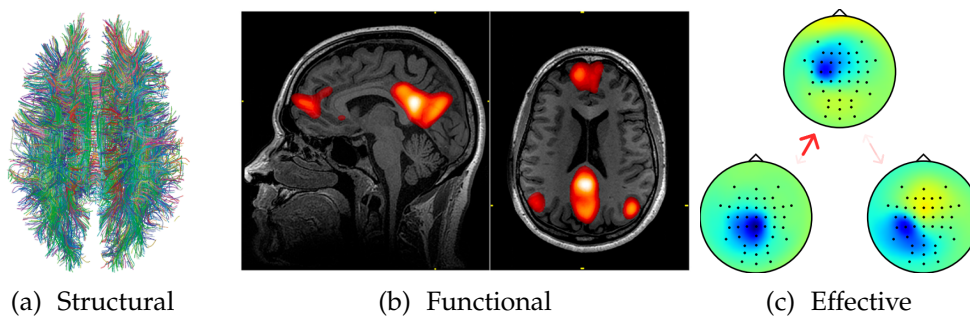


Figure 1.4.: Examples of connectivity categories: (a) Structural connectivity measured with diffusion tensor imaging [67], (b) Functional connectivity measured with functional magnetic resonance imaging [68], (c) Effective connectivity measured with EEG.

(a) Source: Wikimedia Commons [http://commons.wikimedia.org/wiki/File:White\\_Matter\\_Connections\\_Obtained\\_with\\_MRI\\_Tractography.png](http://commons.wikimedia.org/wiki/File:White_Matter_Connections_Obtained_with_MRI_Tractography.png), License: Creative Commons Attribution 2.5 Generic <http://creativecommons.org/licenses/by/2.5/deed.en>

(b) Source: Wikimedia Commons [http://commons.wikimedia.org/wiki/File:Default\\_mode\\_network-WRNMMC.jpg](http://commons.wikimedia.org/wiki/File:Default_mode_network-WRNMMC.jpg), License: Public Domain

## 1.2. Connectivity

### 1.2.1. Overview

Each of the human brain's 20 billion neurons connects on average to about 7000 other neurons via chemical synapses [63]. Only by forming such vast and dynamic networks, groups of relatively simple neurons can perform complex tasks such as learning, motor control, or writing a PhD thesis. Obviously, inter-connectivity is an important characteristic of the brain. Connectivity in the brain can be observed at different scales; from synaptic connections that link individual neurons up to brain regions linked by fiber pathways. With steadily increasing computational power and improvements in neuroimaging techniques, scientists are now able to study brain connectivity at different time and spatial scales. Relevant examples for connectivity research include anatomical tracing of white matter fibers [64] and measuring functionally coupled brain activity [65].

### 1.2.2. Categories of Brain Connectivity

Brain connectivity is fundamentally categorized as structural, functional, or effective connectivity (Figure 1.4). While structural connectivity is concerned with anatomical structures such as fiber pathways, functional connectivity is related to the activity of brain areas, and is often expressed in terms of correlations between the brain signals of different areas. However, functional connectivity does not provide information about the direction of interaction. Inspecting functional connectivity in detail may reveal causal relations between correlated brain areas. Such causal or directed interaction is measured with effective connectivity [66].

### 1.2.3. Connectivity Estimation

Functional connectivity measures such as coherence or phase coupling are typically computed from the auto- and cross-spectra of signal pairs [69]. Accordingly, effective connectivity (causality) can be inferred to some extent from spectral phase differences between signals. However, this can lead to misinterpretations in networks that contain more than two sources. Causality analysis in general is very susceptible to unobserved sources or confounders [65]. Thus, causality is often modeled with vector autoregressive (VAR) models that generalize AR models to multivariate signals. VAR models describe the causal interactions of all observed sources together. This section explains these models and discusses how to obtain connectivity measures from VAR models.

#### Autoregressive Models

AR models (1.1) are mathematical models that predict a signal or time series from its own past. The current sample  $x(n)$  is predicted by the sum of  $P$  previous samples, each weighted with a weight  $a_k$ , and an additive white noise term  $\epsilon(n)$ <sup>1</sup>.

$$x(n) = \sum_{k=1}^p a_k x(n-k) + \epsilon(n) \quad (1.1)$$

An interesting interpretation of AR models is that they form an infinite impulse response (IIR) filter of order  $p$ . This filter takes a white noise signal  $\epsilon(n)$  as input, and produces an output signal whose spectrum resembles that of the original signal  $x$ . Thus, by fitting an AR model to a signal we effectively model the signal's spectrum. This has an important application in power spectral density (PSD) estimation. Parametric PSD estimation is a way of estimating a signal's PSD by fitting an AR model to the signal to estimate the spectrum [70]. The model order  $p$  determines the number of spectral peaks the estimate can have and is therefore a parameter for the smoothness of the estimated spectrum, as illustrated in Figure 1.5.

#### Vector Autoregressive Models

AR models can be extended to model multiple signals simultaneously (1.2).  $\mathbf{x}[n]$  is a vector containing the current sample of each signal,  $\mathbf{e}[n]$  is an additive vector of white noise, and  $\mathbf{B}^{(k)}$  are matrices that describe how previous samples  $\mathbf{x}[n-k]$  contribute to the current sample. Thus each signal can potentially contribute to any other signal. This makes fitting such models more complex, but has the advantage

---

<sup>1</sup>In the AR literature the noise term is often restricted to Gaussian white noise. However, Gaussianity is not strictly a requirement. It mainly simplifies the mathematics of fitting the model in a least-squares sense. Later in this thesis, AR models will be applied to independent components, which would contradict an assumption of Gaussianity because independent component analysis (ICA) cannot separate multiple Gaussian components.

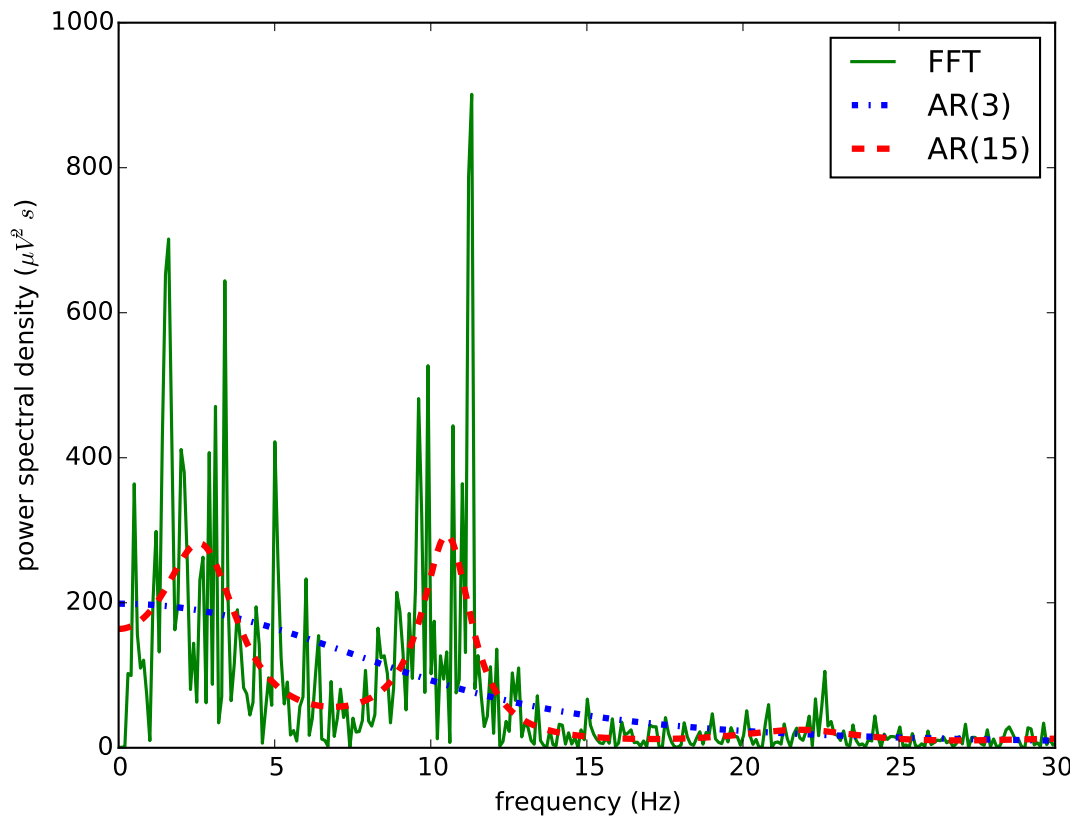


Figure 1.5.: Autoregressive power spectrum estimation. The figure shows the PSD of a 10 s EEG window with  $100\text{ s}^{-1}$  sample rate at location C3. The PSD was estimated from the FFT of the signal, and from autoregressive models with orders 3 and 15. The AR-PSD are much smoother than the FFT-PSD estimates. However, a very low model order only captures the  $1/f$ -characteristic of the EEG spectrum, while a higher model order can capture more spectral peaks, such as the 10 Hz alpha peak in this example. Note that the spurious peak below 3 Hz is caused by a high-pass filter cutting off the lower end of the spectrum.

## 1. Introduction

---

of capturing causal relations between the signals. In other words, a VAR model is time-domain model of functional connectivity between multiple signals.

$$\mathbf{x}[n] = \sum_{k=1}^p \mathbf{B}^{(k)} \mathbf{x}[n-k] + \mathbf{e}[n] \quad (1.2)$$

### Model Fitting

Methods to estimate AR or VAR coefficients from data include solving the Yule-Walker equations [71, 72], Burg's method [70], or least squares regression. The latter is performed by rewriting the the AR/VAR model as a set of linear equations of the form  $\mathbf{Ax} = \mathbf{b}$ . Regardless of which method is used, the number of unknown coefficients is  $\gamma = m^2p$ , where  $m$  is the number of signal (1 for an AR model), and  $p$  is the model order. The amount of independent expressions is approximately  $\beta = mn$ , where  $n$  is the length of the estimation window in samples. Thus, the window must be longer than  $n_{\min} = mp$ . However, in practice, the window length should be at least 5-10 times larger in order to get reliable estimates [73]. Consider typical values of  $m = 21$  signals, model order  $p = 15$ , and a sample rate of 100 Hz: the estimation window length should be at least 3.15 s, ideally more than 15 s. A time resolution of several seconds poses a severe limitation to data analysis. However, the estimation window can be shortened by utilizing multiple trials. Instead of one long window multiple shorter windows that correspond to the same condition are used to provide additional data [74]. The minimum window length becomes  $n_{\min} = mp/t$ , where  $t$  is the number of trials. In consequence, the window length can be reduced significantly with a sufficient number of trials. This approach can be understood as a way to average VAR estimates over multiple trials.

### Connectivity Measures

VAR coefficients can be interpreted as filter coefficients. The diagonal elements of  $\mathbf{B}^{(k)}$  form IIR filters where the input is noise and the output is a signal. The off-diagonal elements form finite impulse response (FIR) filters where the input is a signal and the output is another signal. A filter is represented in the time domain by its impulse response and in the frequency domain by its transfer function. Like conventional filters, VAR models can be represented in the frequency domain. Various combinations and normalizations of frequency domain VAR coefficients lead to different connectivity measures (Table 1.1). Some of these measures depend on the noise covariance matrix, which ideally is a diagonal matrix.

Measures such as the coherence (COH), partial coherence (pCOH), or even cross spectral density (S) are symmetric, which means they do not show information about direction or causality. Thus, they measure functional connectivity. Measures from the partial directed coherence (PDC) or the directed transfer function (DTF) families can be asymmetric, which allows them to measure causality (effective connectivity). However, the DTF does not distinguish between direct and indirect connections (Figure 1.6).

## 1. Introduction

---

Table 1.1.: Summary of connectivity measures. Strictly speaking,  $\mathbf{A}$ ,  $\mathbf{H}$ ,  $\mathbf{S}$  and  $\mathbf{G}$  are no connectivity measures, but were included for completeness.

Measure	Definition	Description
$\mathbf{A}(z)$	$= \mathbf{I} - \sum_{k=1}^p \mathbf{B}^{(k)} z^{-k}$	Spectral VAR coefficients [73]
$\mathbf{H}(z)$	$= \mathbf{A}(z)^{-1}$	Multivariate transfer function [73]
$\mathbf{S}(z)$	$= \mathbf{H}(z) \Sigma_e \mathbf{H}(z)^\top$	Cross-spectral density [73]
$\mathbf{G}(z)$	$= \mathbf{A}(z)^\top \Sigma_e^{-1} \mathbf{A}(z)$	Inverse cross-spectral density [73]
$\text{COH}_{ij}(z)$	$= \frac{ \mathbf{S}_{ij}(z) }{\sqrt{\mathbf{S}_{ii}(z) \mathbf{S}_{jj}(z)}}$	Coherence [69]
$\text{pCOH}_{ij}(z)$	$= \frac{ \mathbf{G}_{ij}(z) }{\sqrt{\mathbf{G}_{ii}(z) \mathbf{G}_{jj}(z)}}$	Partial coherence [75]
$\text{PDC}_{ij}(z)$	$= \frac{ \mathbf{A}_{ij}(z) }{\sqrt{\mathbf{A}_{.j}^\top(z) \mathbf{A}_{.j}(z)}}$	Partial directed coherence [76]
$\text{PDCF}_{ij}(z)$	$= \frac{ \mathbf{A}_{ij}(z) }{\sqrt{\mathbf{A}_{.j}^\top(z) \Sigma_e^{-1} \mathbf{A}_{.j}(z)}}$	PDC factor [76]
$\text{GPDC}_{ij}(z)$	$= \frac{ \mathbf{A}_{ij}(z) }{\sigma_i \sqrt{\mathbf{A}_{.j}^\top(z) \text{diag}(\Sigma_e)^{-1} \mathbf{A}_{.j}(z)}}$	Generalized PDC [77]
$\text{DTF}_{ij}(z)$	$= \frac{ \mathbf{H}_{ij}(z) }{\sqrt{\mathbf{H}_{i.}(z) \mathbf{H}_{.i}^\top(z)}}$	Directed transfer function [78]
$\text{ffDTF}_{ij}(z)$	$= \frac{ \mathbf{H}_{ij}(z) }{\sqrt{\Sigma_e \mathbf{H}_{i.}(z) \mathbf{H}_{.i}^\top(z)}}$	Full frequency DTF [79]
$\text{dDTF}_{ij}(z)$	$= \text{pCOH}_{.i}(z) \cdot \text{ffDTF}_{ij}(z)$	Direct DTF [79]
$\text{GDTF}_{ij}(z)$	$= \frac{\sigma_j  \mathbf{H}_{ij}(z) }{\sqrt{\mathbf{H}_{i.}(z) \text{diag}(\Sigma_e) \mathbf{H}_{.i}^\top(z)}}$	Generalized DTF [77]

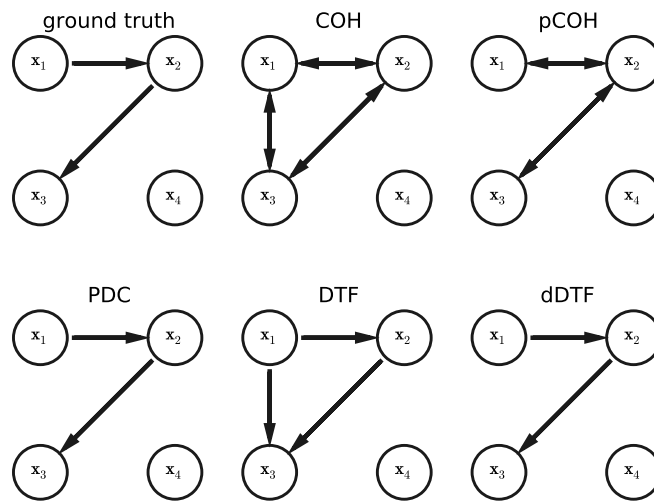


Figure 1.6.: A qualitative example of various connectivity measures. The ground truth consists of four sources  $x_i$ , where  $x_3$  is causally related to  $x_2$ , which in turn is related to  $x_1$ . Coherence (top middle) only reveals that some of the sources are related, but gives no information about direction or indirect connections. Partial coherence (top right) lacks directional information but only shows direct connections. Partial directed coherence (bottom left) shows only direct connections and their direction, while the directed transfer function (bottom middle) also shows indirect connections. The direct DTF (bottom right) resolves only direct connections and their direction. All measures have different normalizations that lead to different connectivity spectra, which is not shown in this figure.

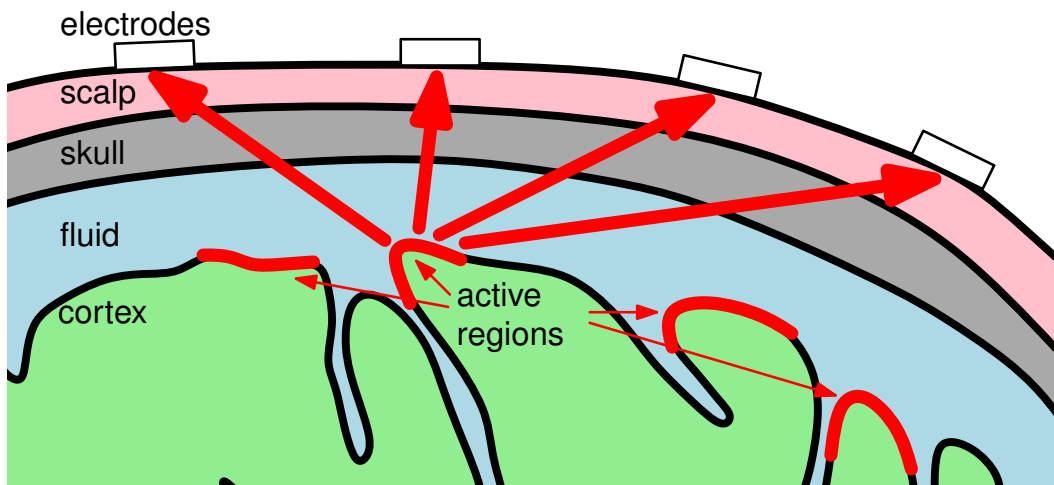


Figure 1.7.: Electrical activity at the cortex spreads to multiple electrodes. Each of the large arrows corresponds to an entry in the mixing matrix  $\mathbf{M}$ . The original signals at the cortex should be modeled with a VAR model instead of trying to interpret connectivity in the mixture of signals at the electrode sites.

#### 1.2.4. Volume Conduction

If a VAR model is unable to explain some interactions between signals, these are expressed as interactions between elements of the residual noise  $\mathbf{e}$ . In other words, if there are correlations in the noise there are also correlations in the signals, but these correlations are not explained by the VAR model. However, ideally all elements of  $\mathbf{e}$  are mutually independent, in which case all relations between signals are explained by the VAR model. When fitting VAR models to EEG data, a common cause for dependencies in the residual noise is volume conduction. Electrical signals spread from cortical sources almost instantly to multiple electrodes (Figure 1.7). However, this instantaneous spread is not modeled by VAR models and leads to correlations in the residual noise. This impedes interpreting actual relations between the signals because the relations are only partially explained by the VAR model.

The problem of volume conduction has been recognized and addressed in the literature [80, 81, 82, 83, 84, 85, 86, 87]. Three approaches are predominant: deriving measures that are invariant to volume conduction [80, 82, 87], adding an instantaneous term to the VAR model [83, 84, 85], and transforming the estimation problem into source space [81, 86]. The first two approaches implicitly assume that the sources of brain signals coincide with the EEG electrode locations. However, EEG electrodes are placed on the surface of the scalp, whereas the electrical signals originate from the brain, which is located inside the skull. Transforming the estimation into source space is done by inversely modeling the way signals spread from the brain to the EEG electrodes, and subsequently finding connectivity between actual brain sources.

### Extended VAR Models

Erla et al. [83] and Faes et al. [84] introduced an extension to VAR models by including an instantaneous term (1.3) in the model equation. This term can model volume conduction under certain conditions. However, solving for  $\mathbf{B}^{(0)}$  is ambiguous. The authors worked around this ambiguity by imposing a triangular structure on  $\mathbf{B}^{(0)}$ . This structure implies that volume conduction can occur only in certain directions that depend on how the signals are ordered. This ordering is a useful assumption if EEG channels are sampled in sequential order. However, sequential sampling interferes with causality analysis. Thus, connectivity analysis on sequentially sampled data is a questionable approach. Furthermore, modern amplifiers typically sample all channels simultaneously or re-align the data to correct for the sampling sequence. For these reasons, extended VAR models are not further considered in this thesis.

$$\mathbf{x}[n] = \mathbf{B}^{(0)}\mathbf{x}[n] + \sum_{k=1}^p \mathbf{B}^{(k)}\mathbf{x}[n-k] + \mathbf{e}[n] \quad (1.3)$$

### The VAR-Mixing Model

By modeling the EEG with a VAR model as in (1.2) or (1.3) signals are implicitly assumed to be generated directly at the EEG electrode locations. In reality however, the EEG is generated in the cortex, which is separated from the EEG electrodes by layers of tissue such as skin and bone. A practical model of the EEG is described in section 1.1.4. Cortical sources representing ensembles of neurons are modeled in (1.4). Activations of cortical sources  $\mathbf{s}$  are modeled by a VAR model, and the signals  $\mathbf{x}$  measured at the EEG electrode sites are related to these activations by the mixing matrix  $\mathbf{M}$  (often referred to as Leadfield matrix) [81].

$$\mathbf{s}[n] = \sum_{k=1}^p \mathbf{B}^{(k)}\mathbf{s}[n-k] + \mathbf{e}(n) \quad (1.4a)$$

$$\mathbf{x}[n] = \mathbf{M}\mathbf{s}[n] \quad (1.4b)$$

Here, model fitting requires an additional step: estimation of the mixing matrix  $\mathbf{M}$  and respective unmixing matrix  $\mathbf{U}$ . These matrices can be obtained in two ways: (1) from electrical forward models that model the conductivity and shape of different tissues in the head, electrode positions, and current sources, or (2) from EEG data alone with blind source decomposition. Electrical forward models mathematically describe how signals propagate from distributed sources in the brain to the EEG electrodes. The equations of the forward model directly correspond to the mixing matrix. However, the unmixing matrix can only be obtained by solving the inverse problem, which does not have a unique solution. Various methods to solve the inverse problem have been proposed. Among them are sLORETA, beam forming, or minimum norm estimation [37]. ICA takes a different approach by

decomposing the EEG into a discrete set of independent components. Some of these ICs relate to artifacts such as eye blinks or muscle activity, but many are of cortical origin. These latter components often have scalp distributions that resemble dipolar sources in the cortex [39] (similar to Figure 1.1b). This thesis focuses on the ICA-based blind source decomposition approach for estimating the unmixing matrix.

The most straight-forward way to obtain source space VAR estimates is to first transform the EEG signals  $\mathbf{x}$  into source space signals  $\mathbf{s}$  with ICA. Subsequently, the VAR model is fitted in source space. This approach was taken in the second paper contributing to this thesis [88]. However, there is a drawback to this method. ICA maximizes independence between the sources, which interferes with the dependence introduced by the VAR process. While this does not in principle interfere with classification (no information is lost in the linear transform), it may invalidate interpretation of connectivity patterns.

Improved source space estimates are obtained by MVARICA, which first fits a VAR model in EEG space, and reconstructs the mixing process by applying ICA to the model's residuals [81]. This approach might seem counter-intuitive at a first glance, but it is important to recognize that a VAR process can be transformed by any mixing matrix  $\mathbf{M}$ . If  $\mathbf{M}^T \mathbf{M}$  is non-singular the models are equivalent<sup>2</sup>. Thus, the VAR model fitted in EEG space is equivalent to a VAR model fitted in source space. Only the interpretation of connectivity is different in both models.

Convulsive ICA was suggested as an alternative to MVARICA [89]. Here, source space VAR coefficients and the mixing process are estimated simultaneously. However, this requires a specially designed ICA algorithm, while MVARICA can use any standard ICA algorithm such as FastICA or Infomax.

### 1.2.5. Dimensionality Reduction

ICA-based methods have one important drawback: They always find exactly as many sources as there are EEG channels. However, there is no guarantee that all these sources are of cortical origin. In fact, sources are often related to artifacts or noise. The number of sources can be reduced with principal component analysis (PCA). First, the EEG signals are pre-transformed with PCA. This transformation has no negative effect on the VAR and ICA estimates because PCA is a linear transformation, and VAR models are invariant to such transformations (see section A.1). However, data dimensionality can be reduced in PCA space by removing low-variance components, which are considered to only contain background noise. This step is part of the original MVARICA procedure [81].

Dimensionality reduction with PCA retains components with high variance. These components include large artifacts like electrooculogram (EOG) or electromyogram (EMG), while potentially task relevant components with lower amplitude may be discarded. By replacing PCA with common spatial patterns (CSP), the criterion for deciding which components to retain is changed. PCA tends to keep large

---

<sup>2</sup>See section A.1 for a formal derivation.

(high variance) components. In contrast, CSP components are optimized to have high variance in one condition and low variance in the other condition. Thus, CSP components are good for distinguishing between conditions. CSPVARICA, a supervised variant of MVARICA was developed in this thesis by replacing the PCA step in MVARICA with CSP. Thus, CSPVARICA can automatically obtain a subset of task relevant sources along with VAR estimates.

### 1.2.6. Relevance for Brain-Computer Interfaces

Typical BCI features such as band power (BP) measure the instantaneous activity of brain areas. However, they do not contain information about interactions of brain areas. Such interactions comprise additional information about processes in the brain and might improve BCI performance. Several previous studies have applied connectivity to BCIs. Most used functional connectivity [90, 91, 92, 93, 94, 95], with a few exceptions of effective connectivity [60, 61, 62]. While functional connectivity, especially phase coupling measures, are well established for BCIs, effective connectivity BCIs have received scant attention. One of the reasons certainly is the difficulty of obtaining reliable single-trial estimates of effective connectivity. Throughout this thesis a rigorous framework was developed for evaluating both effective and functional connectivity measures for use in BCIs. Using connectivity in BCIs poses two important challenges. First, the EEG is strongly affected by volume conduction, which leads to spurious connectivity. Second, BCIs need to operate online with short response times, which severely limits the amount of data available for estimation.

### 1.3. Aim of this Thesis

One of the main weaknesses of current BCIs is their accuracy. Under controlled conditions some individuals achieve almost perfect control over two classes while many people perform just above chance level [96]. The situation gets even worse when moving BCIs out of the lab into real-life applications. This challenge needs to be tackled from many sides. Improving control paradigms, mobile data acquisition, and signal processing strategies are some of the approaches that are under active research. In order to find better signal processing strategies researchers need a broad set of tools to choose from.

The aim of this thesis is to add connectivity to the pool of feature extraction methods currently available for BCI research. Apart from BCIs, other applications might benefit from connectivity estimation. These include online visualization and functional monitoring of wakefulness, workload, or brain surgery. To accomplish this aim, existing methods need to be adapted to work on single-trial basis in a BCI framework. This framework can be used to evaluate different connectivity measures for BCIs in an offline study. Finally, the framework needs to be moved to an online setting in order to demonstrate the feasibility of online connectivity estimation.

## 1. Introduction

---

To start with, it is not clear if established connectivity measures based on linear models are sufficient for use in BCIs, or if a non-linear approach is required. The first study aims to clarify whether VAR, AR, or bilinear AR models are more suitable for motor imagery classification [54]. Based on these results existing connectivity estimation methods can be adapted for single-trial use, or new methods may need to be developed.

Obtaining connectivity measures from VAR models is straight-forward. However, correctly fitting the model is challenging in an online application. The basic idea behind this thesis is to first solve the challenge of VAR model fitting, and subsequently determine which of the numerous connectivity measures (Table 1.1) are suitable for BCIs. Finally, an online implementation demonstrates the feasibility of the methods. Furthermore, the implementation of the methods is made publicly available as a more practical contribution to the field of brain connectivity research.

The thesis comprises four main scientific papers [88, 54, 97, 98] and several secondary publications [99, 100, 101, 102, 103]. According to the concept outlined above, [54, 99] looked at different aspects of AR models, [100] proposed a method to automatically select spectral features, and [103] discussed performance metrics for BCIs. A framework for evaluating connectivity-based BCIs was developed and presented in [88, 101, 102] and further refined in [97, 104]. Finally, online connectivity estimation was presented in [98].

### 1.4. Organization of the Thesis

Chapter 1 gives an introduction to the topics covered by the thesis. Brain-computer interfaces are introduced and an overview of brain connectivity is given. The aim of the thesis – combining BCIs and connectivity – is explained in the last part of this chapter.

The publications that comprise the thesis are summarized in chapter 2. Each main publication is dedicated a short section that summarizes the publication and sets it in relation to the thesis. The last publication is currently in review. Thus, the full text is included as part of this section.

Chapter 3 contains the thesis' overall discussion and conclusions. Here, the main contributions of the thesis to the scientific community are listed. Design choices, results and insights are discussed in detail, followed by an outlook on future directions that single-trial connectivity research might take.

Finally, the appendix A mathematically proves that VAR models are invariant to linear transformations and appendix B contains copies of the published main papers.

## 2. Materials and Methods

### 2.1. Primary Publications

#### 2.1.1. A comparison of univariate, vector, bilinear autoregressive, and band power features for brain–computer interfaces

- [54] C. Brunner, M. Billinger, C. Vidaurre, and C. Neuper. “A comparison of univariate, vector, bilinear autoregressive, and band power features for brain–computer interfaces.” In: *Medical & Biological Engineering & Computing* 49 (11 2011), pp. 1337–1346. ISSN: 0140-0118. DOI: [10.1007/s11517-011-0828-x](https://doi.org/10.1007/s11517-011-0828-x)

The main goal of this thesis is the application of connectivity to BCIs, and a very versatile way to estimate connectivity is provided by VAR models. Thus, the aim of the first study was to determine if it is feasible to use VAR models in motor imagery BCIs. The study was designed to answer two questions: (1) Do linear models sufficiently represent the EEG during motor imagery? (2) Is information about signal interactions as provided by VAR models useful for BCIs?

Univariate AR models, bilinear autoregressive (bAR) models, and VAR models were compared for EEG based motor imagery classification. VAR and bAR models are extensions to univariate AR models. While univariate AR models are linear models of each individual signal, VAR models model all signals together and explain causal interactions. bAR models are nonlinear univariate models that can model bursts or arc-shaped oscillations such as the  $\mu$ -rhythm. To compare the different models they were fitted adaptively to motor imagery EEG data, and the model coefficients were then used as features for classification in an offline study. VAR models achieved reasonable classification performance and were significantly better than the other models.

**Contribution to this work** Showing that VAR models are superior to univariate and bilinear models supports the hypothesis that BCIs can indeed benefit from features that contain information about signal interactions. This result encouraged further research towards online BCIs driven by VAR-based connectivity.

### 2.1.2. Single-trial connectivity estimation for classification of motor imagery data

- [88] M. Billinger, C. Brunner, and G. R. Müller-Putz. "Single-trial connectivity estimation for classification of motor imagery data." In: *Journal of Neural Engineering* 10 (2013), p. 046006

The first study showed that VAR models adequately model the EEG. Thus, the information about connectivity they contain seems to be useful for motor imagery classification. In this second study a BCI framework was developed for evaluating and comparing connectivity measures based on VAR models.

VAR models describe the EEG in the time domain, and model the full spectrum. However, only certain frequency bands contain task relevant information. Among the most prominent bands are the  $\mu$  and  $\beta$  bands during motor execution or imagery. Analysis can be limited to such bands by using spectral connectivity measures. Spectral connectivity measures represent connectivity as a function of frequency, which facilitates selection of interesting frequency bands. Note that the VAR model still models the whole spectrum, and interesting frequency bands are picked afterwards.

In this second work, a framework was developed for offline BCI classification of motor imagery (MI) with connectivity features (Figure 2.1). The EEG was decomposed into ICs prior to connectivity estimation, instead of using the raw EEG like in the previous study. A BCI requires single-trial feature extraction but ICA is difficult to perform on a single-trial basis. Thus, a two-stage approach was developed where ICA was performed only in the initialization estimate of the unmixing matrix. By pruning the unmixing matrix, components were selected based on pre-calculated connectivity between all available sources. Single-trial connectivity estimation was then performed on selected components which were extracted from novel data using the pruned unmixing matrix. Finally, the connectivity in automatically selected frequency bands was used as features for classification.

**Contribution to this work** This is the first publication that compared a large number of connectivity measures in a rigorous BCI framework. It directly supports the main goal of the thesis: development of a connectivity-based BCI. The offline BCI results showed that some connectivity measures can perform en par with band power features. This result encouraged further development and improvement of the estimation procedures.

## 2. Materials and Methods

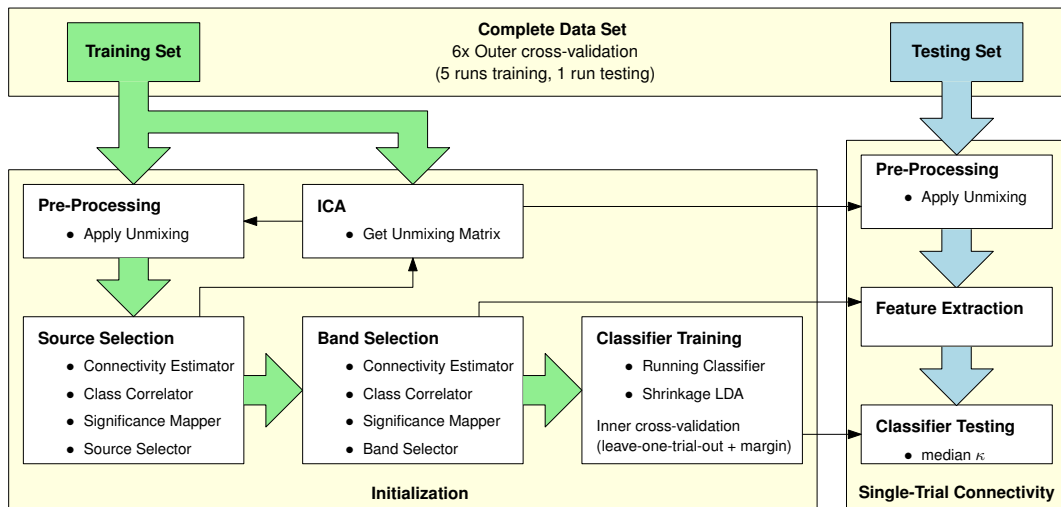


Figure 2.1.: The single-trial connectivity framework resembles the workflow of a typical BCI: parameters are optimized on available data and applied to unseen data. This workflow is embedded in a cross-validation procedure, where parts of the pre-recorded data serve as the novel testing set. Broad arrows depict data flow and narrow arrows correspond to system parameters. This figure was taken from [88].

### 2.1.3. SCoT: a Python toolbox for EEG source connectivity

[97] M. Billinger, C. Brunner, and G. R. Müller-Putz. “SCoT: A Python Toolbox for EEG Source Connectivity.” In: *Front. Neuroinform.* 8 (2014)

The second study showed that spectral connectivity measures can be used in a motor imagery BCI. However, the source selection procedures are rather cumbersome. The initialization step requires two passes of connectivity estimation to select sources, frequency bands and train the classifier. Furthermore, applying ICA to the raw EEG prior to VAR model fitting is not the ideal approach. Joint estimation methods such as MVARICA [81] have been shown to perform better [89]. In this third study the complexity of the connectivity BCI framework was reduced, and source decomposition and VAR model fitting were improved.

A new method, CSPVARICA, was developed for the SCoT toolbox. CSPVARICA is a combination of CSP, ICA, and VAR model. CSPVARICA is similar to MVARICA, but replaces PCA with CSP. Both PCA and CSP are used for dimensionality reduction. While PCA selects dimensions along which the original signal varies most, CSP selects dimensions along which there is most difference between conditions. Thus, CSPVARICA automatically selects sources that are most discriminative for two conditions and jointly estimates ICA and a VAR model. This results in sources that are well suited for connectivity estimation.

Additionally, the VAR model fitting procedure was adapted to support regularization of the coefficients. Regularization penalizes the magnitude of the VAR model coefficients. This imposes an external constraint on the model coefficients, and in

## 2. Materials and Methods

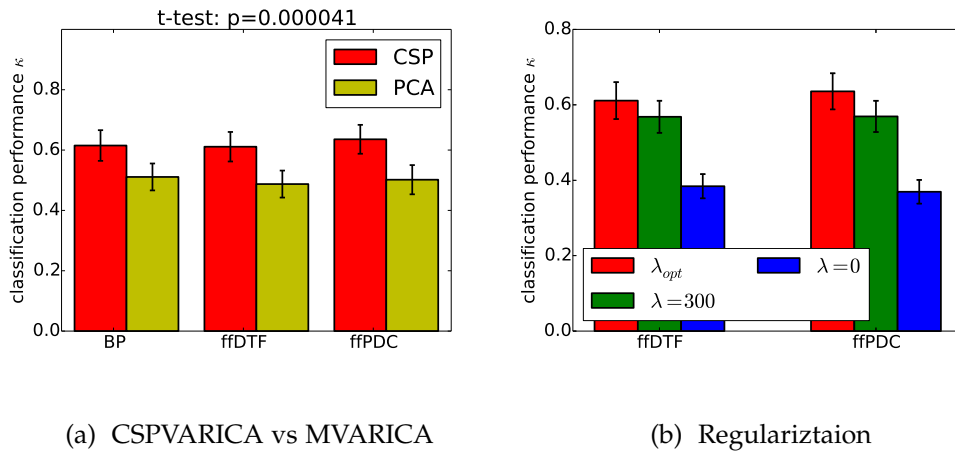


Figure 2.2.: (a) CSPVARICA gives better classification performance than MVARICA. Sources in CSPVARICA are selected based on how well they discriminate classes, which makes it an important tool for BCIs. (b) Regularized VAR model fitting significantly improves classification performance. The figure shows that regularization can be applied generously: the classification performance is less sensitive to too much regularization than to no regularization at all. These figures were taken from [97].

consequence less data is required for fitting the model. This improves the quality of the model in the single-trial situation where data is scarce. Furthermore, all these methods were made publicly available in SCoT, the first open source Python toolbox for connectivity estimation.

**Contribution to this work** The development of CSPVARICA was an important step (Figure 2.2). It is not only useful for BCIs, but for any application where connectivity is compared between two conditions. Also, SCoT is a contribution to the entire research community. Furthermore, streamlining the initialization step for single-trial connectivity estimation made the procedures ready for use in an online system.

### 2.2. Online Visualization of Brain Connectivity

The goal of this final study was to apply single-trial connectivity in an online setting. A system for live visualization of connectivity patterns in the ongoing EEG was implemented. Such a system may have applications in biofeedback or brain surgery. The system was tested with twelve participants, who performed two motor execution tasks (left/right wrist extension) and resting tasks with eyes open and closed. Monitoring connectivity during these tasks revealed in most subjects increased cross-talk between occipital areas while their eyes were closed, but only some subjects had different connectivity patterns for left and right wrist extension.

Implementing the online system required adaptations to the framework that allowed it to run in a parallel signal processing environment. Furthermore, new strategies for online visualization of connectivity had to be developed. In contrast to a static representation, online connectivity changes constantly, and there is little time to take in details. However, online visualization offers possibilities not available to the static representation. Colors and particularly animations help visualizing the “flow” of connectivity between sources.

At the time of writing the thesis, this paper has not been published but is still in the review process. Therefore, the submitted manuscript is included in this section.

**Contribution to this work** This study concludes the thesis by showing that the single-trial connectivity estimation methods are feasible for use in an online system.

#### 2.2.1. Introduction

Functional and effective connectivity can be estimated from various measures of brain activity such as fMRI [105], EEG [106], MEG [107], functional near infrared spectroscopy (fNIRS), or positron emission tomography (PET) [108] in different temporal and spatial resolutions. In our work, we focus on EEG, because it is an inexpensive and portable technique that directly captures neural activity on a millisecond scale. Estimation of connectivity from the EEG faces two challenges: (1) EEG channels are highly correlated due to volume conduction and a common reference, and (2) EEG sensor locations are not the actual sources of cortical brain activity. These challenges can be solved by measuring connectivity in the cortical source space rather than in the sensor space [106].

Routines for connectivity analysis are included in many popular EEG analysis tools such as MNE-Python [109], Fieldtrip [110], and EEGLAB [86]. However, most of these tools are designed for offline analysis. This means that they can utilize multiple repetitions of the experimental conditions to increase time and frequency resolution of the connectivity estimates. Using connectivity in online applications such as BCIs or brain activity visualizations requires more advanced estimation strategies.

## 2. Materials and Methods

---

Recently, we developed a framework for single-trial connectivity estimation [88], where EEG channel data is transformed into the source space with ICA prior to VAR based connectivity estimation. In contrast to multi-trial connectivity estimation, single-trial estimation can be applied online during ongoing EEG recordings. Online connectivity estimation may have applications in workload monitoring, biofeedback, monitoring awakesness in minimally conscious patients, or brain surgery, where other visualization strategies have already been successfully deployed [111, 112, 62, 113].

In this work, we demonstrate online visualization of source-based connectivity from ongoing EEG recordings. Previously, we applied single-trial connectivity estimation only in cross-validated offline studies [88]. Here, we transfer the knowledge gained from offline experiments to an online validation of our single-trial connectivity estimation concept. Even though a system for online connectivity visualization has been proposed before [62] and the Glass Brain<sup>1</sup> project has received recent attention in popular science magazines [114], this is the first time that actual online visualization of source-based connectivity is performed and validated in a study with several participants.

### 2.2.2. Methods

#### Connectivity estimation

A common practice in connectivity estimation is to model the signals with a VAR model. Such a model describes causal interactions in the time domain. Various spectral connectivity measures can be extracted from frequency domain representations of the model [73]. In this manuscript, we will refer to the two steps of VAR model fitting and subsequent extraction of connectivity measures simply as connectivity estimation.

When performing multi-trial connectivity estimation, a large amount of data is available from many repetitions of the experiment. If one considers a typical experiment with 64 EEG channels, 100 trials and an estimation window length of 100 samples, 640,000 data points are available for estimation. Thus, reliable estimates including statistical measures such as the mean and its confidence interval can be obtained in offline analyses. Figure 2.3 shows an example of multi-trial PDC estimation.

In contrast, only a fraction of data is available in the single-trial case – typically only one short time window. This would amount to only 6,400 data points in the example above. In general, this is not sufficient for meaningful interpretation of connectivity estimates and leads to large inter-trial variance. However, this variance can be reduced by imposing constraints on the VAR model. In particular, regularization of the VAR model leads to more consistent single-trial estimates compared to unconstrained VAR models. We use ridge regression to regularize our VAR models. Ridge regression imposes a penalty on the  $l_2$ -norm of the model coefficients, which

---

<sup>1</sup><http://neuroscapelab.com/projects/glass-brain/>

## 2. Materials and Methods

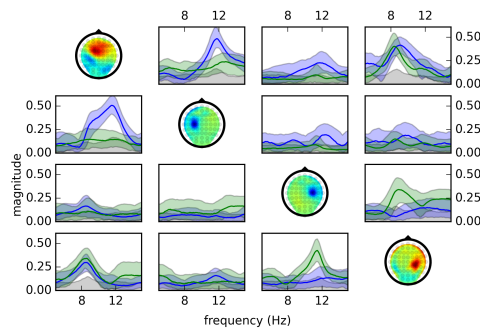


Figure 2.3.: Multi-trial connectivity. Each plot shows the mean PDC (bold lines) with 95 % confidence intervals for left (blue) and right (green) wrist extension. The gray area indicates the 95 % confidence interval under the null hypothesis of no connectivity. The topoplots on the diagonal represent cortical sources used in this example. The direction of connectivity is always from the source in the column to the source in the row.

leads to smaller coefficients and limits the influence of noise. Figure 2.4 illustrates the impact of regularization on single-trial connectivity estimation.

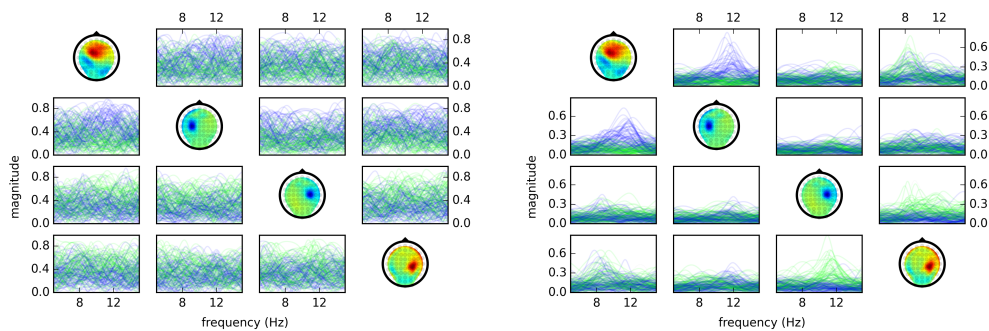


Figure 2.4.: Single-trial connectivity without (left) and with (right) regularization. The plots show PDC spectra for individual single trials for left (blue) and right (green) wrist extension. The topoplots on the diagonal represent cortical sources used in this example. The direction of connectivity is always from the source in the column to the source in the row.

In this study, we extend our previously developed single-trial connectivity framework [88, 97] to online visualization of connectivity. This framework facilitates a two-step approach for single-trial connectivity estimation. In the first step, offline analysis is performed to initialize the single-trial analysis in the second step. In the initialization step, we decompose EEG channels into independent components. By manually selecting ICs that represent cortical sources, we derive an unmixing matrix that we can later use to extract signals from the same sources, but using new recordings. Furthermore, we determine hyper-parameters such as VAR model order and the regularization penalty weight in this step.

Finally, in the second single-trial estimation step, we obtain ICs by applying the unmixing matrix to the ongoing EEG. This is a very fast operation and always returns

## 2. Materials and Methods

---

the same sources. Subsequently, we estimate single-trial connectivity between these sources by fitting a VAR model and extracting the direct directed transfer function (dDTF). The dDTF is a spectral connectivity measure that measures causality between all source pairs as a function of frequency. It shows the inflow of causality from directly connected sources only [73].

To obtain the unmixing matrix, we use CSPVARICA. This supervised method finds a subset of ICs that maximizes the contrast between two conditions. We describe CSPVARICA in more detail elsewhere [97].

### Connectivity Visualization

Connectivity is a measure of how signal sources interact. In order to visualize connectivity, a large amount of information must be presented concisely, including a good representation of the sources. Existing representations are suitable for offline analysis and presentation of results in scientific papers. For online visualization, a new approach is required.

When estimating spectral connectivity measures, we do not only estimate which sources interact, but also how strong and at which frequencies sources are connected. Consequently, connectivity contains four dimensions of information: (1) source pair, (2) direction, (3) frequency, and (4) magnitude. For offline visualization, we use a matrix representation to visualize connectivity along these four dimensions. That is, the connectivity spectrum is plotted for all pairs of sources in both directions (as shown in Figures 2.3 and 2.4).

Interpretation of such a relatively complex cartoon can be challenging in an online setting, because connectivity can vary rapidly in time. Therefore, we reduce the amount information during online representation by showing only a single relevant frequency band. Spectral connectivity is averaged over this band. Thus, connections can be represented by simple arrows instead of spectra.

However, continuously changing arrows are still not ideal in an online setting. Instead of visualizing online connectivity with arrows, we decided to engage different visual modalities to represent the information efficiently to facilitate rapid evaluation of continuously changing connectivity patterns. Figure 2.5 shows a screenshot of our online visualization. First, we marked each source with a unique color (circles around sources in Figure 2.5). Active connections between sources are indicated by arcs connecting these circles. There are up to two arcs between any two sources, representing forward and backward connections. To distinguish directions, the arcs have the same color as the originating sources (i. e. a red arc always indicates an outgoing connection from the red source). In addition to color-coding the direction of information, we also use an animation. The arcs are shaded with a pattern that moves along the arc in the direction of the connection, representing the flow of information. Additionally, we map connectivity magnitude (strength) to the intensity of the arc color and the velocity of the flow animation. Furthermore, we limit the number of visible connections by only showing connections that exceed a certain threshold.

## 2. Materials and Methods

---

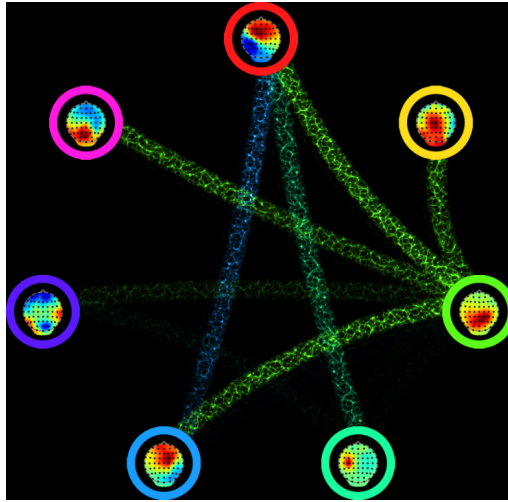


Figure 2.5.: Screenshot of our online connectivity visualization. Each source is assigned a unique color. Arcs between pairs of sources indicates an active connection, with the intensity representing the strength of the connection. The color of an arc corresponds to the color of the originating source, thus indicating the direction of causality. Additionally, causality is visualized by the pattern moving along the arcs, which is not apparent in the screenshot.

### Experimental Procedures

Twelve healthy participants aged between 22 and 30 years took part in our study. They were seated in a comfortable chair 1.5 m from a 21.5" flat panel display. Two BrainAmp MR plus amplifiers (Brain Products, Germany) recorded 64 EEG channels (Table 2.1) with passive Ag/AgCl ring electrodes. Electrode impedances were below 10 k $\Omega$ . Furthermore, a twin axis XM series goniometer (Biometrics Ltd, UK) was attached to each wrist in order to continuously measure the angle of extension of the left and right hand. All signals were sampled at 1 kHz and filtered between 0.016 and 250 Hz. A notch filter at 50 Hz was enabled to remove power line noise.

Participants completed two different paradigms, the rest paradigm and the motor paradigm. The rest paradigm had two conditions: eyes open and eyes closed. In the motor paradigm, participants were instructed to perform slow extension of the left or the right wrist. A total of three and five runs were recorded with the rest paradigm and the motor paradigm, respectively.

**Rest paradigm** The goal of the rest paradigm was to compare resting with eyes open and resting with eyes closed. One trial per condition was recorded during each run of this paradigm. Trials started with a fixation cross on the screen, followed by a visual cue that instructed the participant which task to perform. The cue appeared 1 second after trial start and showed an image of open or closed eyes for 3 seconds. After 60 seconds, the fixation cross disappeared and a short beep tone

## 2. Materials and Methods

Table 2.1.: EEG electrode names and approximate locations.

			Fp1	Fpz	Fp2			
		AF7	AF3	AFz	AF4	AF8		
F7	F5	F3	F1	Fz	F2	F4	F6	F8
FT7	FC5	FC3	FC1	FCz	FC2	FC4	FC6	FC8
T7	C5	C3	C1	Cz	C2	C4	C6	T8
TP7	CP5	CP3	CP1	CPz	CP2	CP4	CP6	TP8
P7	P5	P3	P1	Pz	P2	P4	P6	P8
		PO7	PO3	POz	PO4	PO8		
			O1	Oz	O2			
			O9	Iz	O10			

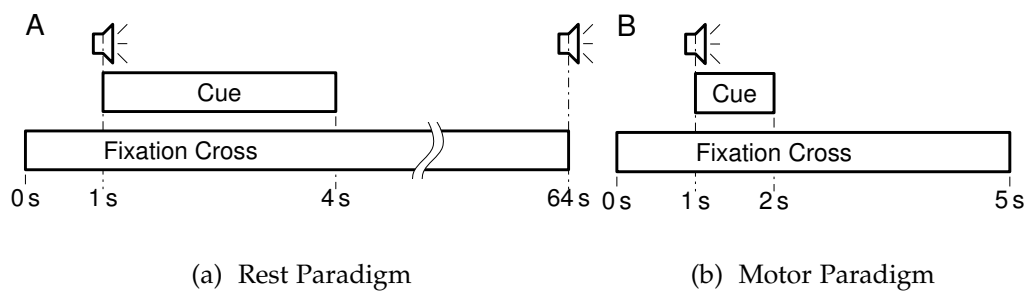


Figure 2.6.: Timing of the rest paradigm (a) and the motor paradigm (b).

indicated the end of the trial. Figures 2.6 (top) and 2.7 (top) show the timing and visuals of the rest paradigm. Participants were instructed to stay relaxed for the duration of the trial and keep their gaze fixed at the center of the screen in the eyes open condition. They were encouraged to avoid swallowing and blinking for the duration of the trial.

**Motor paradigm** The goal of the motor paradigm was to compare extension of the left and the right wrist. 25 trials per condition were performed in randomized order during each run of the motor paradigm. Trials started with a fixation cross on the screen, followed by a visual cue that instructed the participant which task to perform. The cue appeared 1 second after trial start and showed a hand pointing left or right for 1 second. A short beep tone accompanied the cue. The motor execution period lasted 3 seconds and was followed by a short break of 1–2 seconds. Figures 2.6 (bottom) and 2.7 (middle) show the timing and visuals of the motor paradigm. Participants were instructed to stay relaxed, keep their gaze fixed on the fixation cross, and blink or swallow in the breaks rather than during the trial. They were instructed to start the movement right after the cue disappeared. Importantly, we told them to perform the movement slowly, smoothly, and consciously. The maximum extension angle should be reached after approximately 1 s, immediately followed by returning the hand to the resting position at the same slow pace.

## 2. Materials and Methods

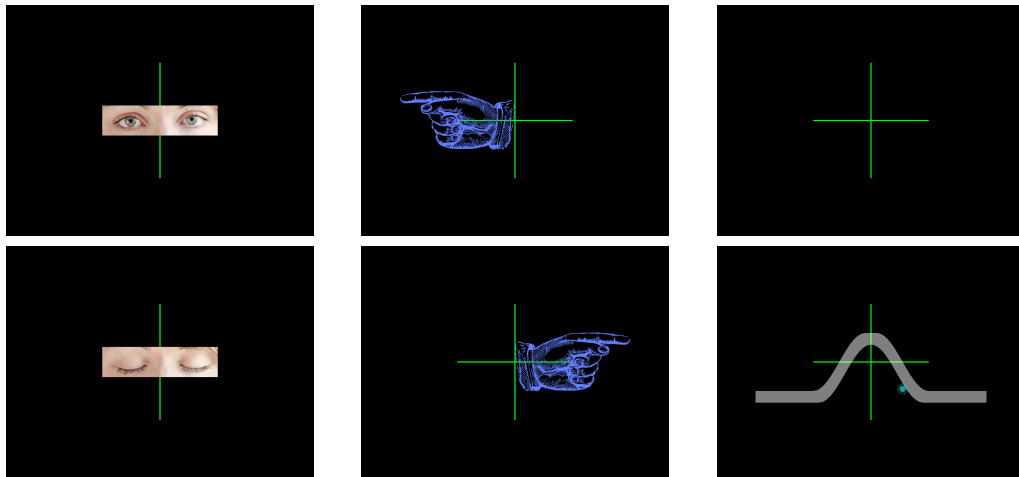


Figure 2.7.: Cues for eyes open/closed (left) and left/right extension (middle) conditions, as well as the fixation cross and visualization during guidance trials (right).

**Guidance trials** These trials were part of the motor paradigm, but are excluded from analysis. Their purpose was to help participants adjust the speed of their movement. These trials were similar to the trials in the motor paradigm, but they additionally provided feedback about the movement as follows. A ball moved horizontally across the screen with constant speed. The vertical position of the ball was controlled by the angle of extension. Furthermore, a curved track was shown on the screen (Figure 2.7 bottom). Participants were instructed to follow this track with the ball, which was possible only if they performed the movement correctly. Two such trials (left and right) were performed at the beginning of the motor paradigm, and after every 10 motor execution trials.

**Session structure** A session consisted of 8 runs. A rest condition run was followed by three motor execution runs. After recording these runs, there was a short break during which connectivity visualization was initialized with the data recorded so far. This amounts to a total of 75 trials per condition for initializing the motor paradigm and 60 s of continuous EEG per condition for initializing the rest paradigm.

After initialization, two runs of each type were performed during which the supervisor monitored online connectivity. This resulted in a total of 50 testing trials per condition for the motor paradigm and 120 s of testing data per condition for the rest paradigm. Note that participants did not see the connectivity visualization during the experiment. Instead, they received the same instructions as in the initialization runs.

### Hardware Setup

Three computers were used to perform this study (Figure 2.8). The operand PC provided the interface to the participant. It was running Windows 7 on an Intel

## 2. Materials and Methods

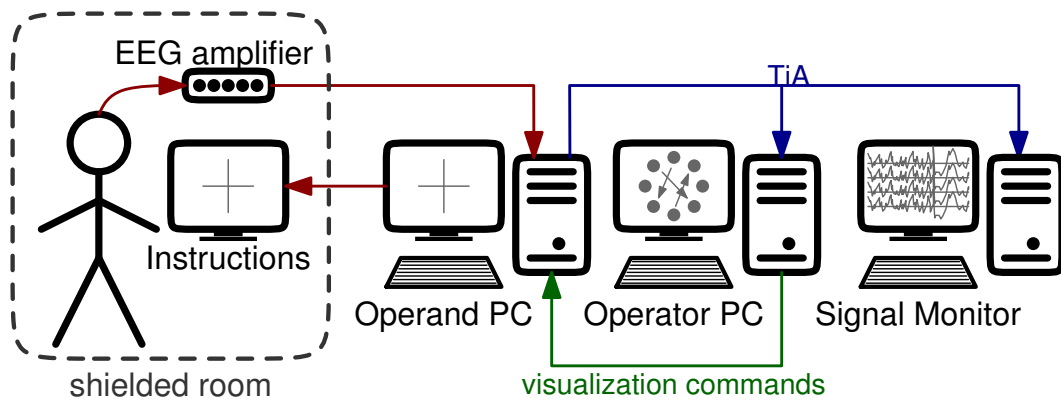


Figure 2.8.: Hardware infrastructure. The operand PC provided the interface to the participant. It recorded physiological signals and presented instructions according to the paradigm. The operator PC performed necessary computations, controlled the paradigm, and showed the connectivity visualization. A third computer was used to continuously monitor recorded EEG signals.

Core 2 machine with 2.4 GHz and 6 GB memory. This computer hosted the TOBI signal server (TSS) [115] for data acquisition and the visualization of the paradigm that instructed the participant. The operator PC provided the computational power for online signal processing and connectivity visualization. It was running Debian Linux on an Intel Core i7 machine with 3.4 GHz and 8 GB memory. The third computer was used to monitor the EEG during the measurements.

### Computational Environment

We selected Python as our main development platform because it is freely available, has numerous libraries for scientific computing, and is suitable for rapid development. Despite being an interpreted programming language, it can perform fast numerical computations and supports multitasking.

Online estimation of connectivity needs to be fast so it can be updated as soon as new data becomes available. Thus, it differs from offline analysis in two important aspects: (1) less data is available for the estimation process, and (2) computational resources need to be carefully managed. Regularization, limiting the model order, and selecting only relevant sources help to deal with these issues.

Parallelization can distribute the workload and allows us to implement a computational pipeline. The typical steps required for online visualization are data acquisition, connectivity estimation, and visualization. In a sequential design, a new chunk of data can enter the processing chain only after the previous chunk has passed through the entire chain. Also, each step has to wait until the previous step is completed, which is an inefficient use of computational resources. In contrast, a parallel pipeline design allows the processing chain to visualize chunk A, while connectivity estimation works on chunk B, and data is collected for chunk C.

## 2. Materials and Methods

---

In general, a program can execute code in parallel using threads or processes. While threads share their memory, processes have their own memory space. Communication between threads does not require copying of data, which makes threads more efficient than processes. However, Python's global interpreter lock (GIL) does not allow multiple threads to access the interpreter simultaneously [116]. Consequently, threads have to wait for each other to complete their computations, which limits their usefulness in a computationally intensive parallel environment. However, this limitation does not apply to processes, which have their own instances of the Python interpreter. While some of the lightweight tasks in the processing pipeline can be put into threads, critical and computationally intensive tasks such as data acquisition or connectivity estimation should be performed in separate processes or even on different computers. Transmitting data between threads, processes, and computers requires different communication mechanisms, which makes the implementation of such an environment cumbersome and error-prone. However, the zero message queue (ØMQ) [117] library solves this problem effectively by providing a communication layer that transparently connects threads, processes or computers. This allowed us to implement functionality in small and highly specialized function blocks that communicate through ØMQ sockets. These blocks can transparently run as threads, processes, or even on different computers to optimally utilize computational resources.

### Initialization Procedure

As alluded to in section 2.2.2, we use a two-stage approach for single-trial connectivity estimation. The first stage is initialization, which was performed separately for the motor and the rest paradigm. Initialization for the motor paradigm was performed with data from runs 2–4, resulting in a total of 75 trials per condition. Initialization for the rest paradigm was performed with data from the first run, resulting in 60 s of data per condition.

The following steps performed for initialization are almost the same for motor and rest paradigms; only step 2 (alignment/segmentation of epochs) is different:

**1. Channel rejection** In order to remove signals from bad EEG locations, signals were excluded from further processing if their standard deviation over the entire recording exceeded  $100 \mu V$ .

**2a. Trial alignment (motor paradigm)** Timing of the movement task is subject to high variability. Thus, trials were temporally re-aligned based on the actual movement. The point where the wrist extension started to reverse direction was chosen for common alignment. This point appears as a peak in the goniometer signals. First, the goniometer signals were low-pass filtered to 3 Hz with a fourth order Butterworth filter. Then, the peak was defined as the first point where the numerical derivative of the filtered signal changed sign from positive to negative.

## 2. Materials and Methods

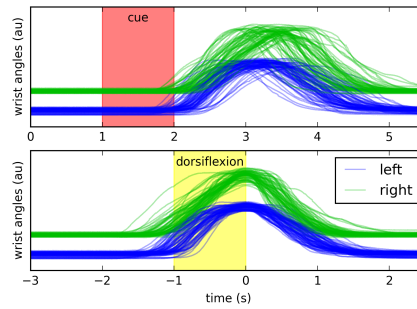


Figure 2.9.: Trial alignment. These plots show the left and right wrist angles measured by the goniometers (in arbitrary units). In the upper panel, the signals are aligned with the cue. In the lower panel, the signals are aligned with the movement peak, which reduces temporal variability in the extension. This information was used to align the EEG segments.

EEG signals were extracted from 1 s windows right before the peaks<sup>2</sup>. Thus, we obtained segmented EEG data for the left and right extension conditions.

**2b. Segmentation (rest paradigm)** The 60 s rest periods were cut into non-overlapping 1 s windows. Thus, we obtained segmented EEG data for the two rest conditions.

**3. Downsampling** EEG signals were downsampled from 1000 Hz to 100 Hz.

**4. Artifact rejection** Trials were rejected if one of the following three criteria was fulfilled: (1) Maximum amplitude exceeds  $75 \mu\text{V}$  anywhere in the trial, (2) the variance of any channel in the trial is higher than three times the variance of the same channel over all trials, or (3) the variance of any ICA component in the trial is higher than three times the variance of the same component over all trials.

**5. Source decomposition** CSPVARICA [97] performs joint VAR model fitting and ICA. In contrast to MVARICA [81], it is designed to yield sources whose signal power varies maximally between conditions. Based on prior experience, we set the number of sources to  $M = 15$  and fitted VAR models of order  $p = 20$  for each of the two conditions. Subsequently, the quality of the VAR model fit was verified by testing the VAR residuals for whiteness with the Ljung-Box test up to a lag of 75. The tests indicated no significant deviation from whiteness for all participants.

<sup>2</sup>With the exception of P12, who performed the movements too fast. Here, we used  $\pm 0.5$  s around the peak.

## 2. Materials and Methods

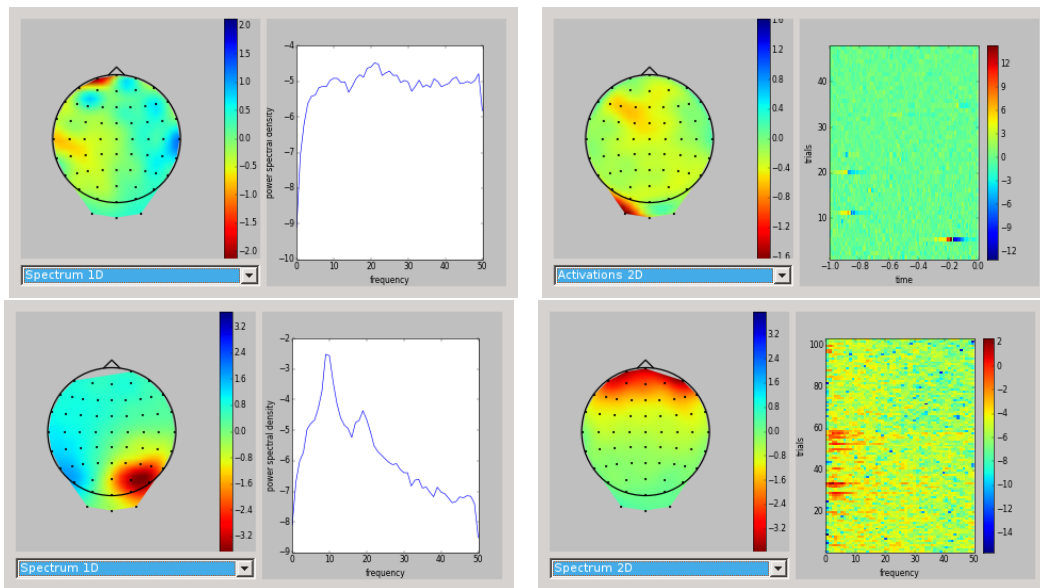


Figure 2.10.: Examples of sources obtained with CSPVARICA. Top left: muscle activity identified by localization at the side of the head and high frequency components. Top right: sporadic neck muscle activity. Bottom left: typical occipital component with alpha peak and  $1/f$  spectrum. Bottom right: EOG is frontally localized, has dominant low frequency components, and occurs sporadically.

**6. Source selection** Sources were manually selected depending on topographic, spectral, and stationarity criteria. Sources were retained if their topography indicated cortical origin, if they had a typical  $1/f$  spectrum, or if they exhibited a clear alpha peak. Sources were removed if they were clearly caused by artifacts or had high activity in only a few trials. Figure 2.10 shows examples of typical sources encountered in this step.

**7. Optimization** The single-trial VAR model order was set to  $p = 15$ , and the optimal ridge penalty was determined with cross-validation and bisection search [97].

**8. Single-trial preview** Finally, single-trial estimates of the dDTF were plotted to show the spectral inflow of causality for each source. From these plots, the frequency band and thresholds were manually chosen for online visualization. The frequency range was selected so that it contained frequencies with strongest differences in the dDTF between conditions. In most cases, this range contained the alpha peak. The threshold was chosen so that the dDTF from most trials of one condition was below the threshold, while most trials of the other condition were above the threshold.

## 2. Materials and Methods

---

### Function Blocks

Figure 2.11 shows an overview of the signal processing pipeline for online visualization. Most parts of the pipeline run as part of the main program on the operator PC. Components that form the interface to the subject (visualization and signal acquisition) run on the operand PC. Each block in the figure corresponds to a sub-program that can either run as a thread, a process, or a stand-alone program. The functionality of each block is described below.

The pipeline receives data from the TSS, which handles the acquisition of data from various sources (EEG, goniometer) and provides the data through the standardized TOBI interface A (TiA) [115]. The **TiA meta** block reads meta information such as sampling rate, number of signals, and signal labels from the TSS and provides them upon request. This information is required for storage and for initializing some of the other blocks (e. g. the resampler). Complementary to the TiA meta block, the **TiA data** block reads data packets from the TSS. Whenever a data packet becomes available, it broadcasts the data to any subscribers. However, for our purposes, the only subscriber is the **Proxy** block, which simply forwards all data it receives to subscribers. It serves as a hub to which data sources and data sinks can connect without having to be aware of one another. For example, the storage block does not need to connect to each individual data/event source separately, but only to the Proxy block. This promotes encapsulation in block design and makes adding new blocks easier.

The **Storage** block continuously streams all data it receives to disk. This includes signals, events, and TiA meta information at the beginning of the stream. After all processing is finished, the raw data stream is converted to a .mat file, which can be opened with MATLAB, Python, and many other platforms.

The following four blocks are used for manipulating data streams. Typically, they perform only simple operations and consist only of a few lines of source code. The **Demux** block extracts an individual data sub-stream (such as EEG or sensor signals). The **Resampler** block downsamples a data stream by applying a low-pass filter and decimating the data. We use a 12<sup>th</sup> order Butterworth 38 Hz low-pass filter to prevent aliasing when downsampling from 1000 Hz to 100 Hz. This filter allowed pass-band attenuation to be less than 0.01 dB with a signal-to-noise ratio (SNR) of at least 60 dB below 30 Hz. The **Sliding Window** block implements a sliding window with a circular buffer (double-ended queue). We use this buffer to estimate connectivity on 1 s EEG windows every 0.1 s. The **o-Hold** block is similar to the Sliding Window block. Basically, it is a 1 sample sliding window that provides zero-order hold functionality. In contrast to the other block, it does not forward the data as soon it becomes available. Instead, the most current data sample is provided upon request. We use this block to sample the goniometer signals, giving the participant feedback about the timing of their movement during the guidance trials.

The remaining five blocks are more complex and very specific to our application. Events that define the paradigm are generated by the **Paradigm** block. This block is responsible for the timing of presenting the fixation cross, showing the cue, clearing

## 2. Materials and Methods

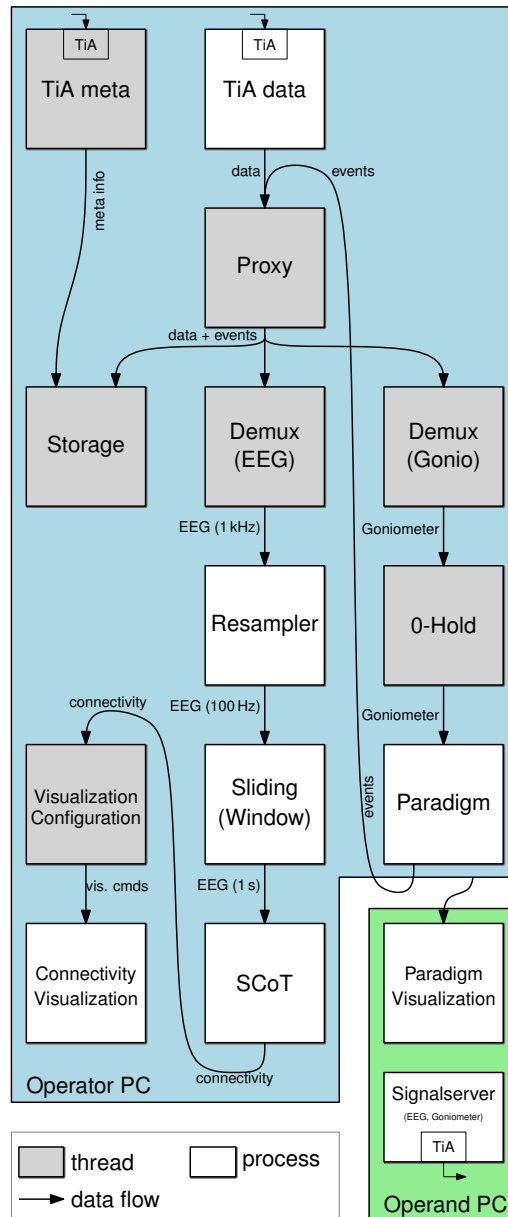


Figure 2.11.: Online signal processing. The figure indicates signal flow between the function blocks. Threads (dark background) run within the main process and share resources, while processes (white background) need to copy resources between each other but are not affected by the global interpreter lock. Note that this figure shows only the signal flow during runtime. Some blocks require information from the *TiA meta* block for initialization, which is not shown here.

## 2. Materials and Methods

Table 2.2.: Participant-specific settings.  $N$  is the number of trials in each class available for training (left/right, eyes open/closed),  $M$  is the number of sources selected for visualization,  $f$  is the visualized frequency band, and “range” is the value range for visualizing the dDTF. Values below the range are not shown as connections, and values above the range are shown at full intensity.

participant	motor paradigm				rest paradigm			
	$N$	$M$	$f$ (Hz)	range	$N$	$M$	$f$ (Hz)	range
Po1	74/72	6	10–12	2–8	54/54	5	8–12	2–10
Po2	70/66	6	7–13	2–10	50/54	6	9–13	4–10
Po3	65/65	5	8–12	3–10	60/56	7	7–11	3.5–10
Po4	69/69	7	10–14	3–10	57/45	6	9–13	3–10
Po5	67/68	7	10–14	2.8–10	58/52	7	10–14	3.4–10
Po6	52/53	4	10–13	3–10	52/55	5	12–16	3.5–10
Po7	56/43	6	10–14	3–10	43/55	5	8–12	3–10
Po8	60/59	6	7–10	3–10	52/53	8	8–12	3–10
Po9	48/52	3	7–30	1–2	40/54	6	9–12	3–10
P10	62/64	9	8–10	6–10	49/40	4	8–10	3–10
P11	55/47	5	12–16	3–10	45/58	5	12–16	3–10
P12	71/66	5	8–12	2–10	54/60	6	8–12	3–10

the screen, selecting the next trial, and so on. The **Paradigm Visualization** block is closely related; it presents the paradigm (cross, cue, beep, etc.) to the participant.

The **SCoT** block estimates connectivity on 1 s windows of EEG data. It projects the data into the source space using the unmixing matrix obtained during initialization, fits a VAR model, and calls connectivity estimation routines from the source connectivity toolbox (SCoT) [97] to estimate the dDTF. The **Visualization Configuration** block processes the connectivity estimates from the previous block and decides if and how to visualize them. This block also presents a GUI dialog where the operator can adjust frequency band and thresholds during the measurement. It sends visualization commands to the **Connectivity Visualization** block, which shows representations of cortical sources and active connections between them.

### 2.2.3. Results

The number of sources, the frequency band, and the visualization threshold were selected individually for each participant. Table 2.2 shows a summary of these settings.

Connectivity visualization was enabled for the last two runs in each paradigm. Quantifying online visualization is not straightforward, because there is no ground truth to compare against. Furthermore, visualization was active throughout the entire run, including breaks, where participants had no specific instructions and generated many artifacts. Thus, we limit the following analysis to the parts of the recordings where instructions were specific. For the motor paradigm, we use

## 2. Materials and Methods

---

the 1-s epoch containing the extension, and for the rest paradigm, we use all non-overlapping 1-s windows. We analyze each paradigm separately, and test if a connection is present in one of the tasks more often than in the other task.

Cohen's Kappa ( $\kappa$ ) [118] is a measure of agreement that we can use here. It measures how well the occurrence of a connection agrees with the tasks. A value of  $\kappa = 0$  means the connection is equally present during both or neither task(s), and  $\kappa = \pm 1$  means that the connection is always present in only one of the tasks. The measure is defined in (2.1), where  $k_i$  is the number of trials in condition  $i$  where a connection exceeds the threshold for one condition,  $\bar{k}_i$  is the number of trials in condition  $i$  where the threshold is not exceeded,  $n_1$  and  $n_2$  are the total number of trials in each condition, and  $p_0$  is the probability of random agreement.

$$\kappa = \frac{\frac{k_1 + \bar{k}_2}{n_1 + n_2} - p_0}{1 - p_0} \quad (2.1)$$

For equal numbers of trials in both conditions ( $n_1 = n_2 = \frac{n}{2}$ ) and  $p_0 = 0.5$ , the equation simplifies to

$$\kappa = 2 \frac{(k_1 - k_2)}{n}. \quad (2.2)$$

We statistically tested  $\kappa$  against the null hypothesis of no connectivity in either condition. To obtain data under the null hypothesis, we generated surrogate source time series by randomly changing the phase of the original time series [119]. This procedure destroys connectivity information in the data, but leaves the power spectra intact. After computing  $\kappa$  for 100 such surrogates, we determined their 95<sup>th</sup> percentile as the critical value  $\kappa_0$ . Connections were considered significantly discriminant if  $\kappa \geq \kappa_0$ .

We visualized significant connections between source pairs with arrows pointing in the direction of causality. The value of  $\kappa$  is mapped to the color of the arrow. Positive values range from white (0) to dark blue (+1), and negative values range from white (0) to dark green (-1). There is, for example, a blue arrow pointing both ways between two sources near the left motor cortex in the top left plot of Figure 2.12. This indicates that these sources often had synchronous activity during the left extension task. Accordingly, the corresponding ERD map shows less desynchronization during the left extension task. Four out of twelve participants had significant discriminative connections in the motor paradigm (Figure 2.12), and seven participants had significant discriminative connections in the rest paradigm (Figure 2.13). Three participants were in both groups, and four participants had no significant connections at all.

An important measure of an online system is the delay introduced by the signal processing pipeline, because this is an upper limit on how fast the system can respond to changes in the signals. We tracked the delay by passing time stamps through the processing pipeline along with the data. This allowed us to measure the time difference between update of the display and acquisition of the most

## 2. Materials and Methods

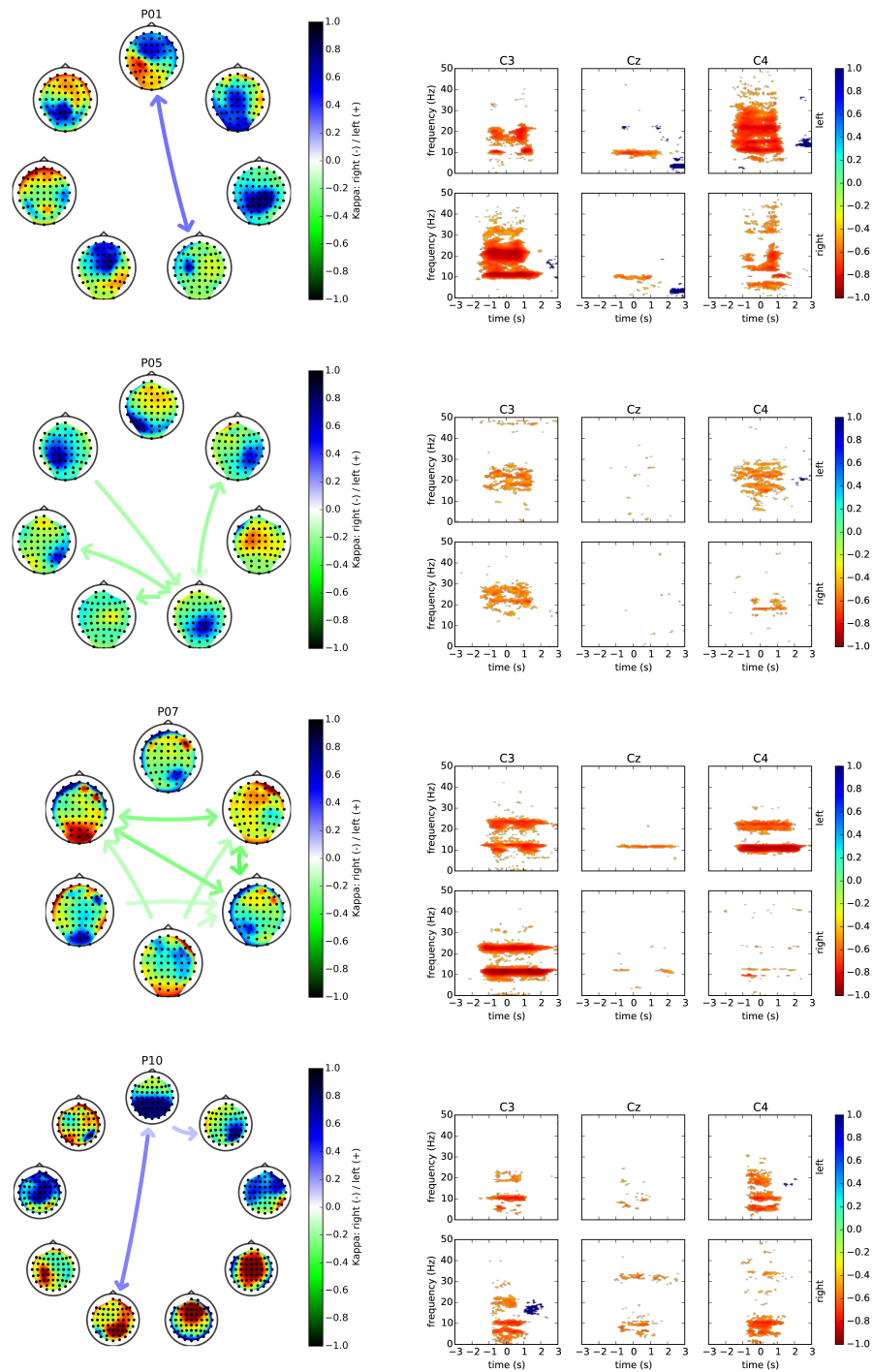


Figure 2.12.: Significant connections (left) and ERD/S maps (right) during motor execution from four subjects (P01, P05, P07, P10). In the left plot, green or blue arrows indicate connections that tended to be more active during right or left extension, respectively. The ERD/S maps show synchronization (blue) and desynchronization (red) of Laplacian EEG channels.

## 2. Materials and Methods

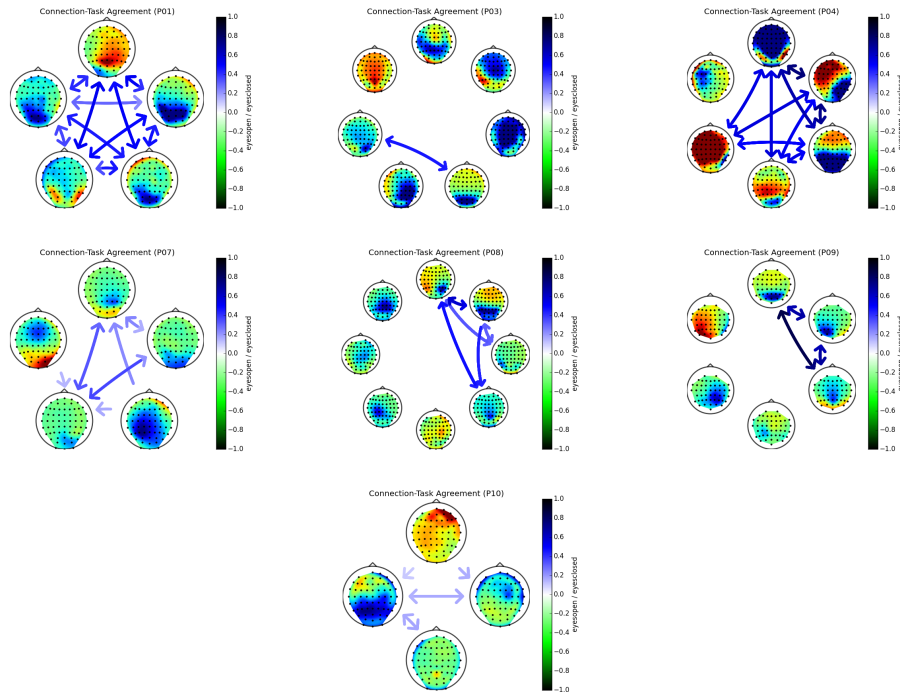


Figure 2.13.: Significant connections during rest. Blue arrows indicate connections that tended to be more active while the participants had their eyes closed.

recent sample in the estimation window. Figure 2.14 shows the distribution of this delay measured with seven sources. Most of the processing delay is approximately normally distributed with mean 68.1 ms and standard deviation 0.57 ms. There is a cluster of lower delays between 66 ms and 67 ms, and the delay never exceeded 72 ms.

### 2.2.4. Discussion

We performed online connectivity visualization during rest and motor execution. This study builds on our previous work [88, 97], where we simulated offline BCIs based on connectivity. We tested the method on two different paradigms: long-duration (60 s) resting, and relatively transient (1 s) motor execution.

We found significant results from seven participants in the resting paradigm, and from four participants in the motor paradigm. This indicates that our methods work better for the rest paradigm. There are two possible explanations for these results. First, the resting state is stationary over a long time period, while the motor task is transient. This might cause instationarities in the estimation window of the motor task, which interfere with connectivity estimation. Second, we observe differences between conditions that are based on the synchronization or desynchronization of task-specific brain rhythms. Occipital alpha synchronization is stronger

## 2. Materials and Methods

---

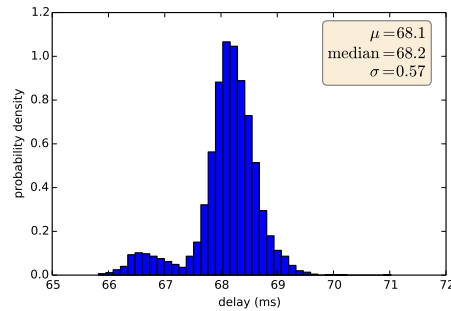


Figure 2.14.: Visualization delay when processing seven sources, measured over a period of 5 minutes. The delay is measured as the time difference between update of the display and acquisition of the most recent sample in the estimation window. This is the time it takes for the sample to pass through the signal processing pipeline.

than  $\mu$ -rhythm desynchronization. Thus, we observe stronger effects in the rest paradigm.

In this study, we based our analysis of the motor task on movement-related  $\mu$ -desynchronization. In other words, absence of the contralateral  $\mu$ -rhythm is the neural correlate of the motor task. However, identifying task-related fine structure in connectivity is difficult in a rhythm that is absent. Thus, future studies could attempt to investigate the post-movement beta synchronization [120, 121] instead, because the increased beta rhythm might exhibit stable task-related connectivity patterns.

Our results show high inter-subject variability. This is not surprising, because sources are selected for each user individually. The results do not only depend on variability in the participants' activation patterns, but also on the quality of the data. This makes comparing results across individuals difficult. Source models that incorporate anatomical information to obtain cortical current source density (CSD) estimates could potentially reduce variability across individuals by mapping activations to anatomical features. However, this might reduce discriminability of conditions. CSPVARICA does not have this drawback because sources are specifically optimized to enhance contrasts between conditions.

A recently published conference paper [62] reports efforts partially similar to ours. The authors successfully tested their connectivity estimation based on cortical CSD with artificial data and pre-recorded EEG channel data from one subject. In contrast, our approach applies ICA based source decomposition. Cortical CSD may give more accurate results, but requires an accurate anatomical head model and is computationally more demanding than our ICA approach. We plan to integrate CSD estimation into our system in the future. However, ICA will remain a feasible fall-back for data-driven source decomposition if no anatomical information is available.

In recent years, different real-time visualization systems have been proposed for use in research and clinical practice. Such systems are mainly used for real-time

## 2. Materials and Methods

---

brain mapping based on EEG [111] or electrocorticography [112, 113]. These systems are concerned with localization of brain activity, but not with interactions within the brain. In contrast, tools such as MNE-Python [109], Fieldtrip [110], or SIFT/EEGLAB [86] that analyze and visualize brain connectivity are typically intended for offline use. Systems for brain monitoring and mapping could benefit from adding online connectivity information. The Glass Brain project has already demonstrated that brain connectivity can not only produce aesthetically pleasing visualizations, but that there is also considerable public interest in the topic [114]. With this paper, we attempt to take a further step towards bridging the gap between real-time monitoring/mapping and connectivity analysis.

### 2.2.5. Conclusion

We provided a proof of concept that online visualization of connectivity is possible. Furthermore, we were able to observe plausible changes in connectivity during different tasks. However, interpreting causality from online results should not be done lightly. The limited number of sources and the strong restrictions on the VAR model might bias the results. Anatomically informed source estimates and advanced VAR model fitting strategies may have the potential to get even more information out of the limited data available online. Therefore, we believe our work is an important first step towards serious real-time causality analysis.

### Acknowledgements

We would like to thank Daniel Hackhofer and Laura Schulz for their invaluable help with the EEG measurements. The project was supported by the Austrian Science Foundation FWF Project *Coupling Measures for BCIs* (P20848-N15) and the FP7 Framework EU Research Projects *ABC* (No. 287774) and *BackHome* (No. 288566).

### 2.3. Secondary Publications

- [99] M. Billinger, C. Brunner, and C. Neuper. "Classification of Adaptive Autoregressive Models at Different Sampling Rates in a motor Imagery-Based BCI." In: *Fourth International BCI Meeting*. 2010
- [100] M. Billinger, V. Kaiser, C. Neuper, and C. Brunner. "Automated frequency band selection for BCIs with ERDS difference maps." In: *Proceedings of the Fifth International BCI Conference* (2011)
- [101] M. Billinger, C. Brunner, R. Scherer, A. Holzinger, and G. R. Müller-Putz. "Towards a framework based on single trial connectivity for enhancing knowledge discovery in BCI." In: *Active Media Technologies, Springer Lecture Notes in Computer Science*. 2012, pp. 658–667
- [102] M. Billinger, C. Brunner, R. Scherer, and G. R. Müller-Putz. "Estimating Brain Connectivity from Single-Trial EEG Recordings." In: *Proceedings of the BMT*. 2013
- [103] M. Billinger, I. Daly, V. Kaiser, J. Jin, B. Z. Allison, G. R. Müller-Putz, and C. Brunner. "Is it Significant? Guidelines for Reporting BCI Performance." In: *Towards Practical BCIs: Bridging the Gap from Research to Real-World Applications*. Springer, 2013, pp. 333–354
- [104] M. Billinger, C. Brunner, and G. R. Müller-Putz. "Analyzing EEG Source Connectivity with SCoT." In: *Proceedings of the 6th International BCI Conference*. 2014

## 3. Discussion and Conclusions

### 3.1. Overview

The research goal of this thesis was to apply connectivity estimation to online applications such as BCIs or brain connectivity monitoring. A very general basis for obtaining various kinds of connectivity measures are vector autoregressive models [73]. Thus, the ability to perform single-trial VAR model fitting was the key to fulfill the thesis' goals. This led to development of new methods and procedures. In consequence, the fundamental contributions of the thesis can be summarized in four points:

1. strategies for estimating single-trial connectivity
2. enhanced source selection with CSPVARICA (by adding class information)
3. SCoT, a publicly available open source toolbox
4. strategies for online visualization of connectivity

### 3.2. Model fitting

Before actually tackling connectivity estimation for BCIs it was necessary to determine which type of AR model is most suitable. The first study compared different types of models: linear univariate AR, linear multivariate AR (VAR), and bilinear univariate AR (bAR) [54]. It showed that VAR models were superior to the other models and there was no significant difference between bAR and AR models. These results indicated that (1) multivariate models improved classification accuracy, and (2) bAR models did not improve classification. Of course this result does not prove that linear models are better than nonlinear models. Bilinear models implement only a specific type of nonlinearity but there are infinitely many possibilities of formulating nonlinear models, some of which may perform better than linear models. However, multivariate models were clearly better than univariate models. Thus, lacking a hypothesis about which type of nonlinearity might prove useful, it was decided to use VAR models for further research on single-trial connectivity.

There are two alternatives to obtain single-trial VAR models: Adaptive fitting with a Kalman filter [53] or fitting with a sliding-window. In principle, adaptive fitting is similar to fitting with an exponential sliding window [122]. However, there are differences in the implementation details. First, the length of the exponential window depends on the adaption rate, which makes it difficult to chose a suitable window length. Furthermore, the adaptive approach needs to process every sample, while a sliding window can be moved in steps of arbitrary size. Thus, a sliding

### 3. Discussion and Conclusions

---

window approach makes the computational load easier to control in an online application. Another drawback of adaptive fitting is that the Kalman filter's memory requirement rises quadratic with the number of coefficients [123]. The number of coefficients is proportional to the squared number of signals modeled in a AR model. Thus, the memory consumption of adaptive fitting rises with the fourth power of the number of signals. In contrast, segmented fitting rises with less than the second power of the number of signals. Because of these reasons the model fitting approach was changed from adaptive Kalman filtering to sliding-window fitting after the first study.

#### 3.3. Source-Connectivity Framework

In this thesis a two-step strategy for single-trial connectivity estimation was developed [88]. The first step is intended as initialization where cortical sources are identified and selected. Only in the second step actual single-trial connectivity estimation is performed. Recently a different approach to a connectivity-based BCI has been proposed [62]. Allegedly, this approach does not rely on a two-step procedure to select sources. Instead, it works with current source densities in pre-defined cortical regions, which requires an inverse solution of an accurate forward model. However, obtaining the model and selecting regions of interest could be understood as an initialization step too. While that approach selects sources using a-priori information about brain anatomy, the approach in this thesis selects sources as ICA components based on actual EEG data. This data-driven approach has the advantage that it does not depend on any a-priori information or explicit forward models.

A common misconception about ICA and connectivity is that these concepts contradict each other. This seems obvious - how can sources be independent if they are related? Independence between sources is often naively understood as "have nothing to do with each other". This is not necessarily the case with ICA sources. Consider the cocktail party example: ICA can separate individual speakers in a room full of people given only the signals of multiple microphones distributed around the room. This is possible even though there may be causal relations between speakers that have a conversation. However, their speech signals are independent because they have different voices and say different things. In summary, while ICA is the process of identifying individual speakers, connectivity analysis is finding out who talks to whom. This also works for neural ensembles in the brain that "talk" to each other. In more technical terms, ICA blindly reconstructs a linear mixture of sources, for example by decorrelating maximally non-Gaussian components, or by minimizing mutual information. Sources are assumed to be statistically independent and non-Gaussian. However, sources are not required to be white (temporally independent), which allows them to be causally related or have an underlying connectivity structure.

Single-trial connectivity estimation relies on two key measures: source selection and regularization [97]. By selecting only a subset sources the total number of possible connections is limited. Regularization of the VAR model penalizes large

### 3. Discussion and Conclusions

---

model coefficients. Both measures reduce the degrees of freedom in the VAR model coefficients, which results in a reduced amount of time samples required for fitting the model. Thus, estimation window lengths as low as 1 s are possible, which is the typical analysis window length in a motor imagery BCI [20].

In the second study source selection was performed by considering how much each IC contributed to connectivity [88]. This requires multiple passes of connectivity estimation, which is a rather cumbersome procedure. In contrast, the number of sources in MVARICA can be limited by reducing the dimensionality of the EEG with PCA [81]. Sources obtained with MVARICA explain a certain percentage of the EEG's variance, which leads to sources with high amplitude signals. While this heuristic is much simpler than selecting sources based on their contribution to connectivity, the sources are not necessarily relevant for BCI operation because they are optimized without knowledge about the tasks. Thus, CSPVARICA was developed [97], which uses CSP instead of PCA. By using CSP CSPVARICA can select sources that have high amplitudes during one condition/task but low amplitudes during another condition/task. In consequence, CSPVARICA tends to select more task relevant sources than MVARICA. Both methods were compared in the third study of this thesis, where CSPVARICA was shown to significantly outperform MVARICA in motor imagery classification [97]. Apart from BCIs, other fields of neuroscience could benefit from CSPVARICA too since it is applicable whenever task-related changes in connectivity are researched.

#### 3.4. Connectivity

Starting with the second study, spectral connectivity measures were used for limiting connectivity estimates to interesting frequency bands. Alternatively, it might seem like a good idea to band-limit the data first. However, the band-pass would become the most prominent feature of the spectrum. Since AR models fit the entire spectrum they would mostly fit the filter's transfer function. On the other hand, downsampling (including an appropriate low-pass filter) helps to reduce the model order required to fit the data [122]. Thus, downsampling is a useful step when analyzing connectivity at lower frequencies ranges such as alpha and beta where a sampling rate of 100 Hz is enough.

Offline results showed that effective connectivity is useful for motor imagery BCIs [88, 97]. However, the results also revealed that classification performance based on connectivity is similar to classification performance based on band power. Similar results were obtained for functional connectivity by Krusienski, McFarland, and Wolpaw [94], who argued that functional connectivity and band power basically carry the same information. If this is also the case for effective connectivity remains an open question. However, this idea is supported by the way causality is defined. Causality is a measure about how much knowledge of one signal can improve prediction of another signal [124]. Signals with a high amplitude are easier to predict than signals with a low amplitude because high amplitude signals have a higher SNR in relation to the noise floor. In consequence, connectivity is easiest to detect during ERS (high amplitudes) and difficult to detect during ERD (low amplitudes).

### 3. Discussion and Conclusions

---

This is reflected in the results of the fourth study, where more connectivity was observed during the eyes closed condition (large occipital alpha oscillations). Also, during motor tasks, connectivity in the mu band drops similarly to band power, which indicates a relation between connectivity and ERD [98].

#### 3.5. Relation to the State of the Art

The current state of the art in motor imagery based BCI features are CSP [48, 49] and band power [47]. Connectivity features performed en par with band power, but currently there is no benefit in using connectivity instead of band power for BCIs. However, other applications might benefit from single-trial connectivity estimation. For example, a recent study used offline connectivity to detect the origin of epileptic seizures [125] for subsequent surgical removal. Single trial connectivity could be applied to online monitoring during brain surgery to help surgeons direct their actions. Thus, the aspect of online connectivity visualization was explored in this thesis. Online visualization of connectivity is different from visualization in printable media. The displayed information evolves constantly. The viewer has little time to take in the whole picture before it changes again. Colors and animation can support the information conveyed in the visualization, which helps to give a rapid impression of the changing “flow” of connectivity [98].

Throughout this thesis, methods that support two-step and joint estimation of connectivity were implemented. These were publicly released in the SCoT<sup>1</sup> toolbox for connectivity analysis in Python. This toolbox contains low-level routines for VAR model fitting, connectivity estimation, source decomposition and visualization. Furthermore, various high level routines are available, among them are MVARICA, CSPVARIACA, and statistics related to VAR models and connectivity. Python is an interpreted programming language that is increasingly gaining importance in scientific programming. However, no tools for connectivity analysis were available for Python so far, while similar toolboxes are available for Matlab (EEGLAB/SIFT [86], Fieldtrip [110]). Currently, core functionality of SCoT is being made available through MNE-Python<sup>2</sup>, the leading MEG/EEG analysis solution in Python, which highlights the need for connectivity analysis software.

#### 3.6. Summary and Conclusions

Only three other studies used effective connectivity measures in BCI related studies [60, 61, 62] although such measures have been applied to the EEG as early as 1991 [78]. This lack of attention is likely caused by the difficulties of single-trial connectivity estimation. The requirement of short time windows, limited amount of available data, and volume conduction stand in the way of successfully performing

---

<sup>1</sup><http://scot-dev.github.io/scot-doc/index.html>

<sup>2</sup><http://martinos.org/mne/stable/mne-python.html>

### 3. Discussion and Conclusions

---

single-trial connectivity estimation on EEG data. This thesis tackled these difficulties and demonstrated successful single-trial connectivity estimation. This opens the door for future research in the direction of BCIs and other applications that utilize connectivity measures. Especially the new SCoT toolbox can help to make single-trial connectivity available to a broad audience.

#### 3.7. Outlook

Connectivity features work well for BCIs but similar performance can be obtained with simpler band power features. However, research towards single-trial connectivity has only just begun yet. Development of improved VAR model fitting techniques, new connectivity measures, or specially designed paradigms may lead to improved connectivity features for BCIs. In particular, different regularization strategies might prove useful. Currently, only regularization with an  $\ell_2$ -norm penalty has been explored. Other regularization strategies might lead to improved results. Especially sparse regularizers such as the group Lasso [126] seem promising because they limit the amount of estimated connections. Another promising approach could be application of shrinkage to VAR models. In a nutshell, shrinkage aims to find the optimal trade-off between a complex model with low bias and high variance, and a simple model with high bias and low variance [127]. In terms of VAR models these could be a low order model and a high order model. In consequence, shrinkage would implicitly resolve model order selection and might replace regularization.

It is important to note that future research might show that connectivity and band power features really carry the same information as far as BCIs are concerned. In this case band power would remain the preferred features for BCIs. However single-trial and online connectivity could still prove useful for alternative applications such as brain surgery or monitoring of wakefulness.

## Bibliography

- [1] V. Kaiser, I. Daly, F. Pichiorri, D. Mattia, G. R. Müller-Putz, and C. Neuper. "Relationship Between Electrical Brain Responses to Motor Imagery and Motor Impairment in Stroke." In: *Stroke* 43 (2012), pp. 2735–2740 (cit. on p. 1).
- [2] I. Daly, M. Billinger, J. Laparra-Hernandez, F. Aloise, M. Lloria Garcia, J. Faller, R. Scherer, and G. R. Müller-Putz. "On the control of brain-computer interfaces by users with cerebral palsy." In: *Clinical Neurophysiology* 124 (2013), pp. 1787–1797 (cit. on p. 1).
- [3] A. Madikians and C. Giza. "A clinician's guide to the pathophysiology of traumatic brain injury." In: *Indian Journal of Neurotrauma* 3 (2006), pp. 9–17 (cit. on p. 1).
- [4] D. Majoor-Krakauer, P. J. Willems, and A. Hofman. "Genetic epidemiology of amyotrophic lateral sclerosis." In: *Clinical Genetics* 63 (2003), pp. 83–101 (cit. on p. 1).
- [5] G. Pfurtscheller, P. Linortner, R. Winkler, G. Korisek, and G. R. Müller-Putz. "Discrimination of motor imagery-induced EEG patterns in patients with complete spinal cord injury." In: *Computational Intelligence and Neuroscience* (2009). DOI: [10.1155/2009/104180](https://doi.org/10.1155/2009/104180) (cit. on p. 1).
- [6] A. Kübler, B. Kotchoubey, J. Kaiser, J. R. Wolpaw, and N. Birbaumer. "Brain-computer communication: unlocking the locked in." In: *Psychological Bulletin* 127 (2001), pp. 358–375. DOI: [10.1037/0033-2909.127.3.358](https://doi.org/10.1037/0033-2909.127.3.358) (cit. on p. 1).
- [7] G. Pfurtscheller and C. Neuper. "Motor imagery and direct brain-computer communication." In: *Proceedings of the IEEE* 89 (2001), pp. 1123–1134 (cit. on p. 1).
- [8] J. R. Millán, R. Rupp, G. Mueller-Putz, R. Murray-Smith, C. Giugliemma, M. Tangermann, C. Vidaurre, F. Cincotti, A. Kubler, R. Leeb, C. Neuper, K. R. Müller, and D. Mattia. "Combining Brain-Computer Interfaces and Assistive Technologies: State-of-the-Art and Challenges." In: *Frontiers in Neuroscience* 4.161 (2010) (cit. on p. 1).
- [9] J. R. Wolpaw, N. Birbaumer, D. J. McFarland, G. Pfurtscheller, and T. M. Vaughan. "Brain-computer interfaces for communication and control." In: *Clinical Neurophysiology* 113 (2002), pp. 767–791. DOI: [10.1016/S1388-2457\(02\)00057-3](https://doi.org/10.1016/S1388-2457(02)00057-3) (cit. on p. 1).
- [10] J. R. Wolpaw and E. Winter Wolpaw. "Brain-Computer Interfaces: Principles and Practice." In: ed. by Jonathan Wolpaw and Elizabeth Winter Wolpaw. New York: Oxford University Press, 2012. Chap. Brain-Computer Interfaces: Something New under the Sun, pp. 3–12 (cit. on p. 1).

## Bibliography

---

- [11] R. Krepki, B. Blankertz, G. Curio, and K.-R. Müller. “The Berlin Brain-Computer Interface (BBCI)—towards a new communication channel for online control in gaming applications.” In: *Multimedia Tools and Applications* 33 (2007), pp. 73–90. DOI: [10.1007/s11042-006-0094-3](https://doi.org/10.1007/s11042-006-0094-3) (cit. on p. 1).
- [12] R. Scherer, M. Pröll, B. Z. Allison, and G. R. Müller-Putz. “New input modalities for modern game design and virtual embodiment.” In: *IEEE Virtual Reality* (2012), pp. 163–164 (cit. on p. 1).
- [13] T. O. Zander and C. Kothe. “Towards passive brain-computer interfaces: applying brain-computer interface technology to human-machine systems in general.” In: *Journal of Neural Engineering* 8 (2011), p. 025005 (cit. on pp. 1, 2).
- [14] A. D. Gerson, L. C. Parra, and P. Sajda. “Cortically-coupled Computer Vision for Rapid Image Search.” In: *IEEE Transactions on Neural Systems and Rehabilitation Engineering* (2006) (cit. on p. 1).
- [15] A. Stoica, A. Matran-Fernandez, D. Andreou, R. Poli, C. Cinel, Y. Iwashita, and C. Padgett. “Multi-brain fusion and applications to intelligence analysis.” In: vol. 8756. 2013. DOI: [10.1117/12.2016456](https://doi.org/10.1117/12.2016456). URL: <http://dx.doi.org/10.1117/12.2016456> (cit. on p. 1).
- [16] N. Birbaumer, N. Ghanayim, T. Hinterberger, I. Iversen, B. Kotchoubey, A. Kübler, J. Perelmouter, E. Taub, and H. Flor. “A spelling device for the paralysed.” In: *Nature* 398 (1999), pp. 297–298. DOI: [10.1038/18581](https://doi.org/10.1038/18581) (cit. on p. 1).
- [17] G. Pfurtscheller, G. R. Müller, J. Pfurtscheller, H. J. Gerner, and R. Rupp. ““Thought”-control of functional electrical stimulation to restore handgrasp in a patient with tetraplegia.” In: *Neuroscience Letters* 351 (2003), pp. 33–36. DOI: [10.1016/S0304-3940\(03\)00947-9](https://doi.org/10.1016/S0304-3940(03)00947-9) (cit. on p. 1).
- [18] G. R. Müller-Putz, R. Scherer, G. Pfurtscheller, and R. Rupp. “EEG-based neuroprosthesis control: a step towards clinical practice.” In: *Neuroscience Letters* 382 (2005), pp. 169–174 (cit. on p. 1).
- [19] M. Rohm, M. Schneiders, and R. Rupp. “Evaluation of MI-BCI performance in ten spinal cord injured end users.” In: *Proc 4th TOBI Workshop 2013*. 2013, p. 19 (cit. on p. 1).
- [20] R. Leeb, D. Friedman, G. R. Müller-Putz, R. Scherer, M. Slater, and G. Pfurtscheller. “Self-paced (asynchronous) BCI control of a wheelchair in virtual environments: a case study with a tetraplegics.” In: *Computational Intelligence and Neuroscience 2007* (2007), p. 79642. DOI: [10.1155/2007/79642](https://doi.org/10.1155/2007/79642) (cit. on pp. 1, 43).
- [21] I. Daly, F. Aloise, P. Arico, J. Belda, M. Billinger, E. Bolinger, F. Cincotti, D. Hettich, M. Josa, J. Laparra-Hernandez, R. Scherer, and G. Müller-Putz. “Rapid Prototyping for hBCI Users With Cerebral Palsy.” In: *Proceedings of the Fifth International Brain-Computer Interface Meeting: Defining the Future*. 2013, pp. 27–28 (cit. on p. 2).

## Bibliography

---

- [22] G. Pfurtscheller, B. Z. Allison, C. Brunner, G. Bauernfeind, T. Solis-Escalante, R. Scherer, T. O. Zander, G. Müller-Putz, C. Neuper, and N. Birbaumer. "The hybrid BCI." In: *Frontiers in Neuroscience* 4 (2010), p. 30. DOI: [10.3389/fnpro.2010.00003](https://doi.org/10.3389/fnpro.2010.00003) (cit. on p. 2).
- [23] G. R. Müller-Putz, C. Breitwieser, F. Cincotti, R. Leeb, M. Schreuder, F. Leotta, M. Tavella, L. Bianchi, A. Kreillinger, A. Ramsay, M. Rohm, M. Sagebaum, L. Tonin, C. Neuper, and J. del R. Millán. "Tools for brain-computer interaction: a general concept for a hybrid BCI." In: *Frontiers in Neuroinformatics* 5 (2011), p. 30 (cit. on p. 2).
- [24] A. Kreilinger, V. Kaiser, R. Martin, R. Leeb, R. Rupp, and G. R. Müller-Putz. "Neuroprosthesis Control via Noninvasive Hybrid Brain-Computer Interface." In: *IEEE Intelligent Systems* 28.5 (2013), pp. 28–43 (cit. on p. 2).
- [25] A. Kreilinger, V. Kaiser, C. Breitwieser, C. Neuper, and G. R. Müller-Putz. "Fusion of Manual Control and BCI Using Long Term and Short Term Quality Measures." In: *International Journal of Bioelectromagnetism* 13.3 (2011), pp. 110–111 (cit. on p. 2).
- [26] J. C. De Munck, P. C. M. Vijn, and F. Lopes da Silva. "A Random dipole model for spontaneous brain activity." In: *IEEE Transactions on Biomedical Engineering* 39 (1992), pp. 791–804 (cit. on p. 2).
- [27] F. Lopes da Silva and A. Van Rotterdam. "Biophysical Aspects of EEG and Magnetoencephalogram Generation." In: *Electroencephalography*. 5th edition. Lippincott Williams & Wilkins, 2005, pp. 107–125 (cit. on pp. 2, 3).
- [28] G. Bauernfeind. "Using Functional Near-Infrared Spectroscopy (fNIRS) for Optical Brain-Computer Interface (oBCI) Applications." PhD thesis. Graz University of Technology, 2012 (cit. on p. 2).
- [29] A. Palmini. "The concept of the epileptogenic zone: a modern look at Penfield and Jaspers's views on the role of interictal spikes." In: *Epileptic Disorders* 8 (2006), pp. 10–15 (cit. on p. 2).
- [30] P. Shenoy, K. J. Miller, J. G. Ojemann, and R. P. N. Rao. "Generalized features for electrocorticographic BCIs." In: *IEEE Transactions on Biomedical Engineering* 55 (2008), pp. 273–280. DOI: [10.1109/TBME.2007.903528](https://doi.org/10.1109/TBME.2007.903528) (cit. on p. 2).
- [31] M. D. Serruya, N. G. Hatsopoulos, L. Paninski, Fellows M. R., and J. P. Donoghue. "Instant neural control of a movement signal." In: *Nature* (2002), pp. 141–142 (cit. on p. 2).
- [32] C. Mehring, J. Rickert, E. Vaadia, S. C. de Oliveira, A. Aertsen, and S. Rotter. "Inference of hand movements from local field potentials in monkey motor cortex." In: *Nature Neuroscience* 6 (2003), pp. 1253–1254 (cit. on p. 2).
- [33] P. R. Kennedy, R. A. E. Bakay, M. M. Moore, K. Adams, and J. Goldwithe. "Direct control of a computer from the human central nervous system." In: *IEEE Transactions on Rehabilitation Engineering* 8.2 (2000), pp. 198–202 (cit. on p. 2).

## Bibliography

---

- [34] L. R. Hochberg, J. Mukand, G. Polykoff, G. Friehs, and J. Donoghue. *Braingate Neuromotor Prosthesis: Nature and Use of Neural Control Signals*. Society of Neuroscience Abst. Program No. 520.17, Online. 2005 (cit. on p. 2).
- [35] J. D. Simeral, S.-P. Kim, M. J. Black, J. P. Donoghue, and L. R. Hochberg. "Neural control of cursor trajectory and click by a human with tetraplegia 1000 days after implant of an intracortical microelectrode array." In: *Journal of Neural Engineering* 8 (2011), p. 025027. DOI: [10.1088/1741-2560/8/2/025027](https://doi.org/10.1088/1741-2560/8/2/025027) (cit. on p. 2).
- [36] S. G. Mason, A. Bashashati, M. Fatourechhi, K. F. Navarro, and G. E. Birch. "A comprehensive survey of brain interface technology designs." In: *Annals of Biomedical Engineering* 35 (2007), pp. 137–169. DOI: [10.1007/s10439-006-9170-0](https://doi.org/10.1007/s10439-006-9170-0) (cit. on pp. 2, 5).
- [37] S. Baillet, J. C. Mosher, and R. M. Leahy. "Electromagnetic brain mapping." In: *IEEE Signal Processing Magazine* 18.6 (2001), pp. 14–30 (cit. on pp. 3, 13).
- [38] R. D. Pascual-Marqui. "Discrete, 3D distributed linear imaging methods of electric neuronal activity. Part 1: exact, zero error localization." In: *arXiv:0710.3341 [math-ph]* (2007) (cit. on p. 3).
- [39] S. Makeig, A. J. Bell, T.-P. Jung, and T. J. Sejnowski. "Independent component analysis of electroencephalographic data." In: *Advances in Neural Information Processing Systems*. MIT Press, 1996, pp. 145–151 (cit. on pp. 3, 14).
- [40] A. T. Boye, U. Q. Kristiansen, M. Billinger, O. Feix do Nascimento, and D. Farina. "Identification of movement-related cortical potentials with optimized spatial filtering and principal component analysis." In: *Biomedical Signal Processing and Control* 3 (2008), pp. 300–304. DOI: [10.1016/j.bspc.2008.05.001](https://doi.org/10.1016/j.bspc.2008.05.001) (cit. on p. 3).
- [41] F. Lopes da Silva. "Event-Related Potentials: Methodology and Quantification." In: *Electroencephalography*. Ed. by Ernst Niedermeyer and Fernando Lopes da Silva. 5th edition. Lippincott Williams & Wilkins, 2005, pp. 991–1002 (cit. on p. 3).
- [42] E. Niedermeyer. "The Normal EEG of the Waking Adult." In: *Electroencephalography*. Ed. by Ernst Niedermeyer and Fernando Lopes da Silva. 5th edition. Lippincott Williams & Wilkins, 2005, pp. 167–192 (cit. on p. 4).
- [43] G. Pfurtscheller and F. Lopes da Silva. "EEG Event-Related Desynchronization (ERD) and Event-Related Synchronization (ERS)." In: *Electroencephalography*. Ed. by Ernst Niedermeyer and Fernando Lopes da Silva. 5th edition. Lippincott Williams & Wilkins, 2005, pp. 1003–1016 (cit. on p. 4).
- [44] G. Pfurtscheller, C. Neuper, and G. Krausz. "Functional dissociation of lower and upper frequency mu rhythms in relation to voluntary limb movement." In: *Clinical Neurophysiology* 111 (2000), pp. 1873–1879. DOI: [10.1016/S1388-2457\(00\)00428-4](https://doi.org/10.1016/S1388-2457(00)00428-4) (cit. on p. 4).
- [45] G. Pfurtscheller and F. H. Lopes da Silva. "Event-related EEG/MEG synchronization and desynchronization: basic principles." In: *Clinical Neurophysiology* 110 (1999), pp. 1842–1857. DOI: [10.1016/S1388-2457\(99\)00141-8](https://doi.org/10.1016/S1388-2457(99)00141-8) (cit. on p. 4).

## Bibliography

---

- [46] B. Graimann, J. E. Huggins, S. P. Levine, and G. Pfurtscheller. "Visualization of significant ERD/ERS patterns in multichannel EEG and ECoG datas." In: *Clinical Neurophysiology* 113 (2002), pp. 43–47. DOI: [10.1016/S1388-2457\(01\)00697-6](https://doi.org/10.1016/S1388-2457(01)00697-6) (cit. on p. 5).
- [47] G. Pfurtscheller, G. R. Müller-Putz, A. Schlögl, B. Graimann, R. Scherer, R. Leeb, C. Brunner, C. Keinrath, F. Lee, G. Townsend, C. Vidaurre, and C. Neuper. "15 years of BCI research at Graz University of Technology: current projects." In: *IEEE Transactions on Neural Systems and Rehabilitation Engineering* 14 (2006), pp. 205–210 (cit. on pp. 5, 44).
- [48] H. Ramoser, J. Müller-Gerking, and G. Pfurtscheller. "Optimal spatial filtering of single trial EEG during imagined hand movement." In: *IEEE Transactions on Rehabilitation Engineering* 8 (2000), pp. 441–446 (cit. on pp. 5, 44).
- [49] B. Blankertz, R. Tomioka, S. Lemm, M. Kawanabe, and K.-R. Müller. "Optimizing spatial filters for robust EEG single-trial analysis." In: *IEEE Signal Processing Magazine* 25 (2008), pp. 41–56. DOI: [10.1109/MSP.2008.4408441](https://doi.org/10.1109/MSP.2008.4408441) (cit. on pp. 5, 44).
- [50] D. Flotzinger, J. Kalcher, and G. Pfurtscheller. "EEG classification by learning vector quantization." In: *Biomedizinische Technik* 37 (1992), pp. 303–309 (cit. on p. 5).
- [51] S. Lemm, B. Blankertz, G. Curio, and K.-R. Müller. "Spatio-spectral filters for improving the classification of single trial EEG." In: *IEEE Transactions on Biomedical Engineering* 52 (2005), pp. 1541–1548. DOI: [10.1109/TBME.2005.851521](https://doi.org/10.1109/TBME.2005.851521) (cit. on p. 5).
- [52] G. Pfurtscheller, G. R. Müller-Putz, J. Pfurtscheller, and R. Rupp. "EEG-based asynchronous BCI controls functional electrical stimulation in a tetraplegic patient." In: *EURASIP Journal on Applied Signal Processing* 19 (2005), pp. 3152–3155 (cit. on p. 5).
- [53] A. Schlögl, D. Flotzinger, and G. Pfurtscheller. "Adaptive autoregressive modeling used for single-trial EEG classification." In: *Biomedizinische Technik* 42 (1997), pp. 162–167 (cit. on pp. 5, 41).
- [54] C. Brunner, M. Billinger, C. Vidaurre, and C. Neuper. "A comparison of univariate, vector, bilinear autoregressive, and band power features for brain-computer interfaces." In: *Medical & Biological Engineering & Computing* 49 (11 2011), pp. 1337–1346. ISSN: 0140-0118. DOI: [10.1007/s11517-011-0828-x](https://doi.org/10.1007/s11517-011-0828-x) (cit. on pp. 5, 16, 17, 41).
- [55] B. Graimann, J. E. Huggins, S. P. Levine, and G. Pfurtscheller. "Toward a direct brain interface based on human subdural recordings and wavelet-packet analysis." In: *IEEE Transactions on Biomedical Engineering* 51 (2004), pp. 954–962. DOI: [10.1109/TBME.2004.826671](https://doi.org/10.1109/TBME.2004.826671) (cit. on p. 5).
- [56] C. Vidaurre, R. Scherer, R. Cabeza, A. Schlögl, and G. Pfurtscheller. "Study of discriminant analysis applied to motor imagery bipolar data." In: *Medical and Biological Engineering and Computing* 45 (2007), pp. 61–68. DOI: [10.1007/s11517-006-0122-5](https://doi.org/10.1007/s11517-006-0122-5) (cit. on p. 5).

## Bibliography

---

- [57] B. Blankertz, S. Lemm, M. Treder, S. Haufe, and K.-R. Müller. "Single-trial analysis and classification of ERP components – a tutorial." In: *NeuroImage* 56 (2011), pp. 814–825 (cit. on p. 5).
- [58] E. Gysels, P. Renevey, and P. Celka. "SVM-based recursive feature elimination to compare phase synchronization computed from broadband and narrowband EEG signals in brain-computer interfaces." In: *Signal Processing* 85 (2005), pp. 2178–2189 (cit. on p. 5).
- [59] H. Cecotti and A. Gräser. "Convolutional neural networks for P300 detection with application to brain-computer interfaces." In: *IEEE Transactions on Pattern Analysis and Machine Intelligence* in press (2010) (cit. on p. 5).
- [60] L. Shoker, S. Sanei, and A. Sumich. "Distinguishing Between Left and Right Finger Movement from EEG using SVM." In: *Engineering in Medicine and Biology Society, 2005. IEEE-EMBS 2005. 27th Annual International Conference. 2005*, pp. 5420–5423. DOI: [10.1109/IEMBS.2005.1615708](https://doi.org/10.1109/IEMBS.2005.1615708) (cit. on pp. 5, 15, 44).
- [61] J. H. Lim, H. J. Hwang, Y. J. Jung, and C. H. Im. "Feature Extraction for Brain-Computer Interface (BCI) Based on the Functional Causality Analysis of Brain Signals." In: *Proceedings of the 5th International Brain-Computer Interface Conference. 2011*, pp. 36–38 (cit. on pp. 5, 15, 44).
- [62] T. Mullen, C. Kothe, Y. M. Chi, A. Ojeda, T. Kerth, S. Makeig, G. Cauwenberghs, and T. P. Jung. "Real-Time Modeling and 3D Visualization of Source Dynamics and Connectivity Using Wearable EEG." In: *35th Annual International Conference of the IEEE EMBS 35 (2013)*, pp. 2184–2187 (cit. on pp. 5, 15, 22, 38, 42, 44).
- [63] D. A. Drachman. "Do we have brain to spare?" In: *Neurology* 64 (2005), pp. 2004–2005. DOI: [10.1212/01.WNL.0000166914.38327.BB](https://doi.org/10.1212/01.WNL.0000166914.38327.BB) (cit. on p. 6).
- [64] S. Wakana, Jiang H., L. M. Nagae-Poetscher, P. C. M. van Zijl, and S. Mori. "Fiber Tract-based Atlas of Human White Matter Anatomy." In: *Radiology* 230 (2004), pp. 77–87 (cit. on p. 6).
- [65] K. J. Friston. "Functional and effective connectivity: a review." In: *Brain Connectivity* 1 (2011), pp. 13–36. ISSN: 2158-0014. DOI: [10.1089/brain.2011.0008](https://doi.org/10.1089/brain.2011.0008) (cit. on pp. 6, 7).
- [66] K. J. Friston. "Functional and effective connectivity in neuroimaging: a synthesis." In: *Human Brain Mapping* 2 (1994), pp. 56–78 (cit. on p. 6).
- [67] X. Gigandet, P. Hagmann, M. Kurant, L. Cammon, R. Meuli, and Thiran J. P. "Estimating the Confidence Level of White Matter Connections Obtained with MRI Tractography." In: *PLoS ONE* 3(12) (2008), e4006 (cit. on p. 6).
- [68] J. Graner, T. R. Oakes, L. M. French, and Riedy G. "Functional MRI in the investigation of blast-related traumatic brain injury." In: *Frontiers in Neurology* 4:16 (2013) (cit. on p. 6).

## Bibliography

---

- [69] P. L. Nunez, R. Srinivasan, A. F. Westdorp, R. S. Wijesinghe, D. M. Tucker, R. B. Silberstein, and P. J. Cadusch. "EEG coherency I: statistics, reference electrode, volume conduction, Laplacians, cortical imaging, and interpretation at multiple scales." In: *Electroencephalography and Clinical Neurophysiology* 103 (1997), pp. 499–515 (cit. on pp. 7, 10).
- [70] J. P. Burg. "A new analysis technique for time series data." In: *Modern Spectrum Analysis*. Ed. by Childers D. G. New York: IEEE Press, 1968 (cit. on pp. 7, 9).
- [71] G. U. Yule. "On a Method of Investigating Periodicities in Disturbed Series, with Special Reference to Wolfer's Sunspot Numbers." In: *Philosophical Transactions of the Royal Society of London* 226 (1927), pp. 267–298 (cit. on p. 9).
- [72] G. Walker. "On Periodicity in Series of Related Terms." In: *Proceedings of the Royal Society of London* 131 (1931), pp. 518–532 (cit. on p. 9).
- [73] A. Schlögl and G. Supp. "Analyzing event-related EEG data with multivariate autoregressive parameters." In: *Event-related dynamics of brain oscillations*. Ed. by C. Neuper and W. Klimesch. Elsevier, 2006, pp. 135–147 (cit. on pp. 9, 10, 22, 24, 41).
- [74] M. Ding, S. L. Bressler, W. Yang, and H. Liang. "Short-window spectral analysis of cortical event-related potentials by adaptive multivariate autoregressive modeling: data preprocessing, model validation, and variability assessment." In: *Biological Cybernetics* 83 (2000), pp. 35–45 (cit. on p. 9).
- [75] P. J. Franaszczuk, K. J. Blinowska, and M. Kowalczyk. "The application of parametric multichannel spectral estimates in the study of electrical brain activity." In: *Biological Cybernetics* 51.4 (1985), pp. 239–247 (cit. on p. 10).
- [76] L. A. Baccalá and K. Sameshima. "Partial directed coherence: a new concept in neural structure determination." In: *Biological Cybernetics* 84 (2001), pp. 463–474 (cit. on p. 10).
- [77] L. Faes, S. Erila, and G. Nollo. "Measuring Connectivity in Linear Multivariate Processes: Definitions, Interpretation, and Practical Analysis." In: *Computational and Mathematical Methods in Medicine* 2012 (2012), pp. 1–18 (cit. on p. 10).
- [78] M. J. Kamiński and K. J. Blinowska. "A new method of the description of the information flow in the brain structures." In: *Biological Cybernetics* 65 (1991), pp. 203–210. DOI: [10.1007/BF00198091](https://doi.org/10.1007/BF00198091) (cit. on pp. 10, 44).
- [79] A. Korzeniewska, M. Mańczak, M. Kamiński, K. J. Blinowska, and S. Kasicki. "Determination of information flow direction among brain structures by a modified directed transfer function (dDTF) method." In: *Journal of Neuroscience Methods* 125 (2003), pp. 195–207. DOI: [10.1016/S0165-0270\(03\)00052-9](https://doi.org/10.1016/S0165-0270(03)00052-9) (cit. on p. 10).
- [80] G. Nolte, O. Bai, L. Wheaton, Z. Mari, S. Vorbach, and M. Hallett. "Identifying true brain interaction from EEG data using the imaginary part of coherency." In: *Clinical Neurophysiology* 115 (2004), pp. 2292–2307 (cit. on p. 12).

## Bibliography

---

- [81] G. Gomez-Herrero, M. Atienza, M. Egiazarian, and J. L. Cantero. "Measuring directional coupling between EEG sources." In: *NeuroImage* 43.3 (2008), pp. 497–508. ISSN: 1053-8119. DOI: [10.1016/j.neuroimage.2008.07.032](https://doi.org/10.1016/j.neuroimage.2008.07.032) (cit. on pp. 12–14, 19, 30, 43).
- [82] G. Nolte, A. Ziehe, V. V. Nikulin, A. Schlögl, N. Krämer, T. Brismar, and K.-R. Müller. "Robustly estimating the flow direction of information in complex physical systems." In: *Physical Review Letters* 100 (2008), p. 234101. DOI: [10.1103/PhysRevLett.100.234101](https://doi.org/10.1103/PhysRevLett.100.234101) (cit. on p. 12).
- [83] S. Erla, L. Faes, E. Tranquillini, D. Orrico, and G. Nollo. "Multivariate Autoregressive Model with Instantaneous Effects to Improve Brain Connectivity Estimation." In: *International Journal of Bioelectromagnetism* 11.2 (2009), pp. 74–79 (cit. on pp. 12, 13).
- [84] L. Faes and G. Nollo. "Extended causal modeling to assess Partial Directed Coherence in multiple time series with significant instantaneous interactions." English. In: *Biological Cybernetics* 103.5 (2010), pp. 387–400. ISSN: 0340-1200. DOI: [10.1007/s00422-010-0406-6](https://doi.org/10.1007/s00422-010-0406-6) (cit. on pp. 12, 13).
- [85] A. Hyvärinen, K. Zhang, S. Shimizu, P. O. Hoyer, and P. Dayan. "Estimation of a Structural Vector Autoregression Model Using Non-Gaussianity." In: *Journal of Machine Learning Research* 11 (2010), pp. 1709–1731 (cit. on p. 12).
- [86] A. Delorme, T. Mullen, C. Kothe, Z. Akalin Acar, N. Bigdely-Shamlo, A. Vankov, and S. Makeig. "EEGLAB, SIFT, NFT, BCILAB, and ERICA: new tools for advanced EEG processing." eng. In: *Comput Intell Neurosci* 2011 (2011), pp. 1–12. DOI: [10.1155/2011/130714](https://doi.org/10.1155/2011/130714) (cit. on pp. 12, 21, 39, 44).
- [87] A. H. Omidvarnia, G. Azemi, B. Boashash, J. M. O. Toole, P. Colditz, and S. Vanhatalo. "Orthogonalized Partial Directed Coherence for Functional Connectivity Analysis of Newborn EEG." In: *Neural Information Processing*. Ed. by Tingwen Huang, Zhigang Zeng, Chuandong Li, and ChiSing Leung. Vol. 7664. Lecture Notes in Computer Science. Springer Berlin Heidelberg, 2012, pp. 683–691. ISBN: 978-3-642-34480-0. DOI: [10.1007/978-3-642-34481-7\\_83](https://doi.org/10.1007/978-3-642-34481-7_83) (cit. on p. 12).
- [88] M. Billinger, C. Brunner, and G. R. Müller-Putz. "Single-trial connectivity estimation for classification of motor imagery data." In: *Journal of Neural Engineering* 10 (2013), p. 046006 (cit. on pp. 14, 16, 18, 19, 22, 23, 37, 42, 43).
- [89] S. Haufe, R. Tomioka, G. Nolte, K.-R. Müller, and M. Kawanabe. "Modeling Sparse Connectivity Between Underlying Brain Sources for EEG/MEG." In: *IEEE Transactions on Biomedical Engineering* 57.8 (Aug. 2010), pp. 1954–1963. ISSN: 0018-9294. DOI: [10.1109/TBME.2010.2046325](https://doi.org/10.1109/TBME.2010.2046325) (cit. on pp. 14, 19).
- [90] E. Gysels and P. Celka. "Phase synchronization for the recognition of mental tasks in a brain computer interface." In: *IEEE Transactions on Neural Systems and Rehabilitation Engineering* 12 (2004), pp. 406–415. DOI: [10.1109/TNSRE.2004.838443](https://doi.org/10.1109/TNSRE.2004.838443) (cit. on p. 15).
- [91] C. Brunner, R. Scherer, B. Graimann, G. Supp, and G. Pfurtscheller. "Online control of a brain-computer interface using phase synchronization." In: *IEEE Transactions on Biomedical Engineering* 53 (2006), pp. 2501–2506. DOI: [10.1109/TBME.2006.881775](https://doi.org/10.1109/TBME.2006.881775) (cit. on p. 15).

## Bibliography

---

- [92] Q. Wei, Y. Wang, X. Gao, and S. Gao. "Amplitude and phase coupling measures for feature extraction in an EEG-based brain-computer interface." In: *Journal of Neural Engineering* 4 (2007), pp. 120–129. DOI: [10.1088/1741-2560/4/2/012](https://doi.org/10.1088/1741-2560/4/2/012) (cit. on p. 15).
- [93] B. Hamner, R. Leeb, M. Tavella, and J. del R. Millán. "Phase-based features for motor imagery brain-computer interfaces." In: *2011 Annual International Conference of the IEEE Engineering in Medicine and Biology Society (EMBC)*. 2011, pp. 2578–2581. DOI: [10.1109/IEMBS.2011.6090712](https://doi.org/10.1109/IEMBS.2011.6090712) (cit. on p. 15).
- [94] D. J. Krusienski, D. J. McFarland, and J. R. Wolpaw. "Value of amplitude, phase, and coherence features for a sensorimotor rhythm-based brain-computer interface." In: *Brain Research Bulletin* 87 (2012), pp. 130–134. DOI: [doi:10.1016/j.brainresbull.2011.09.019](https://doi.org/10.1016/j.brainresbull.2011.09.019) (cit. on pp. 15, 43).
- [95] I. Daly, S. J. Nasuto, and K. Warwick. "Brain computer interface control via functional connectivity dynamics." In: *Pattern Recognition* 45.6 (2012), pp. 2123–2136. DOI: [10.1016/j.patcog.2011.04.034](https://doi.org/10.1016/j.patcog.2011.04.034) (cit. on p. 15).
- [96] C. Guger, G. Edlinger, W. Harkam, I. Niedermayer, and G. Pfurtscheller. "How many people are able to operate an EEG-based brain-computer interface (BCI)?" In: *IEEE Transactions on Neural Systems and Rehabilitation Engineering* 11 (2003), pp. 145–147. DOI: [10.1109/TNSRE.2003.814481](https://doi.org/10.1109/TNSRE.2003.814481) (cit. on p. 15).
- [97] M. Billinger, C. Brunner, and G. R. Müller-Putz. "SCoT: A Python Toolbox for EEG Source Connectivity." In: *Front. Neuroinform.* 8 (2014) (cit. on pp. 16, 19, 20, 23, 24, 30, 31, 34, 37, 42, 43).
- [98] M. Billinger, C. Brunner, and G. R. Müller-Putz. "Online Visualization of Connectivity." In: *tba.* (2014-2015), in preparation (cit. on pp. 16, 44).
- [99] M. Billinger, C. Brunner, and C. Neuper. "Classification of Adaptive Autoregressive Models at Different Sampling Rates in a motor Imagery-Based BCI." In: *Fourth International BCI Meeting*. 2010 (cit. on pp. 16, 40).
- [100] M. Billinger, V. Kaiser, C. Neuper, and C. Brunner. "Automated frequency band selection for BCIs with ERDS difference maps." In: *Proceedings of the Fifth International BCI Conference* (2011) (cit. on pp. 16, 40).
- [101] M. Billinger, C. Brunner, R. Scherer, A. Holzinger, and G. R. Müller-Putz. "Towards a framework based on single trial connectivity for enhancing knowledge discovery in BCI." In: *Active Media Technologies, Springer Lecture Notes in Computer Science*. 2012, pp. 658–667 (cit. on pp. 16, 40).
- [102] M. Billinger, C. Brunner, R. Scherer, and G. R. Müller-Putz. "Estimating Brain Connectivity from Single-Trial EEG Recordings." In: *Proceedings of the BMT*. 2013 (cit. on pp. 16, 40).
- [103] M. Billinger, I. Daly, V. Kaiser, J. Jin, B. Z. Allison, G. R. Müller-Putz, and C. Brunner. "Is it Significant? Guidelines for Reporting BCI Performance." In: *Towards Practical BCIs: Bridging the Gap from Research to Real-World Applications*. Springer, 2013, pp. 333–354 (cit. on pp. 16, 40).

## Bibliography

---

- [104] M. Billinger, C. Brunner, and G. R. Müller-Putz. “Analyzing EEG Source Connectivity with SCoT.” In: *Proceedings of the 6th International BCI Conference*. 2014 (cit. on pp. 16, 40).
- [105] Stephen M. Smith. “The future of fMRI connectivity.” In: *Neuroimage* 62(2) (2012), pp. 1257–1266 (cit. on p. 21).
- [106] Christoph M. Michel and Micah M. Murray. “Towards the utilization of EEG as a brain imaging tool.” In: *Neuroimage* 61.2 (June 2012), pp. 371–385. DOI: [10.1016/j.neuroimage.2011.12.039](https://doi.org/10.1016/j.neuroimage.2011.12.039) (cit. on p. 21).
- [107] M. J. Brookes, M. W. Woolrich, and G. R. Barnes. “Measuring functional connectivity in MEG: a multivariate approach insensitive to linear source leakage.” In: *Neuroimage* 63 (2 2012), pp. 910–920 (cit. on p. 21).
- [108] K. J. Friston, Frith C. D., P. F. Liddle, and R. S. Frackowiak. “Functional connectivity: the principal-component analysis of large (PET) data sets.” In: *Journal of Cerebral Blood Flow and Metabolism* 13 (1993), pp. 5–14 (cit. on p. 21).
- [109] Alexandre Gramfort, Martin Luessi, Eric Larson, Denis A Engemann, Daniel Strohmeier, Christian Brodbeck, Roman Goj, Mainak Jas, Teon Brooks, Lauri Parkkonen, and Matti Hinen. “MEG and EEG data analysis with MNE-Python.” In: *Frontiers in Neuroscience* 7.267 (2013). ISSN: 1662-453X. DOI: [10.3389/fnins.2013.00267](https://doi.org/10.3389/fnins.2013.00267) (cit. on pp. 21, 39).
- [110] R. Oostenveld, P. Fries, E. Maris, and JM. Schoffelen. “FieldTrip: Open Source Software for Advanced Analysis of MEG, EEG, and Invasive Electrophysiological Data.” In: *Computational Intelligence and Neuroscience* (2011). DOI: [10.1155/2011/156869](https://doi.org/10.1155/2011/156869) (cit. on pp. 21, 39, 44).
- [111] P. M. Birgani and M. Ashtiyani. “Wireless Real-time Brain Mapping.” English. In: *3rd Kuala Lumpur International Conference on Biomedical Engineering 2006*. Ed. by Fatimah Ibrahim, NoorAzuanAbu Osman, Juliana Usman, and NahrizulAdib Kadri. Vol. 15. IFMBE Proceedings. Springer Berlin Heidelberg, 2007, pp. 444–446. ISBN: 978-3-540-68016-1 (cit. on pp. 22, 39).
- [112] Peter Brunner, Anthony L Ritaccio, Timothy M Lynch, Joseph F Emrich, J Adam Wilson, Justin C Williams, Erik J Aarnoutse, Nick F Ramsey, Eric C Leuthardt, Horst Bischof, and Gerwin Schalk. “A Practical Procedure for Real-Time Functional Mapping of Eloquent Cortex Using Electrocor-ticographic Signals in Humans.” In: *Epilepsy & behavior : E&B* 15.3 (2009), pp. 278–286. ISSN: 1525-5069 (cit. on pp. 22, 39).
- [113] Hiroshi Ogawa, Kyousuke Kamada, Christoph Kapeller, Satoru Hiroshima, Robert Prueckl, and Christoph Guger. “Rapid and Minimum Invasive Functional Brain Mapping by Real-Time Visualization of High Gamma Activity During Awake Craniotomy.” In: *World Neurosurgery* (2014). DOI: [10.1016/j.wneu.2014.08.009](https://doi.org/10.1016/j.wneu.2014.08.009) (cit. on pp. 22, 39).
- [114] L. Greenmeier. “Glass Brain” Offers Tours of the Space between Your Ears. Sept. 2014. URL: <http://www.scientificamerican.com/article/glass-brain-offers-tours-of-the-space-between-your-ears/> (cit. on pp. 22, 39).

## Bibliography

---

- [115] C. Breitwieser, I. Daly, C. Neuper, and G. R. Müller-Putz. "Proposing a Standardized Protocol for Raw Biosignal Transmission." In: *IEEE Transactions on Biomedical Engineering* 59 (3 2012), pp. 852–859 (cit. on pp. 28, 32).
- [116] David Beazley. "Understanding the Python GIL." In: *PyCon*. 2010 (cit. on p. 29).
- [117] Pieter Hintjens. *ZeroMQ: Messaging for Many Applications*. O'Reilly Media, 2013 (cit. on p. 29).
- [118] J. Cohen. "A coefficient for agreement for nominal scales." In: *Educational and Psychological Measurement* 20 (1960), pp. 37–46 (cit. on p. 35).
- [119] Luca Faes, Alberto Porta, and Giandomenico Nollo. "Surrogate data approaches to assess the significance of directed coherence: application to EEG activity propagation." In: *Conf Proc IEEE Eng Med Biol Soc 2009* (2009), pp. 6280–6283. DOI: [10.1109/IEMBS.2009.5332477](https://doi.org/10.1109/IEMBS.2009.5332477) (cit. on p. 35).
- [120] G. Pfurtscheller, A. Stancák Jr., and C. Neuper. "Post movement beta synchronization: a correlate of an idling motor area?" In: *Electroencephalography and Clinical Neurophysiology* 98 (1996), pp. 281–293 (cit. on p. 38).
- [121] M. T. Jurkiewicz, W. C. Gaetz, A. C. Bostan, and D. Cheyene. "Post-movement beta rebound is generated in motor cortex: evidence from neuromagnetic recordings." In: *NeuroImage* 32 (2006), pp. 1281–1289 (cit. on p. 38).
- [122] D. J. McFarland and J. R. Wolpaw. "Sensorimotor rhythm-based brain-computer interface (BCI): model order selection for autoregressive spectral analysis." In: *Journal of Neural Engineering* 5 (2008), pp. 155–162. DOI: [10.1088/1741-2560/5/2/006](https://doi.org/10.1088/1741-2560/5/2/006) (cit. on pp. 41, 43).
- [123] J. M. Mendel. "Computational Requirements for a Discrete Kalman Filter." In: *IEEE Transactions on Automatic Control* 16(6) (1971), pp. 748–758 (cit. on p. 42).
- [124] B. P. Bezruchko and D. A. Smirnov. *Extracting Knowledge From Time Series: An Introduction to Nonlinear Empirical Modeling*. Springer, 2010 (cit. on p. 43).
- [125] M. Miyakoshi, A. Delorma, T. Mullen, K. Kojima, S. Makeig, and E. Asano. "Automated detection of cross-frequency coupling in the electrocorticogram for clinical inspection." In: *Engineering in Medicine and Biology Society. 35th Annual International Conference of the IEEE*. 2013 (cit. on p. 44).
- [126] S. Haufe, K.-R. Müller, G. Nolte, and N. Krämer. "Sparse Causal Discovery in Multivariate Time Series." In: *JMLR Workshop and Conference Proceedings* 6 (2008), pp. 97–106 (cit. on p. 45).
- [127] J. Schäfer and K. Strimmer. "A Shrinkage Approach to Large-Scale Covariance Matrix Estimation and Implications for Functional Genomics." In: *Statistical Applications in Genetics and Molecular Biology* 4 (2005) (cit. on p. 45).

# Appendix

## Appendix A.

# Mathematical Derivations

### A.1. VAR Model Transformations

Consider a data set consisting of  $M$  signals and  $N$  samples. Each multivariate sample in the data set is a vector  $\mathbf{x}[n]$  of size  $M$ . When fitting a VAR model (A.1) to this data set, we attempt to find linear combinations of  $p$  previous samples that best predict the current sample  $\mathbf{x}[n]$ . This linear combination is expressed by the model coefficients as  $M \times M$  matrices  $\mathbf{B}^{(k)}$ , where  $k = 1 \dots p$ .

$$\mathbf{x}[n] = \sum_{k=1}^p \mathbf{B}^{(k)} \mathbf{x}[n-k] + \mathbf{r}[n] \quad (\text{A.1})$$

We want to find the model coefficients that give on average the best prediction over all samples in the data set. In other words, we try to minimize the sum of the squared model residuals  $\mathbf{r}$ . This leads to the cost function  $J$  (A.2), which can be written as a sum of partial cost functions  $J_n$ .

$$J = \sum_n J_n = \sum_n \mathbf{r}^T[n] \mathbf{r}[n] \quad (\text{A.2})$$

The partial cost function is given by (A.3). Apparently, this function is quadratic in the coefficient matrices  $\mathbf{B}^{(k)}$ , and we can find the minimum by setting the gradient of  $J$  to zero and solving for each  $B_{ij}^{(k)}$ . Although there are more practical approaches to actually fit a VAR model, this approach is well suited for a formal derivation.

$$J_n = \mathbf{x}^T[n] \mathbf{x}[n] - 2 \sum_{u=1}^p \mathbf{x}^T[n] \mathbf{B}^{(u)} \mathbf{x}[n-u] + \sum_{v=1}^p \sum_{w=1}^p \mathbf{x}^T[n-v] \mathbf{B}^{(v)T} \mathbf{B}^{(w)} \mathbf{x}[n-w] \quad (\text{A.3})$$

The gradient of the cost function  $\nabla J$  is formed by partially deriving  $J$  by each element  $B_{ij}^{(k)}$ . Grouping the elements of the gradient by  $k$  leads to a compact representation (A.4, A.5). We could solve for the model coefficients by setting  $\nabla J = \mathbf{0}$ . However, we will stop here, because comparing the gradients of the basic VAR model and a transformed VAR model is sufficient for our derivation.

$$\nabla J = \left[ \nabla J^{(1)} \dots \nabla J^{(p)} \right] \quad (\text{A.4})$$

$$\nabla J^{(k)} = \frac{\partial J}{\partial \mathbf{B}^{(k)}} = 2 \sum_n \left( \sum_{u=1}^p \mathbf{B}^{(u)} \mathbf{x}[n-u] \mathbf{x}^T[n-k] - \mathbf{x}[n] \mathbf{x}^T[n-k] \right) \quad (\text{A.5})$$

## Appendix A. Mathematical Derivations

---

Next, we will derive the gradient of the cost function in a transformed VAR model. Consider the transformed signals  $\mathbf{y}[n] = \mathbf{M}\mathbf{x}[n]$ , with inverse transform  $\mathbf{x}[n] = \mathbf{U}\mathbf{y}[n]$ . Expressing the model from (A.1) in  $\mathbf{y}$  leads to (A.6) with residuals  $\mathbf{e} = \mathbf{M}\mathbf{r}$ .

$$\mathbf{y}[n] = \sum_{k=1}^p \mathbf{M}\mathbf{B}^{(k)}\mathbf{U}\mathbf{y}[n-k] + \mathbf{e}[n] \quad (\text{A.6})$$

Again, the cost function  $J'$  of the transformed model (A.7) is a sum of partial cost functions (A.8).

$$J' = \sum_n J'_n = \sum_n \mathbf{e}[n]^\top \mathbf{e}[n] = \sum_n \mathbf{r}^\top[n] \mathbf{M}^\top \mathbf{M} \mathbf{r}[n] \quad (\text{A.7})$$

$$\begin{aligned} J'_n &= \mathbf{x}^\top[n] \mathbf{M}^\top \mathbf{M} \mathbf{x}[n] - 2 \sum_{u=1}^p \mathbf{x}^\top[n] \mathbf{M}^\top \mathbf{M} \mathbf{B}^{(u)} \mathbf{x}[n-u] \\ &\quad + \sum_{v=1}^p \sum_{w=1}^p \mathbf{x}^\top[n-v] \mathbf{B}^{(v)\top} \mathbf{M}^\top \mathbf{M} \mathbf{B}^{(w)} \mathbf{x}[n-w] \end{aligned} \quad (\text{A.8})$$

Finally, the gradient of the transformed cost function simplifies to the gradient of the original model transformed with  $\mathbf{M}^\top \mathbf{M}$  (A.10).

$$\frac{\partial J'}{\partial \mathbf{B}^{(k)}} = 2\mathbf{M}^\top \mathbf{M} \sum_n \left( \sum_{u=1}^p \mathbf{B}^{(u)} \mathbf{x}[n-u] \mathbf{x}^\top[n-k] - \mathbf{x}[n] \mathbf{x}^\top[n-k] \right) \quad (\text{A.9})$$

$$\nabla J' = \mathbf{M}^\top \mathbf{M} \nabla J \quad (\text{A.10})$$

From (A.10) it is easy to see that both cost functions  $J$  and  $J'$  have the same minimum if  $\mathbf{M}^\top \mathbf{M}$  is invertible:

$$\begin{aligned} \nabla J' &= \mathbf{0} \\ \mathbf{M}^\top \mathbf{M} \nabla J &= \mathbf{0} \\ \nabla J &= (\mathbf{M}^\top \mathbf{M})^{-1} \mathbf{0} = \mathbf{0} \end{aligned}$$

This has important practical implications. First, it does not matter in which signal space a VAR model is fitted. The same model can be obtained from cortical sources, EEG signals, principal components, or ICs. However, if information is lost during the transform,  $\mathbf{M}^\top \mathbf{M}$  becomes singular and the original model can no longer be recovered. This is for example the case if  $\mathbf{y}$  contains less signals than  $\mathbf{x}$ . Second, although both models are equivalent, the model coefficients in the transformed model are  $\mathbf{M}\mathbf{B}^{(k)}\mathbf{U}$ . These are different from the coefficients in the original model  $\mathbf{B}^{(k)}$ . When interpreting connectivity, it is important to check in which space the model was fitted, and if an interpretation of connectivity is valid in this space.

## Appendix B.

### Primary Publications

#### B.1. Contributions

This section lists the approximate amount of work each author has contributed to each of the four main publications.

	Author	work	contribution
1	C. Brunner	30 %	idea, writing
	<b>M. Billinger</b>	55 %	programming, analysis, proofreading
	C. Vidaurre	10 %	technical advice, proofreading
	C. Neuper	5 %	general advice, proofreading
2	<b>M. Billinger</b>	70 %	idea, programming, analysis, writing
	C. Brunner	20 %	technical advice, partial writing, proofreading
	G. Müller-Putz	10 %	general advice, proofreading
3	<b>M. Billinger</b>	70 %	idea, programming, writing
	C. Brunner	20 %	idea, technical advice, proofreading
	G. Müller-Putz	10 %	general advice, proofreading
4	<b>M. Billinger</b>	70 %	idea, programming, measurements, video, writing
	C. Brunner	20 %	idea, technical advice, proofreading
	G. Müller-Putz	10 %	idea, advice on paradigm, proofreading

# A comparison of univariate, vector, bilinear autoregressive, and band power features for brain–computer interfaces

Clemens Brunner · Martin Billinger ·  
Carmen Vidaurre · Christa Neuper

Received: 4 March 2011 / Accepted: 8 September 2011 / Published online: 25 September 2011  
© The Author(s) 2011. This article is published with open access at Springerlink.com

**Abstract** Selecting suitable feature types is crucial to obtain good overall brain–computer interface performance. Popular feature types include logarithmic band power (logBP), autoregressive (AR) parameters, time-domain parameters, and wavelet-based methods. In this study, we focused on different variants of AR models and compare performance with logBP features. In particular, we analyzed univariate, vector, and bilinear AR models. We used four-class motor imagery data from nine healthy users over two sessions. We used the first session to optimize parameters such as model order and frequency bands. We then evaluated optimized feature extraction methods on the unseen second session. We found that band power yields significantly higher classification accuracies than AR methods. However, we did not update the bias of the classifiers for the second session in our analysis procedure. When updating the bias at the beginning of a new session, we found no significant differences between all methods anymore. Furthermore, our results indicate that subject-specific optimization is not better than globally optimized parameters. The comparison within the AR methods

showed that the vector model is significantly better than both univariate and bilinear variants. Finally, adding the prediction error variance to the feature space significantly improved classification results.

**Keywords** Brain–computer interface · Autoregressive model · Logarithmic band power · Feature extraction · Motor imagery

## 1 Introduction

A brain–computer interface (BCI) is a device that measures signals from the brain and translates them into control commands for an application such as a wheelchair, an orthosis, or a spelling device [43]. By definition, a BCI does not use signals from muscles or peripheral nerves. Furthermore, a BCI operates in real-time, presents feedback, and requires goal-directed behavior from the user [27].

Most non-invasive BCIs record the electroencephalogram (EEG) from the surface of the scalp [19]. In general, there are several components which process the raw EEG signals before an actual output of the system is available. Typically, signals are first preprocessed with temporal or spatial filters. Examples of preprocessing techniques include bandpass filters, bipolar filters, or more advanced approaches such as common spatial patterns (CSP) [4]. The next stage extracts suitable features from the preprocessed signals, that is, relevant (discriminative) signal characteristics are isolated. Popular features for BCIs include logarithmic band power (logBP) [25, 26], autoregressive (AR) parameters [35], time-domain parameters [42], and wavelet-based methods [11]. Finally, a classification or regression algorithm translates the features into an output signal

C. Brunner (✉) · M. Billinger · C. Neuper  
Laboratory of Brain-Computer Interfaces, Institute for  
Knowledge Discovery, Graz University of Technology,  
Krenngasse 37, 8010 Graz, Austria  
e-mail: clemens.brunner@tugraz.at

C. Vidaurre  
Department of Software Engineering and Theoretical Computer  
Science, Technische Universität Berlin, Franklinstraße 28/29,  
10587 Berlin, Germany

C. Neuper  
Department of Psychology, University of Graz, Universitätsplatz  
2/III, 8010 Graz, Austria

for a specific application. Examples of widely used classifiers in BCI research are linear discriminant analysis (LDA), support vector machines, neural networks, and nearest neighbor classifiers [18, 19, 40]. Optionally, and depending on the application, the output of the classification stage can be post-processed, for example by averaging over time or by introducing additional constraints such as a dwell time and refractory period [37].

Selecting suitable features is crucial to obtain good overall BCI performance [7, 8]. In this study, we focus on BCIs based on event-related desynchronization [28] and explore extensions of the simple AR model and compare the resulting features with logBP features. More specifically, we compare the performance of a standard univariate AR (UAR) model, a vector AR (VAR) model, and a bilinear AR (BAR) model on BCI data. We also study the influence of adding the error variance as a feature for all three AR model types. Similar to logBP, AR parameters can be used to estimate the power spectral density [20], but they can also serve directly as features for BCIs [35]. Many groups have used AR parameters as features for BCIs in either way; some groups used short segments of time and fitted an AR model to this data segment [9, 30], whereas others adapted the model coefficients continuously [35, 39] (for example with a Kalman filter approach).

Most studies used UAR models, which means that each EEG channel is described with a separate AR model. This means that information about the relationships between signals is completely neglected. In contrast, a VAR model describes all channels at once and therefore includes information about the correlation between individual signals. Only a few studies have described VAR parameters applied to BCI data, but they reported promising results [2, 24]. Furthermore, the additional information inherent in VAR models can be used to compute explicit coupling measures such as the partial directed coherence and the directed transfer function [34].

Another extension of the AR model is the BAR model. In contrast to the classical linear AR model, a BAR model can describe certain non-linear signal properties [29] such as non-Gaussian signals. Many real-world time series exhibit such behavior, for example the arc-shaped sensorimotor mu rhythm [10] in the case of EEG signals. Consequently, a bilinear model (which is a special case of general non-linear models) should be better suited to model such data.

The objective of this study is to assess the influence of different feature types based on AR models on the performance of a BCI (for example as measured by the classification accuracy). More specifically, we compared standard UAR models with VAR and BAR models, and variants including the prediction error variance as an additional feature. We also used logBP features as state-of-

the-art features for comparison. We hypothesized that both VAR and BAR models could yield higher BCI performance than UAR parameters, because they contain more information on the underlying signals and/or describe the signals more accurately. Moreover, adding the error variance as a feature could add discriminative information and thus increase BCI performance.

## 2 Methods

### 2.1 Data

We used data set 2a from the BCI Competition IV<sup>1</sup>, which comprises data from nine users over two sessions each (recorded on separate days). The data was recorded with prior consent of all participants, and the study conformed to guidelines established by the local ethics commission. In each trial, participants performed one out of four different motor imagery tasks: movement imagination of left hand, right hand, both feet, and tongue. In total, each of the two sessions consists of 288 trials (72 trials per class) in random order.

Subjects were sitting in front of a computer monitor. At the beginning of a trial, a cross appeared on the black screen. In addition, subjects heard a tone indicating trial onset. After 2 s, subjects viewed an arrow that pointed either to the left, right, top or bottom of the screen. They performed the corresponding motor imagery task until the cross disappeared after 6 s. A short break between 1.5 and 2.5 s followed before the next trial.

The data set consists of 22 EEG signals recorded monopolarly (referenced to the left mastoid and grounded to the right mastoid). Signals were sampled at 250 Hz and bandpass-filtered between 0.5 and 100 Hz. An additional 50 Hz notch filter removed line noise. In this study, we used only three bipolar channels, calculated by subtracting channels anterior to C3, Cz, and C4 from sites posterior to these locations (the inter-electrode distance was 3.5 cm).

### 2.2 Features

We compared three different AR variants, namely (1) a UAR model, (2) a VAR model, and (3) a BAR model. In all three cases, we used the corresponding AR coefficients as features. In addition, we enhanced each AR method by adding the prediction error variance to the feature space. In summary, we analyzed six different AR-based feature types, described in more detail in the following paragraphs.

<sup>1</sup> <http://www.bbc.de/competition/iv/>.

2.2.1 UAR model

A UAR( $p$ ) model is defined as

$$x_k = \sum_{i=1}^p a_i x_{k-i} + e_k, \tag{1}$$

where  $x_k$  is the value of the time series  $x$  at time point  $k$ . The current value of  $x_k$  can be predicted by the weighted sum of  $p$  past values  $x_{k-i}$  plus an additional error term  $e_k$ . The weights  $a_i$  are called the AR parameters. In a typical BCI,  $x_k$  corresponds to the amplitude of an EEG channel at time  $k$ .

2.2.2 VAR model

A VAR( $p$ ) model is an extension of the UAR case described above, because it simultaneously describes several time series. Thus, it is defined as

$$\mathbf{x}_k = \sum_{i=1}^p \mathbf{A}_i \mathbf{x}_{k-i} + \mathbf{e}_k, \tag{2}$$

where  $\mathbf{x}_k$  is a vector of time series at time  $k$ . The  $p$  AR parameters from the UAR model generalize to  $p$  matrices  $\mathbf{A}_i$ , and the error term  $\mathbf{e}_k$  becomes a vector. In contrast to a UAR model, a VAR model explicitly models the correlation between the different time series. Applied to EEG data, VAR models can describe the relationships between different EEG channels, which might contain discriminable information for BCIs [5].

2.2.3 BAR model

In contrast to UAR and VAR models (which are linear time series models), non-linear models can describe non-linear characteristics such as large bursts or extremely rapid and large fluctuations [29]. A BAR( $p, q_1, q_2$ ) model is an extension of a linear UAR( $p$ ) model and a special case of general non-linear models with finite parameters. It is defined as

$$x_k = \sum_{i=1}^p a_i x_{k-i} + e_k + \sum_{i=1}^{q_1} \sum_{j=1}^{q_2} b_{ij} x_{k-i} e_{k-j}, \tag{3}$$

where the first part is a UAR( $p$ ) model and the last part describes the bilinear contribution with the  $q_1 \cdot q_2$  bilinear coefficients  $b_{ij}$ .

BAR models might be more suitable to describe EEG signals, because EEG signals may contain non-linear features such as the arc-shaped mu rhythm [10]. Such characteristics cannot be captured by linear time series models [29].

2.2.4 Parameter estimation

We estimated AR parameters adaptively for all AR-based methods (UAR, VAR, and BAR) using a Kalman filter

[14]. A Kalman filter operates in the state space, which is defined by the following two equations:

$$\mathbf{z}_k = \mathbf{G} \cdot \mathbf{z}_{k-1} + \mathbf{w}_{k-1} \tag{4}$$

$$\mathbf{y}_k = \mathbf{H} \cdot \mathbf{z}_k + \mathbf{v}_k \tag{5}$$

Here,  $\mathbf{z}_k$  is the state at time  $k$ ,  $\mathbf{G}$  is the state transition matrix, and  $\mathbf{w}_{k-1}$  is the process noise with  $\mathbf{w}_{k-1} \sim \mathcal{N}(0, \mathbf{W})$ . Furthermore,  $\mathbf{y}_k$  is the measurement sensitivity matrix, and  $\mathbf{v}_k$  is the measurement noise with  $\mathbf{v}_k \sim \mathcal{N}(0, \mathbf{V})$ . For univariate models UAR and BAR,  $\mathbf{y}_k$  and  $\mathbf{v}_k$  reduce to scalars  $y_k$  and  $v_k$  (with  $v_k \sim \mathcal{N}(0, V)$ ), respectively.

We used these equations to estimate AR parameters by assigning  $\mathbf{z}_k = \mathbf{a}_k$  (where  $\mathbf{a}_k = [a_1, a_2, \dots, a_p]^T$  is a vector containing all AR coefficients),  $y_k = x_k$ ,  $\mathbf{G} = \mathbf{I}$  (the identity matrix), and  $\mathbf{H} = [x_{k-1}, x_{k-2}, \dots, x_{k-p}]$ . These assignments hold for the UAR model only, but they can be easily generalized for the VAR case by using matrix equivalents of the corresponding variables, and for the BAR model by extending  $\mathbf{z}_k$  and  $\mathbf{H}$ .

We adopted an estimation approach based on results presented in [36] and as recommended and implemented in the BioSig<sup>2</sup> toolbox [33] function `tvaar.m`. We implemented this function in C and added a MATLAB<sup>3</sup> interface, which speeded up computation time significantly.

In the first step, we tried to find suitable initial values for parameters such as the AR coefficients, the process noise covariance, and the measurement noise covariance. We updated all parameters in this first run over the complete first data session. Once we found initial values with this procedure, we estimated AR parameters in a second run over the session using another update mode, which essentially keeps the process noise and measurement noise covariances constant at the previously found values. In the final evaluation step on the unseen second session, we only used mode the latter mode, but initialized parameters with values found in the optimization step using the first session (see Sects. 2.3, 2.4 for more details).

2.2.5 Features based on AR models

The prediction error  $\mathbf{e}_k$  at time  $k$  can be estimated by subtracting the prediction ( $\mathbf{H} \cdot \mathbf{z}_k$ ) from the measurement  $\mathbf{y}_k$ :

$$\mathbf{e}_k = \mathbf{y}_k - \mathbf{H} \cdot \mathbf{z}_k \tag{6}$$

We used the logarithm of the estimated covariance of the prediction error  $\log(E \langle \mathbf{e}_k \mathbf{e}_k^T \rangle)$  to augment the feature

<sup>2</sup> <http://biosig.sourceforge.net/>.

<sup>3</sup> <http://www.mathworks.com/>.

space of UAR, VAR, and BAR models, thus yielding three additional AR feature types termed xUAR, xVAR, and xBAR. Note that we adapted the covariance estimation in each step directly with UC.

In summary, we compared the following six AR-based feature extraction methods: (1) UAR, (2) xUAR, (3) VAR, (4) xVAR, (5) BAR, and (6) xBAR.

2.2.6 LogBP

We compared our AR features with results obtained from logBP, which is commonly used in many BCI systems [19]. The calculation procedure is as follows:

- Bandpass-filter raw EEG signal in a specific frequency band (we used a fifth order Butterworth filter)
- Square samples
- Smooth over a one second time window (we used a moving average filter)
- Compute the logarithm

2.3 Parameter optimization

We conducted two independent parameter optimization procedures. In the first analysis (individual optimization), we optimized parameters for each subject individually. In the second analysis (global optimization), we searched for parameters that were optimal for all subjects in the data set. Importantly, we used only data from the first session in both procedures; we never used data from the second session during parameter optimization.

2.3.1 Individual optimization

For each AR method, we optimized model order(s) and update coefficient UC (a parameter which determines the update speed in each iteration of the Kalman filter algorithm) for each subject individually. We used a grid search to find the optimal parameter combination. Table 1 lists the search spaces for the different methods. In summary, we searched in  $41 \cdot 20 = 820$  (UAR, xUAR),  $41 \cdot 15 = 615$  (VAR, xVAR), and  $41 \cdot 15 \cdot 3 \cdot 3 = 5535$  (BAR, xBAR) parameter combinations, respectively.

For each parameter combination and method, we performed the following steps:

- Extract features (see Sects. 2.2.4, 2.2.5)
- Find best segment for classifier setup using a running classifier [22] (we divided a trial into 1 s segments with 0.5 s overlap and used all samples within a segment for the running classifier procedure; see Sect. 2.4 for more details on the classifier)
- Leave-8-trials-out cross-validation (train a classifier on best segment found in the previous step, test on whole trial)
- Use 0.9 quantile of classification accuracy  $p_0$  as performance measure

Finally, we selected the parameter combination associated with the highest performance measure.

In contrast to the grid search optimization for AR methods, we used a method based on neurophysiological principles instead of classification results to optimize log-BP features; we refer to this method as band power difference maps [3], which is similar to the approach described in [4]. The procedure is as follows (applied to each EEG channel separately):

- Compute time-frequency maps of signal power for each motor imagery task and the three remaining tasks combined (using only data from within trials)
- Calculate difference maps by subtracting the map of one task from the map of the three remaining tasks combined
- Iteratively find and remove connected patches in maps (corresponding to largest differences)
- Combine adjacent or overlapping bands.

We calculated time–frequency maps with high time and frequency resolution (we varied time from 0–8 s in steps of 0.04 s and frequency from 5 to 40 Hz with 1 Hz bands in steps of 0.1 Hz). We also calculated confidence intervals for each time–frequency point by first applying a Box-Cox transformation and then computing confidence intervals from the normal distribution.

In summary, we calculated eight time–frequency maps for the following motor imagery tasks and combination of tasks: 1, 2, 3, 4, 234, 134, 124, and 123 (the numbers 1, 2, 3, and 4 correspond to left hand, right hand, feet, and

**Table 1** Search spaces for the AR-based feature extraction methods

Methods	log(UC)	$p$	$q_1$	$q_2$
UAR, xUAR	–8..0	1..20	–	–
VAR, xVAR	–8..0	1..15	–	–
BAR, xBAR	–8..0	1..15	1..3	1..3

We varied linear and bilinear model orders  $p$ ,  $q_1$ , and  $q_2$  in steps of 1, and the logarithmic update coefficient log UC in steps of 0.2

tongue motor imagery, respectively; the numbers 234, 134, 124, and 123 are combinations of these tasks). Next, we calculated four difference maps, namely 1–234, 2–134, 3–124, and 4–123. Within each difference map, we iteratively searched for connected significant patches (inspired by a four-way flood fill algorithm), starting with the pixel with the largest difference. If the area of such a patch was over a predefined threshold of 1 s Hz, we used its upper and lower frequency borders to define a band for the logBP feature extraction method. We then removed this patch from the map and repeated the search procedure, searching again for the pixel with the largest difference. We continued this procedure until the algorithm had removed all patches from the map. Finally, we combined all frequency bands found in the four difference maps and combined adjacent or overlapping frequency bands.

### 2.3.2 Global optimization

In addition to the individual optimization, we also tried to find parameters that are optimal for all subjects. For each AR method, we averaged the performance measures (calculated for all parameter combinations) over all nine subjects. From these averaged results, we selected the combination of linear model order(s) and update coefficient with the highest performance measure.

For logBP, we simply selected standard frequency bands 8–12 and 16–24 Hz (containing alpha and beta bands) for all channels.

## 2.4 Evaluation

We evaluated all feature extraction methods in two different ways. First, we calculated the cross-validated (XV) classification accuracy  $p_0$  on the second session. Second, we estimated the session transfer (ST) by calculating classifier weights on the first session and computing the classification accuracy  $p_0$  on the second session. We carried out this evaluation for both individually and globally optimized features (see Sect. 2.2.4).

### 2.4.1 Cross-validation (XV)

With the optimized parameter values found in the optimization step (using data from the first session only), we calculated the cross-validated classification accuracy  $p_0$  on the second session. Therefore, we used a similar classification procedure as described in Sect. 2.2.4. First, we extracted features from the second session. Next, we determined the best segment for classifier setup using a running classifier [22]. As before, we divided each trial into 1 s segments with 0.5 s overlap. We used a combination of LDA classifiers in a one-versus-rest scheme; this classifier assigned one out of

four classes to the class with the highest discriminant value. We performed a leave-8-trials-out cross-validation, which means that we used segments of 280 trials to train and eight trials to test a classifier. We repeated this procedure until all segments had been used as a test set once. Finally, we averaged over all folds, and we calculated the 0.9 quantile of the cross-validated classification accuracy. That is, instead of reporting the maximum of the classification accuracy within a trial, we chose the 0.9 quantile as a more robust measure of performance, because it effectively removes outliers.

### 2.4.2 Session transfer

The ST estimates the performance of a real-world BCI system more realistically, but it requires a sufficiently high number of unseen test data trials. In this analysis, we determined optimal parameters and classifier weights from the first session. After that we extracted features from the second session and applied the classifier from the previous step. We used the same one-versus-rest classifier scheme as in the cross-validation analysis.

### 2.4.3 Statistical analysis

We used repeated measures analysis of variance (ANOVA) to statistically analyze the classification results. First, we checked the sphericity assumption with Mauchly's sphericity test. Then, we performed the ANOVA and corrected degrees of freedom if necessary. If we found significant effects, we used Newman–Keuls post-hoc tests to determine significant differences.

Basically, we performed ANOVAs for XV and ST results separately. First, we wanted to assess differences over all seven feature extraction methods (factor “method”; 7 levels; UAR, xUAR, VAR, xVAR, BAR, xBAR, and logBP) and optimization strategies (factor “optimization”; 2 levels; individual and global). Second, we were also interested in differences between the three AR-based methods only (factor “method”; 3 levels; U, V, and B), the influence of the prediction error variance feature (factor “x”; 2 levels; yes or no), and the optimization strategies (factor “optimization”; 2 levels; individual or global).

We repeated these analyses with both XV and ST results combined into a factor “ST/XV” (2 levels; ST and XV). In summary, we performed six repeated measures ANOVAs.

## 3 Results

### 3.1 Parameter optimization

Tables 2 and 3 show the results of the optimization procedure for both the individual and global optimization,

**Table 2** Results of parameter optimization for AR-based methods UAR, VAR, and BAR without the prediction error variance feature

	UAR			VAR			BAR			
	$p_0$	$p$	log(UC)	$p_0$	$p$	log(UC)	$p_0$	$p$	$q$	log(UC)
A01	0.582	13	-2.8	0.612	4	-2.6	0.601	8	2, 2	-0.8
A02	0.446	6	-3.0	0.461	6	-2.8	0.461	14	1, 1	-0.6
A03	0.573	12	-2.6	0.625	2	-2.8	0.578	12	1, 3	-2.6
A04	0.418	10	-2.2	0.395	4	-2.2	0.421	12	2, 2	-2.6
A05	0.406	4	-2.6	0.410	2	-2.4	0.418	5	1, 2	-2.2
A06	0.429	15	-2.2	0.434	12	-2.2	0.457	15	1, 1	-2.6
A07	0.544	14	-2.6	0.533	13	-2.4	0.559	14	1, 3	-2.6
A08	0.635	15	-2.4	0.673	4	-2.4	0.639	5	1, 2	-2.4
A09	0.614	3	-2.2	0.640	3	-2.0	0.623	7	1, 2	-2.2
Global	0.494	13	-2.6	0.507	4	-2.6	0.499	13	1, 1	-2.4

All nine subjects (A01, A02, ...) are shown. Columns show the 0.9 quantile of the classification accuracy  $p_0$ , linear model order  $p$ , bilinear model order  $q$ , and update coefficient logUC. The last row shows the results of the global optimization

**Table 3** Results of parameter optimization for AR-based methods xUAR, xVAR, and xBAR (including the prediction error variance feature)

	xUAR			xVAR			xBAR			
	$p_0$	$p$	log(UC)	$p_0$	$p$	log(UC)	$p_0$	$p$	$q$	log(UC)
A01	0.619	12	-2.6	0.626	4	-2.6	0.619	13	1, 1	-2.6
A02	0.509	8	-2.8	0.506	4	-3.0	0.509	8	1, 1	-2.8
A03	0.654	5	-2.6	0.651	2	-2.8	0.651	5	1, 1	-2.6
A04	0.410	18	-2.0	0.400	3	-2.0	0.425	15	2, 2	-2.2
A05	0.418	2	-2.8	0.410	6	-2.4	0.414	5	1, 2	-2.2
A06	0.436	2	-2.2	0.434	13	-2.2	0.457	15	1, 2	-2.6
A07	0.556	14	-2.6	0.541	13	-2.4	0.563	15	2, 3	-2.0
A08	0.654	16	-2.4	0.677	4	-2.6	0.639	4	1, 1	-2.6
A09	0.629	3	-2.2	0.653	3	-2.0	0.640	7	1, 2	-2.2
Global	0.511	13	-2.6	0.518	4	-2.4	0.513	12	1, 1	-2.4

The notation is the same as in Table 2

respectively. On average, univariate methods (UAR, BAR, xUAR, and xBAR) require a higher model order  $p$  as opposed to vector models (VAR and xVAR). The optimized values of the update coefficient UC are similar for all methods, except in the case of BAR for subjects A01 and A02, where the UC is significantly lower (see Fig. 1). This might be due to our optimization procedure, where we selected the parameter combination with the highest fitness function. However, only a slightly lower classification accuracy is associated with a log(UC) around -2.5, a value found for all other subjects.

Finally, note that we used the achieved classification accuracies only within our optimization procedure. We report it here only for the sake of completeness, and stress that we did not use these accuracies for evaluation of the methods. The evaluation results are described in the next section.

### 3.2 Evaluation

Using the optimal parameter combinations found in the optimization step, we evaluated the methods on the second session. Table 4 shows the results for the ST analysis, whereas Table 5 shows the cross-validated (XV) results. As expected, classification accuracies are generally higher in the cross-validated case than in the ST analysis. In both cases, there is no obvious difference in the means for the individual and global optimization. The following paragraphs describe the outcomes of the statistical analyses.

#### 3.2.1 Overall comparison

A two-way repeated measures ANOVA for the ST case (factors “method” and “optimization”) found a significant main effect of “method” ( $F_{6,48} = 8.104$ , Greenhouse-

## Appendix B. Primary Publications

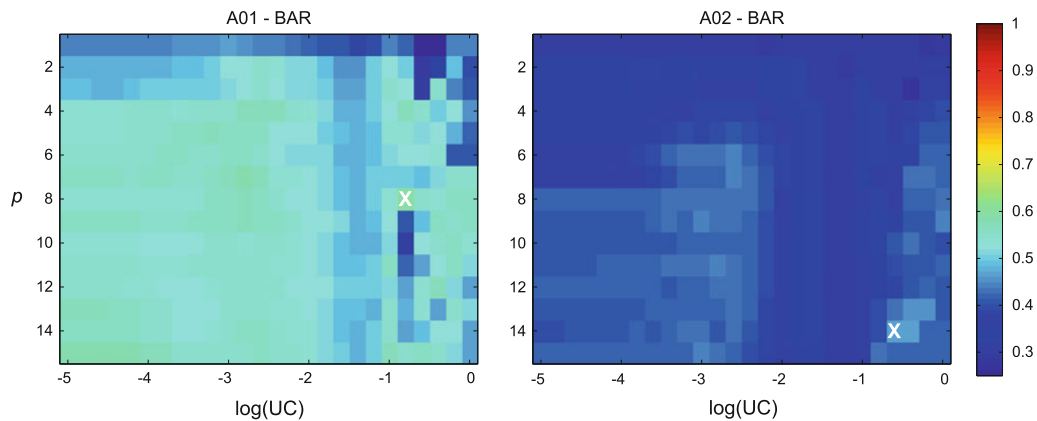


**Fig. 1** Optimization results for subjects A01 (left) and A02 (right) for BAR with the best bilinear model order  $q$ . Maps show the 0.9 quantile of the classification accuracy for all parameter combinations of  $\log(\text{UC})$  ( $x$ -axis) and model order  $p$  ( $y$ -axis). The white cross marks the location of the maximum

**Table 4** ST evaluation results (0.9 quantile of the classification accuracy) for each feature extraction method and optimization strategy on the second session

	Individual							Global						
	UAR	xUAR	VAR	xVAR	BAR	xBAR	LogBP	UAR	xUAR	VAR	xVAR	BAR	xBAR	LogBP
A01	0.471	0.571	0.521	0.550	0.275	0.600	0.650	0.554	0.611	0.521	0.575	0.511	0.593	0.596
A02	0.340	0.376	0.351	0.372	0.294	0.351	0.340	0.312	0.379	0.390	0.411	0.326	0.390	0.351
A03	0.357	0.555	0.452	0.529	0.379	0.548	0.645	0.360	0.467	0.563	0.599	0.419	0.511	0.601
A04	0.273	0.282	0.291	0.379	0.282	0.273	0.410	0.260	0.282	0.317	0.292	0.269	0.300	0.441
A05	0.258	0.298	0.273	0.258	0.273	0.265	0.287	0.291	0.291	0.258	0.276	0.273	0.284	0.305
A06	0.374	0.308	0.350	0.336	0.369	0.369	0.369	0.360	0.355	0.294	0.318	0.369	0.355	0.369
A07	0.239	0.239	0.239	0.326	0.239	0.239	0.395	0.239	0.290	0.239	0.250	0.239	0.264	0.471
A08	0.467	0.407	0.581	0.567	0.563	0.533	0.641	0.481	0.481	0.548	0.585	0.552	0.504	0.641
A09	0.498	0.498	0.487	0.597	0.327	0.498	0.608	0.259	0.304	0.380	0.517	0.270	0.430	0.601
Mean	0.364	0.393	0.394	0.435	0.333	0.408	0.483	0.346	0.384	0.390	0.425	0.359	0.403	0.486
SD	0.10	0.12	0.12	0.13	0.10	0.14	0.15	0.11	0.11	0.13	0.15	0.11	0.11	0.13

The last two rows show the mean and standard deviation (SD)

Geisser-adjusted  $P < 0.01$ ). A Newman–Keuls post-hoc test found that  $\log\text{BP}$  is significantly better than all six AR-based methods (mean classification accuracies of 0.355, 0.389, 0.392, 0.430, 0.346, 0.406, and 0.485 for UAR, xUAR, VAR, xVAR, BAR, xBAR, and  $\log\text{BP}$ , respectively). Furthermore, xVAR is significantly better than both UAR and BAR. The factor “optimization” was not significant ( $F_{1,8} = 0.030$ ,  $P = 0.87$ ).

In the XV case, an ANOVA with the same factors as in the ST analysis also found a significant main effect of “method” ( $F_{6,48} = 3.247$ ,  $P < 0.01$ ). A Newman–Keuls post-hoc test revealed that BAR (mean accuracy of 0.460) is significantly worse than xUAR, VAR, xVAR, and  $\log\text{BP}$  (mean accuracies of 0.507, 0.509, 0.525, and 0.510, respectively). Again, the factor “optimization” was not significant ( $F_{1,8} = 2.901$ ,  $P = 0.13$ ).

We also conducted a repeated measures ANOVAs as described above for the combined evaluation results (that is, we combined ST and XV results and introduced a new factor “ST/XV”). This analysis yielded significant main effects “ST/XV” ( $F_{1,8} = 22.797$ ,  $P < 0.01$ ) and “method” ( $F_{6,48} = 6.700$ ,  $P < 0.01$ ), as well as a significant interaction between “ST/XV” and “method” ( $F_{6,48} = 5.746$ , Greenhouse-Geisser-adjusted  $P < 0.01$ ). Post-hoc tests showed that XV results (mean accuracy 0.499) are significantly higher than ST results (0.400). Furthermore,  $\log\text{BP}$  yielded significantly higher results than UAR, VAR, BAR, and xBAR. BAR was significantly worse than xUAR, VAR, xVAR, and  $\log\text{BP}$ . Finally, xVAR was significantly better than UAR. The mean accuracies for UAR, xUAR, VAR, xVAR, BAR, xBAR, and  $\log\text{BP}$  were 0.420, 0.448, 0.451, 0.477, 0.403, 0.452, and 0.497, respectively.

## Appendix B. Primary Publications

**Table 5** Cross-validated evaluation results (0.9 quantile of the classification accuracy) for each feature extraction method and optimization strategy on the second session

	Individual							Global						
	UAR	xUAR	VAR	xVAR	BAR	xBAR	LogBP	UAR	xUAR	VAR	xVAR	BAR	xBAR	LogBP
A01	0.621	0.664	0.611	0.629	0.318	0.657	0.650	0.639	0.664	0.611	0.646	0.618	0.664	0.614
A02	0.382	0.420	0.427	0.444	0.299	0.392	0.375	0.406	0.410	0.417	0.392	0.385	0.406	0.377
A03	0.502	0.603	0.610	0.658	0.518	0.603	0.680	0.496	0.599	0.627	0.647	0.518	0.610	0.603
A04	0.425	0.463	0.408	0.421	0.379	0.454	0.458	0.430	0.451	0.391	0.405	0.421	0.434	0.524
A05	0.411	0.377	0.406	0.400	0.364	0.363	0.293	0.375	0.367	0.404	0.407	0.393	0.389	0.329
A06	0.332	0.355	0.309	0.356	0.326	0.333	0.424	0.343	0.350	0.358	0.378	0.356	0.343	0.424
A07	0.489	0.504	0.482	0.518	0.496	0.411	0.418	0.486	0.507	0.532	0.543	0.493	0.500	0.489
A08	0.620	0.612	0.642	0.645	0.599	0.609	0.647	0.600	0.598	0.645	0.632	0.602	0.602	0.643
A09	0.599	0.613	0.619	0.646	0.608	0.615	0.615	0.581	0.577	0.672	0.683	0.581	0.570	0.624
Mean	0.487	0.512	0.502	0.524	0.434	0.493	0.507	0.484	0.503	0.517	0.526	0.485	0.502	0.514
SD	0.11	0.11	0.12	0.12	0.12	0.13	0.14	0.10	0.11	0.13	0.13	0.10	0.11	0.12

The last two rows show the mean and standard deviation (SD)

### 3.2.2 Comparison of AR-based methods

We also analyzed the six AR-based methods in more detail and performed three-way repeated measures ANOVAs (factors “method”, “x”, and “optimization”). In the ST case, we found significant main effects of “method” ( $F_{2,16} = 3.939, P < 0.05$ ) and “x” ( $F_{1,8} = 6.324, P < 0.05$ ). Post-hoc tests revealed that vector methods (mean accuracy of 0.411) are significantly better than bilinear methods (mean accuracy of 0.376). Furthermore, methods including the prediction error variance are significantly better (mean accuracy 0.408) than their counterparts without this additional feature (mean accuracy 0.364). In the XV case, we found a significant main effect of “method” ( $F_{2,16} = 6.753, P < 0.01$ ). Post-hoc tests showed that vector models (mean accuracy of 0.517) are significantly better than bilinear models (mean accuracy of 0.479).

Finally, we analyzed the six AR methods for the combined ST and XV results (by introducing the factor “ST/XV”). We found significant main effects of “ST/XV” ( $F_{1,8} = 20.604, P < 0.01$ ), “method” ( $F_{2,16} = 5.597, P < 0.05$ ), and “x” ( $F_{1,8} = 6.778, P < 0.05$ ). Post-hoc tests showed that cross-validated results (mean accuracy 0.497) were significantly higher than ST results (mean accuracy 0.386). Furthermore, vector models (mean accuracy of 0.464) were significantly better than both univariate and bilinear models (mean accuracies of 0.434 and 0.427, respectively). Finally, results were significantly higher for methods using the prediction error variance feature (mean accuracy of 0.459) compared to methods that did not use this feature (mean accuracy of 0.425).

## 4 Discussion

In summary, logBP features yielded the highest classification results in this study. In the ST analysis, where features and classifiers are determined on the first session and then applied to the second (completely unseen) session, logBP was significantly better than all AR-based methods. When assessing this result in more detail, we found out that it might be due to our optimization and evaluation procedure, which resembles a practical BCI setup. In such a setup, users control the BCI in different sessions on different days, and only data from previous sessions can be used to tune parameters. However, this only works if the features are stable over sessions, that is, the bias of the classifiers does not change significantly. In fact, it turned out that all AR methods led to a much higher bias in the second session compared to logBP features, where the bias was about as small as in the first session. A statistical analysis comparing all feature extraction methods after adapting the bias in the second session resulted in no significant differences in the ST analysis. Therefore, adapting the bias of the classifier [15] or using adaptive classifiers [12, 38, 41] to improve ST is necessary for AR features.

Due to the high dimensionality of the feature space in our globally optimized features (see Tables 2, 3), and because similarly high classification accuracies could be obtained for lower model orders in the optimization step, we assessed the performance of univariate models with a lower model order of  $p = 5$  for all subjects. It turned out that classification accuracies improved slightly, but statistical analyses showed that the overall results did not change. That is, all results described above are also valid

for univariate models with lower model orders. Therefore, we can safely rule out overfitting effects that might have explained the inferior performance of (univariate) AR models, especially in the ST analysis. Other studies such as [20] have also found similarly high or higher model orders (although they did not use AR coefficients directly for classification, but calculated the power spectrum).

Furthermore, we have shown that optimizing parameters for individual subjects does not result in better classification rates. Indeed, there was no significant difference between globally and individually optimized parameters. This implies that using logBP with default bands (8–12 and 16–24 Hz) works as well as with subject-specific bands. Note that we used bipolar channels in this study, which is very common in BCI research [1, 6, 16, 17, 23, 32, 31, 40]. Had we used subject-specific spatial filters such as CSP, subject-specific bands might have yielded better results than default bands [4].

The comparison of all analyzed AR methods showed that vector models yielded higher classification results than both univariate and bilinear models. On the one hand, this is not surprising, because vector models consider more information, namely the relationships between individual signals. On the other hand, the potentially more accurate signal description with bilinear models could not be translated into improved classification results. This could be due to two reasons: first, the EEG might not contain signal characteristics that cannot be described by linear models; or second, although bilinear signal properties might improve the model fit, they do not contribute discriminative information for BCIs.

Clearly, all AR methods benefited from the inclusion of the prediction error variance as an additional feature. This feature makes initialization of parameters even more important, because the prediction error variance is updated directly with the update coefficient UC. Without initialization to suitable values, it would take a long time until this feature was in its operating range. This underscores the importance of estimating good initial values, for example with a first run over the optimization data set as implemented in our study.

In conclusion, logBP is superior to AR-based methods, at least with the procedure and implementation used in this study. However, as described above, the performance of AR features can be improved when adapting the bias of the classifiers in new sessions [21, 41]. We also found that low model orders generalized better, and the high model orders determined in our optimization step on the first session resulted in significantly lower classification accuracies on the unseen second session. Moreover, for the settings used in this study (which is very common in BCI experiments), it is not necessary to optimize features for each user individually globally optimized parameters for all users yield equally high classification rates. In particular, we recommend using

low model orders (such as a model order of 5) for univariate models to ensure generalization of the features. Finally, vector models should be preferred over univariate models, and the prediction error variance improved classification performance of all AR models. Future study should apply these findings to online BCIs, where users receive feedback based on their brain patterns, for example to control a prosthesis [13]. Although we are confident that our results will generalize to online sessions with feedback, we are currently working on an online study to verify our findings. Another follow-up study could explore the combination of AR and logBP features to assess whether they contain complimentary information on the data.

**Acknowledgments** This study was supported by the Austrian Science Fund FWF, P20848-N15 (Coupling Measures in BCIs), PAS-CAL-2 ICT-216886, and MU 987/3-2. This publication only reflects the authors' views. Funding agencies are not liable for any use that may be made of the information contained herein. We would also like to thank Alois Schlögl for helpful discussions and Vera Kaiser for support with statistical questions.

**Open Access** This article is distributed under the terms of the Creative Commons Attribution Noncommercial License which permits any noncommercial use, distribution, and reproduction in any medium, provided the original author(s) and source are credited.

## References

- Allison BZ, Brunner C, Kaiser V, Müller-Putz GR, Neuper C, Pfurtscheller G (2010) Toward a hybrid brain–computer interface based on imagined movement and visual attention. *J Neural Eng* 7:026007. doi:10.1088/1741-2560/7/2/026007
- Anderson CW, Stolz EA, Shamsunder S (1998) Multivariate autoregressive models for classification of spontaneous electroencephalographic signals during mental tasks. *IEEE Trans Biomed Eng* 45:277–286. doi:10.1109/10.661153
- Billinger M, Kaiser V, Neuper C, Brunner C (2011) Automatic frequency band selection for BCIs with ERDS difference maps. In: Proceedings of the fifth international brain–computer interface conference. Graz
- Blankertz B, Tomioka R, Lemm S, Kawanabe M, Müller KR (2008) Optimizing spatial filters for robust EEG single-trial analysis. *IEEE Signal Process Mag* 25:41–56. doi:10.1109/MSP.2008.4408441
- Brunner C, Scherer R, Gaimann B, Supp G, Pfurtscheller G (2006) Online control of a brain–computer interface using phase synchronization. *IEEE Trans Biomed Eng* 53:2501–2506. doi:10.1109/TBME.2006.881775
- Brunner C, Allison BZ, Krusienski DJ, Kaiser V, Müller-Putz GR, Pfurtscheller G, Neuper C (2010) Improved signal processing approaches in an offline simulation of a hybrid brain–computer interface. *J Neurosci Methods* 188:165–173. doi:10.1016/j.jneumeth.2010.02.002
- Cabrera AF, Farina D, Dremstrup K (2010) Comparison of feature selection and classification methods for a brain–computer interface driven by non-motor imagery. *Med Biol Eng Comput* 48:123–132
- Dias NS, Kamrunnahr M, Mendes PM, Schiff SJ, Correia JH (2010) Feature selection on movement imagery discrimination and attention detection. *Med Biol Eng Comput* 48:331–341

9. Garrett D, Peterson DA, Anderson CW, Thaut MH (2003) Comparison of linear, nonlinear, and feature selection methods for EEG signal classification. *IEEE Trans Neural Syst Rehabil Eng* 11:141–144
10. Gastaut H, Dongier M, Courtois G (1954) On the significance of “wicket rhythms” (“rythmes en arceau”) in psychosomatic medicine. *Electroencephalogr Clin Neurophysiol* 6:687
11. Graimann B, Huggins JE, Levine SP, Pfurtscheller G (2004) Toward a direct brain interface based on human subdural recordings and wavelet-packet analysis. *IEEE Trans Biomed Eng* 51:954–962. doi:[10.1109/TBME.2004.826671](https://doi.org/10.1109/TBME.2004.826671)
12. Hasan BAS, Gan JQ (2010) Unsupervised movement onset detection from EEG recorded during self-paced real hand movement. *Med Biol Eng Comput* 48:245–253
13. Horki P, Solis-Escalante T, Neuper C, Müller-Putz G (2011) Combined motor imagery and SSVEP based BCI control of a 2 DoF artificial upper limb. *Med Biol Eng Comput* 49:567–577
14. Kalman RE (1960) A new approach to linear filtering and prediction problems. *Trans ASME J Basic Eng* 82:35–45
15. Krauledat M, Tangermann M, Blankertz B, Müller KR (2008) Towards zero training for brain–computer interfacing. *PLoS ONE* 3:e2967. doi:[10.1371/journal.pone.0002967](https://doi.org/10.1371/journal.pone.0002967)
16. Leeb R, Lee F, Keinrath C, Scherer R, Bischof H, Pfurtscheller G (2007a) Brain–computer communication: motivation, aim and impact of exploring a virtual apartment. *IEEE Trans Neural Syst Rehabil Eng* 15:473–482. doi:[10.1109/TNSRE.2007.906956](https://doi.org/10.1109/TNSRE.2007.906956)
17. Leeb R, Settgast V, Fellner DW, Pfurtscheller G (2007b) Self-paced exploring of the Austrian National Library through thoughts. *Int J Bioelectromagn* 9:237–244
18. Lotte F, Congedo M, Lécuyer A, Lamarche F, Arnaldi B (2007) A review of classification algorithms for EEG-based brain–computer interfaces. *J Neural Eng* 4:R1–R13. doi:[10.1088/1741-2560/4/2/R01](https://doi.org/10.1088/1741-2560/4/2/R01)
19. Mason SG, Bashashati A, Fatourech M, Navarro KF, Birch GE (2007) A comprehensive survey of brain interface technology designs. *Ann Biomed Eng* 35:137–169. doi:[10.1007/s10439-006-9170-0](https://doi.org/10.1007/s10439-006-9170-0)
20. McFarland DJ, Wolpaw JR (2008) Sensorimotor rhythm-based brain–computer interface (BCI): model order selection for autoregressive spectral analysis. *J Neural Eng* 5:155–162. doi:[10.1088/1741-2560/5/2/006](https://doi.org/10.1088/1741-2560/5/2/006)
21. McFarland DJ, Krusienski DJ, Sarnacki WA, Wolpaw JR (2008) Emulation of computer mouse control with a noninvasive brain–computer interface. *J Neural Eng* 5:101–110. doi:[10.1088/1741-2560/5/2/001](https://doi.org/10.1088/1741-2560/5/2/001)
22. Müller-Gerking J, Pfurtscheller G, Flyvbjerg H (2000) Classification of movement-related EEG in a memorized delay task experiment. *Clin Neurophysiol* 111:1353–1365
23. Müller-Putz GR, Scherer R, Pfurtscheller G, Rupp R (2005) EEG-based neuroprosthesis control: a step towards clinical practice. *Neurosci Lett* 382:169–174
24. Pei XM, Zheng CX (2004) Feature extraction and classification of brain motor imagery task based on MVAR model. In: *Proceedings of the third international conference on machine learning and cybernetics* doi:[10.1109/ICMLC.2004.1380465](https://doi.org/10.1109/ICMLC.2004.1380465)
25. Pfurtscheller G, Kalcher J, Neuper C, Flotzinger D, Pregenzer M (1996) On-line EEG classification during externally-paced hand movements using a neural network-based classifier. *Electroencephalogr Clin Neurophysiol* 99:416–425. doi:[10.1016/S0013-4694\(96\)95689-8](https://doi.org/10.1016/S0013-4694(96)95689-8)
26. Pfurtscheller G, Neuper C, Flotzinger D, Pregenzer M (1997) EEG-based discrimination between imagination of right and left hand movement. *Electroencephalogr Clin Neurophysiol* 103:642–651. doi:[10.1016/S0013-4694\(97\)00080-1](https://doi.org/10.1016/S0013-4694(97)00080-1)
27. Pfurtscheller G, Allison BZ, Brunner C, Bauernfeind G, Solis-Escalante T, Scherer R, Zander TO, Müller-Putz G, Neuper C, Birbaumer N (2010a) The hybrid BCI. *Front Neurosci* 4:30. doi:[10.3389/fnpro.2010.00003](https://doi.org/10.3389/fnpro.2010.00003)
28. Pfurtscheller G, Brunner C, Leeb R, Scherer R, Müller-Putz GR, Neuper C (2010b) The Graz brain–computer interface. In: Graimann B, Allison BZ, Pfurtscheller G (eds) *Brain–computer interfaces: revolutionizing human–computer interaction*. Springer, Berlin, pp 79–96
29. Priestley MB (1988) *Non-linear and non-stationary time series analysis*. Academic Press, London
30. Sajda P, Gerson A, Müller KR, Blankertz B, Parra L (2003) A data analysis competition to evaluate machine learning algorithms for use in brain–computer interfaces. *IEEE Trans Neural Syst Rehabil Eng* 11:184–185. doi:[10.1109/TNSRE.2003.814453](https://doi.org/10.1109/TNSRE.2003.814453)
31. Scherer R, Müller GR, Neuper C, Graimann B, Pfurtscheller G (2004) An asynchronously controlled EEG-based virtual keyboard: improvement of the spelling rate. *IEEE Trans Neural Syst Rehabil Eng* 51:979–984
32. Scherer R, Lee F, Schlögl A, Leeb R, Bischof H, Pfurtscheller G (2008) Toward self-paced brain–computer communication: navigation through virtual worlds. *IEEE Trans Biomed Eng* 55:675–682. doi:[10.1109/TBME.2007.903709](https://doi.org/10.1109/TBME.2007.903709)
33. Schlögl A, Brunner C (2008) BioSig: a free and open source software library for BCI research. *IEEE Comput Mag* 41:44–50. doi:[10.1109/MC.2008.407](https://doi.org/10.1109/MC.2008.407)
34. Schlögl A, Supp G (2006) Analyzing event-related EEG data with multivariate autoregressive parameters. In: Neuper C, Klimesch W (eds) *Event-related dynamics of brain oscillations*. Elsevier, Amsterdam, pp 135–147
35. Schlögl A, Flotzinger D, Pfurtscheller G (1997) Adaptive autoregressive modeling used for single-trial EEG classification. *Biomed Tech* 42:162–167
36. Schlögl A, Vidaurre C, Müller KR (2010) Adaptive methods in BCI research—an introductory tutorial. In: Graimann B, Allison BZ, Pfurtscheller G (eds) *Brain–computer interfaces: revolutionizing human–computer interaction*. Springer, Berlin, pp 331–355
37. Townsend G, Graimann B, Pfurtscheller G (2004) Continuous EEG classification during motor imagery—simulation of an asynchronous BCI. *IEEE Trans Neural Syst Rehabil Eng* 12:258–265. doi:[10.1109/TNSRE.2004.827220](https://doi.org/10.1109/TNSRE.2004.827220)
38. Tsui CSL, Gan JQ, Roberts SJ (2009) A self-paced brain–computer interface for controlling a robot simulator: an online event labelling paradigm and an extended Kalman filter based algorithm for online training. *Med Biol Eng Comput* 47:257–265
39. Vidaurre C, Schlögl A, Cabeza R, Scherer R, Pfurtscheller G (2005) Adaptive on-line classification for EEG-based brain computer interfaces with AAR parameters and band power estimates. *Biomed Tech* 50:350–354. doi:[10.1515/BMT.2005.049](https://doi.org/10.1515/BMT.2005.049)
40. Vidaurre C, Scherer R, Cabeza R, Schlögl A, Pfurtscheller G (2007a) Study of discriminant analysis applied to motor imagery bipolar data. *Med Biol Eng Comput* 45:61–68. doi:[10.1007/s11517-006-0122-5](https://doi.org/10.1007/s11517-006-0122-5)
41. Vidaurre C, Schlögl A, Cabeza R, Scherer R, Pfurtscheller G (2007b) Study of on-line adaptive discriminant analysis for EEG-based brain computer interfaces. *IEEE Trans Biomed Eng* 54:550–556. doi:[10.1109/TBME.2006.888836](https://doi.org/10.1109/TBME.2006.888836)
42. Vidaurre C, Krämer N, Blankertz B, Schlögl A (2009) Time domain parameters as a feature for EEG-based brain computer interfaces. *Neural Netw* 22:1313–1319. doi:[10.1016/j.neunet.2009.07.020](https://doi.org/10.1016/j.neunet.2009.07.020)
43. Wolpaw JR, Birbaumer N, McFarland DJ, Pfurtscheller G, Vaughan TM (2002) Brain–computer interfaces for communication and control. *Clin Neurophysiol* 113:767–791. doi:[10.1016/S1388-2457\(02\)00057-3](https://doi.org/10.1016/S1388-2457(02)00057-3)

# Single-trial connectivity estimation for classification of motor imagery data

Martin Billinger, Clemens Brunner and Gernot R Müller-Putz

Institute for Knowledge Discovery, Graz University of Technology, Graz, Austria

E-mail: [clemens.brunner@tugraz.at](mailto:clemens.brunner@tugraz.at)

Received 26 March 2013

Accepted for publication 24 May 2013

Published 11 June 2013

Online at [stacks.iop.org/JNE/10/046006](http://stacks.iop.org/JNE/10/046006)

## Abstract

*Objective.* Many brain–computer interfaces (BCIs) use band power (BP) changes in the electroencephalogram to distinguish between different motor imagery (MI) patterns. Most current approaches do not take connectivity of separated brain areas into account. Our objective is to introduce single-trial connectivity features and apply these features to BCI data.

*Approach.* We introduce a procedure for extracting single-trial connectivity estimates from vector autoregressive (VAR) models of independent components in a BCI setting.

*Main results.* In a simulated BCI, we demonstrate that the directed transfer function (DTF) with full-frequency normalization and the direct DTF give classification results similar to BP, while other measures such as the partial directed coherence perform significantly worse.

*Significance.* We show that single-trial MI classification is possible with connectivity measures extracted from VAR models, and that a BCI could potentially utilize such measures.

(Some figures may appear in colour only in the online journal)

## 1. Introduction

A brain–computer interface (BCI) is a communication device that classifies brain activity and controls a device such as a spelling application, a neuroprosthesis, or a wheelchair [1]. Most non-invasive BCIs rely on the electroencephalogram (EEG) to record brain signals. A typical signal processing pipeline for such a BCI comprises preprocessing, feature extraction, and classification stages. In the preprocessing stage, signals are typically filtered in the spatial and/or spectral domain. Spatial filters usually create a linear mixture of existing signal channels; popular techniques include bipolar derivations, Laplace filters, and common spatial patterns (CSP) [2]. Next, the preprocessed data is further processed in the feature extraction stage. To date, most non-invasive BCIs have used features derived from individual channels. Commonly used feature types include band power (BP), autoregressive (AR) model coefficients, and wavelets [3]. Using suitable classification algorithms in the next stage, these features allow BCIs to discriminate between different brain states or mental

tasks. However, these features do not contain information about causal relationships between channels. It is reasonable to assume that such information could provide useful features for BCIs.

The interaction of spatially separated brain areas can be observed through functional or effective connectivity [4, 5]. Functional connectivity reflects statistically related activation of brain areas, while effective connectivity explains the causality of these observed dependencies [5]. Numerous connectivity measures have been developed and applied in neuroscientific studies, including coherence (COH), partial directed coherence (PDC) [6], directed transfer function (DTF) [7], and many others [8, 9]. Some of these measures have also been used in BCI studies [10–18]. Most of these measures are related to vector autoregressive (VAR) models and can be extracted from the model coefficients.

Volume conduction or instantaneous connectivity causes spurious connectivity between raw EEG channels [19]. Different solutions to this problem have been proposed. These solutions can be divided into three groups: (1) connectivity measures designed to suppress instantaneous effects [20–22], (2) inclusion of an instantaneous term in VAR models [23–25], and (3) modeling the EEG as a mixture of sources [26, 27].



Content from this work may be used under the terms of the [Creative Commons Attribution 3.0 licence](https://creativecommons.org/licenses/by/3.0/). Any further distribution of this work must maintain attribution to the author(s) and the title of the work, journal citation and DOI.

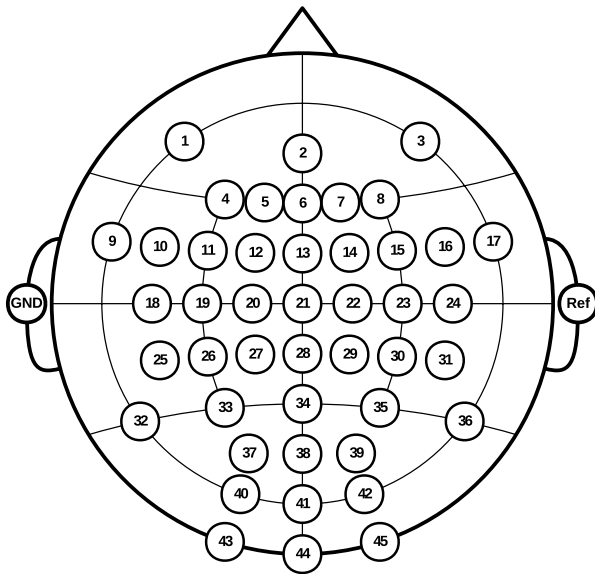


**Figure 1.** Layout of the EEG electrode montage. Left mastoid: ground. Right mastoid: reference. EEG locations in order: AF7, AFz, AF8, F3, F1, Fz, F2, F4, FT7, FC5, FC3, FC1, FCz, FC2, FC4, FC6, FT8, C5, C3, C1, Cz, C2, C4, C6, CP5, CP3, CP1, Pz, CP2, CP4, CP6, P7, P3, Pz, P4, P8, PO3, POz, PO4, O1, Oz, O2, I1, Iz, I2.

We decided to tackle the problem of instantaneous connectivity by applying a VAR model to EEG sources. In contrast to measures specifically designed to suppress volume conduction, our procedures can be easily extended to include new connectivity measures, provided that these new measures can be extracted from VAR models.

Adding an additional instantaneous term in the VAR model definition, as suggested in [23], imposes certain restrictions on the structure of this term. Specifically, the instantaneous term cannot contain any cycles [25]. This implies that instantaneous interaction in any pair of signals can originate from only one of these signals. In other words, if the signal spreads from electrode A to B, it cannot spread from B to A.

In contrast, modeling the EEG as a mixture of sources does not impose such restrictions. Instead, sources are assumed to be independent and non-Gaussian, which is a reasonable assumption for EEG sources [28]. This assumption makes blind source identification possible with independent component analysis (ICA). Since these sources are independent, they exhibit minimal instantaneous interaction. Therefore, they can be modeled with simple VAR models.

For our purposes, modeling the EEG as a mixture of sources results in a better model than adding an instantaneous term, because EEG is commonly assumed to be the result of mostly cortical sources that appear smeared over the scalp due to volume conduction [28]. Thus, we use the connectivity estimation approach recommended and implemented in EEGLAB with the SIFT toolbox [27]: fitting of VAR models to component signals obtained by extended Infomax ICA [29].

For use in BCIs, connectivity measures need to be extracted online from the on-going EEG. However, in practice, many connectivity measures are extracted from VAR models, which are fitted to data that contains multiple realizations of the EEG time series (multiple trials) [30]. Single-trial estimation is inherently more difficult, because only a fraction of the data is available for model fitting.

In this paper, we propose a procedure for obtaining single-trial estimates of connectivity measures between ICA sources for motor imagery (MI) classification. We solve the problem of single-trial estimation by automatically selecting a subset of signals for analysis to reduce the amount of data. This procedure enables us to evaluate different measures in a BCI simulation. The measures we test include univariate measures as well as functional and effective connectivity measures for classification of BCI tasks. Although we use pre-recorded data in our analysis, our work flow easily generalizes to online applications.

## 2. Methods

### 2.1. Data acquisition

We recorded 45 EEG and three electrooculogram (EOG) channels with sintered Ag/AgCl ring electrodes. The locations of the EEG channels corresponded to the extended international 10–20 system (see figure 1 for montage details). We recorded all signals at a sampling rate of 300 Hz with three synchronized g.USBamp amplifiers (g.tec, Guger Technologies OEG, Graz, Austria). The amplifiers filtered the raw data with a 0.5–100 Hz bandpass and a 50 Hz notch filter. EOG components in the EEG were reduced with a regression-based approach [31]. For this study, the signals were further resampled to 100 Hz.

Fourteen healthy volunteers (five male, age  $29.6 \pm 4.2$  and nine female, age  $24.8 \pm 2.3$ ) without prior experience in BCI control participated in our BCI experiment. All participants except one female were right-handed. Each participant took part in two sessions on separate days, with six screening and three feedback runs on each day. At the beginning of each session, participants performed an artifact run to estimate the influence of EOG artifacts on the EEG. The screening runs were based on the synchronous Graz BCI training paradigm [32], which we modified to visually resemble the feedback runs in this study. We only use data from the artifact and screening runs in this study. During feedback runs, we instructed the participants to steer a virtual plane along a path using hand and foot MI. After four screening runs, one feedback run, two further screening runs, and two final feedback runs followed.

Each session comprised 90 right hand MI and 90 foot MI trials. Figure 2 illustrates the timing of a trial. A trial lasted 7 s, followed by a break of  $3 \pm 0.5$  s. An acoustic beep and the appearance of a fixation symbol indicated the start of a trial. 2.5 s after the start of the trial, an arrow appeared, pointing either up or down to instruct participants to perform hand or foot MI, respectively.

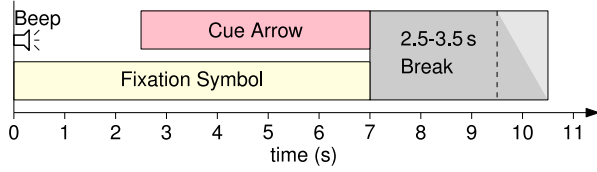


**Figure 2.** Timing of the experimental paradigm. Trial duration is 7 s with a break of 3 s (on average) between trials. Trial start is indicated with an acoustic beep and the appearance of the fixation symbol. After 2.5 s, participants are cued as to which MI task to perform.

### 2.2. Autoregressive models for connectivity estimation.

We can derive various connectivity measures from VAR models, which are a multivariate generalization of univariate AR models. VAR models consist of univariate and multivariate terms. Univariate terms model individual channels, whereas multivariate terms describe how channels depend on past values of other channels. As such, VAR models are related to the concept of Granger causality. Their structure mirrors effective connectivity in the time domain, as shown in (1), where the  $[M \times 1]$  vectors  $\mathbf{y}[n]$  and  $\mathbf{x}[n]$  are the  $M$ -channel EEG sample and residual at time instant  $n$ , and  $\boldsymbol{\beta}^{(k)}$  is the  $[M \times M]$  AR coefficient matrix at time lag  $k$ . By transforming the model equations into the frequency domain, we obtain (2), a spectral representation of the model. The  $[M \times 1]$  vectors  $\mathbf{y}(z)$  and  $\mathbf{x}(z)$  correspond to EEG and residuals in the  $z$ -domain. We define the  $[M \times M]$  matrix function  $\mathbf{A}(z)$  in (3), which is the inverse of the multivariate transfer function  $\mathbf{H}(z)$ , as shown in (4):

$$\mathbf{y}[n] = \sum_{k=1}^p \boldsymbol{\beta}^{(k)} \mathbf{y}[n-k] + \mathbf{x}[n] \quad (1)$$

$$\mathbf{x}(z) = \left( \mathbf{I} - \sum_{k=1}^p \boldsymbol{\beta}^{(k)} z^{-k} \right) \mathbf{y}(z) \quad (2)$$

$$\mathbf{A}(z) = \mathbf{I} - \sum_{k=1}^p \boldsymbol{\beta}^{(k)} z^{-k} \quad (3)$$

$$\mathbf{y}(z) = \mathbf{A}(z)^{-1} \mathbf{x}(z) = \mathbf{H}(z) \mathbf{x}(z). \quad (4)$$

### 2.3. Instantaneous connectivity

Applying VAR models directly to raw EEG data is problematic. Volume conduction causes EEG channels to be highly correlated. This is expressed as instantaneous connectivity between EEG channels, which is not included in the VAR model. Instead, the residuals  $\mathbf{x}$  are no longer independent; they have non-zero covariances. Some connectivity measures such as the PDC or DTF do not include the residual covariance matrix in their definition. Thus, they are distorted by instantaneous connectivity.

We propose a solution based on blind source separation, which does not impose directional restrictions as is the case when adding an instantaneous term. It is possible to use ICA as a preprocessing step to transform the EEG from the electrode

space into the source space. ICA minimizes the statistical dependence between signals. We use the extended Infomax ICA algorithm [29] to minimize instantaneous dependencies. Delayed dependencies between signals are preserved and can thus be modeled with VAR models.

In this paper, we refer to data channels obtained from ICA as sources, although they are not necessarily related to cortical sources or dipoles.

### 2.4. Connectivity measures

Using the above equations, we can derive connectivity measures from VAR models (see [8] for more details).

The cross-spectral density (S) is obtained by

$$\mathbf{S}(z) = \mathbf{H}(z) \boldsymbol{\Sigma}_x \mathbf{H}(z)^H. \quad (5)$$

The COH is similar to S, but normalized by the corresponding auto-spectra:

$$\text{COH}_{ij}(z) = \frac{|\mathbf{S}_{ij}(z)|}{\sqrt{\mathbf{S}_{ii}(z) \mathbf{S}_{jj}(z)}}. \quad (6)$$

Variations of COH are imaginary coherence (iCOH) and partial coherence (pCOH):

$$\text{iCOH}_{ij}(z) = \frac{\Im\{\mathbf{S}_{ij}(z)\}}{\sqrt{\mathbf{S}_{ii}(z) \mathbf{S}_{jj}(z)}} \quad (7)$$

$$\text{pCOH}_{ij}(z) = \frac{|\mathbf{G}_{ij}(z)|}{\sqrt{\mathbf{G}_{ii}(z) \mathbf{G}_{jj}(z)}} \quad (8)$$

with

$$\mathbf{G}_{ij}(z) = \mathbf{A}(z)^H \boldsymbol{\Sigma}_x^{-1} \mathbf{A}(z). \quad (9)$$

While the above measures are symmetric, the PDC provides directional connectivity information:

$$\text{PDC}_{ij}(z) = \frac{|\mathbf{A}_{ij}(z)|}{\sqrt{\mathbf{A}_{ij}^H(z) \mathbf{A}_{ij}(z)}}. \quad (10)$$

The partial directed coherence factor (PDCF) incorporates the residual error covariance in the normalization:

$$\text{PDCF}_{ij}(z) = \frac{|\mathbf{A}_{ij}(z)|}{\sqrt{\mathbf{A}_{ij}^H(z) \boldsymbol{\Sigma}_x^{-1} \mathbf{A}_{ij}(z)}}. \quad (11)$$

The generalized partial directed coherence (GPDC) is a generalization of the PDC that does not depend on signal scale:

$$\text{GPDC}_{ij}(z) = \frac{|\mathbf{A}_{ij}(z)|}{\sigma_i \sqrt{\mathbf{A}_{ij}^H(z) \text{diag}(\boldsymbol{\Sigma}_x)^{-1} \mathbf{A}_{ij}(z)}}. \quad (12)$$

Another measure that provides directed connectivity information is the DTF:

$$\text{DTF}_{ij}(z) = \frac{|\mathbf{H}_{ij}(z)|}{\sqrt{\mathbf{H}_{i:}(z) \mathbf{H}_{i:}^H(z)}}. \quad (13)$$

The full-frequency DTF (ffDTF) is similar to the DTF, except that normalization is performed over the full frequency range:

$$\text{ffDTF}_{ij}(z) = \frac{|\mathbf{H}_{ij}(z)|}{\sqrt{\sum_z \mathbf{H}_{i:}(z) \mathbf{H}_{i:}^H(z)}}. \quad (14)$$

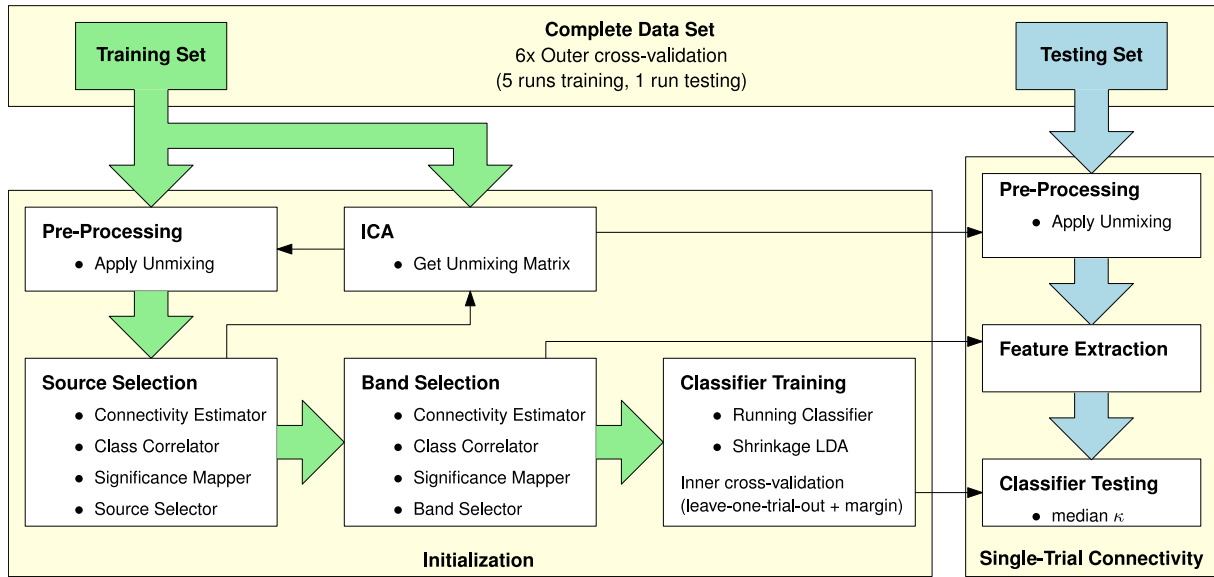


**Figure 3.** The proposed procedure resembles the workflow of a typical BCI: parameters are optimized on available data and applied to unseen data. This workflow is embedded in a cross-validation procedure, where parts of the pre-recorded data serve as the novel testing set. Broad arrows depict data flow and narrow arrows correspond to system parameters.

While the ffDTF reveals direct and indirect connections, the direct DTF (dDTF) only shows direct connections:

$$\mathbf{dDTF}_{ij}(z) = \mathbf{pCOH}_{ij}(z) \cdot \mathbf{ffDTF}_{ij}(z). \quad (15)$$

The directed coherence (DCOH) can be understood as a generalization of the DTF, just like GPDC is a generalization of the PDC:

$$\mathbf{DCOH}_{ij}(z) = \frac{\sigma_j |\mathbf{H}_{ij}(z)|}{\sqrt{\mathbf{H}_i(z) \mathbf{diag}(\Sigma_x) \mathbf{H}_i^H(z)}}. \quad (16)$$

### 2.5. BCI simulation

Application of connectivity measures in BCIs based on MI requires estimation of these measures from a single realization of the time series. More channels and higher frequency resolution (model order) require longer estimation windows. However, we cannot increase the estimation window length indefinitely, because the time series are required to be stationary throughout the window. In addition, long estimation windows lead to a slow BCI response.

We propose a procedure that solves the problem of single-trial connectivity estimation in two steps. First, we compute connectivity estimates with low time and frequency resolution from all 45 available sources with estimation windows of length 4.5 s. Sources are ranked based on these estimates, and eight sources are selected for further use (a detailed description of source ranking and selection follows below). Second, the final connectivity estimates are obtained from the subset of eight sources with windows of length 1.5 s. In both steps, optimal model orders are determined by Akaike's final prediction error (FPE) [33].

In a typical BCI experiment, the first step (initialization) is performed on training data recorded without feedback.

Then, single-trial connectivity estimation and classification can be performed on the ongoing EEG. We simulate this strategy on pre-recorded data with an outer cross-validation loop. Classifier training requires a further nested cross-validation loop to optimize the time of training. Figure 3 shows schematically the functional blocks of our procedure. In the following sections, we will describe each block in detail.

**2.5.1. Outer cross-validation.** We employ a cross-validation scheme for validating the BCI system. From six available runs in a recording session, one is used for testing and the five remaining runs for training. This is repeated until every run was in the testing set once. Thus, trials from the same run can never occur in both the training and the testing set, and every trial is used for testing exactly once (see also [34]). The training sets are used for initialization of our procedure, and results are obtained from the respective testing sets.

**2.5.2. Initialization.** First, the unmixing matrix for extracting source signals from the EEG is estimated. This is accomplished by applying Infomax ICA [29] to the training data set. The unmixing matrix serves as a spatial filter that extracts the source signals from the EEG.

Next, the connectivity estimator fits VAR models to a sliding window of length 4.5 s over all 45 source signals, and subsequently extracts connectivity measures. The window is moved in steps of 0.3 s from  $t = 0$  (cue) to  $t = 6$  (end of trial), creating 21 time segments. This results in a four-dimensional data set  $c_k(i, j, f, t)$  for each trial  $k$ , which describes a measure of connectivity from channel  $j$  to channel  $i$  at frequency  $f$  and time  $t$  relative to the cue. BP is estimated from the source autospectra obtained by fast Fourier transform. Although BP is not a connectivity measure, it can be treated as  $c_k(i, j, f, t) = 0$

## Appendix B. Primary Publications

for  $i \neq j$ . We extract connectivity measures in the frequency range from 0–50 Hz in steps of 0.5 Hz. Once all connectivity measures are extracted, the following steps are performed for each measure separately.

The class correlator estimates the correlation coefficient  $r(i, j, f, t)$  of  $c_k$  with corresponding class labels  $l_k$ . A class label is a numeric value that indicates if a trial contains hand MI ( $l_k = 1$ ) or foot MI ( $l_k = -1$ ). Thus,  $r$  indicates how strongly a connectivity measure can distinguish between both types of MI in channel pair  $(i, j)$  at time  $t$  and frequency  $f$ . A high positive correlation means the measure’s magnitude is higher during hand MI and lower during foot MI. Likewise, negative correlation relates to foot MI.

With the information obtained so far, the eight most important sources are selected. Sources that form a network with connections that differentiate strongly between classes are considered the most important. Thus, sources are ranked by the amount of correlation found in their in- and out-going connections, according to the ranking criterion  $e$  defined in (17).

$$e_m = \sum_f \sum_t \left( \sum_i r^2(i, m, f, t) + \sum_j r^2(m, j, f, t) \right). \quad (17)$$

Once a subset of sources is selected, the unmixing matrix is pruned to only yield the selected sources. Connectivity estimates are obtained for these sources in a sliding window of length 1.5 s and the class-correlation  $r(i, j, f, t)$  is obtained for the estimates.

$p(i, j, f, t)$ -values are obtained from the asymptotic normal distribution of  $r$ , for testing against the null-hypothesis of no correlation. To determine which correlations are statistically significant, the significance mapper attempts to control the false discovery rate (FDR) [35] so that the probability of falsely detected correlations does not exceed 0.01. To reduce noise in the significance maps, we modified the FDR method so that correlations are only considered significant if they form a cluster of minimum size in the  $t/f$ -plane. Minimum cluster size was set to an area of 2 s Hz.

Features for classification are extracted from frequency bands where the connectivity exhibits significant class-correlation. The band selector identifies a list of frequency bands and connections  $(i, j)$  where  $r$  is significant for a duration of at least 2 s. For functional connectivity measures, where  $c_k$  is symmetric, only one of the equivalent connections  $(j, i)$  and  $(i, j)$  is used. If no bands are found, the system resorts to a broad default band from 8 to 28 Hz for each connection.

A shrinkage linear discriminant analysis classifier [36] is trained on the features as follows. We use a nested cross-validation loop to estimate the classification performance for each time segment. In a leave-one-out procedure, each trial of the original training set is used for validation exactly once. A margin of ten trials before and after the validation trial is excluded from classifier training. This is repeated for each time segment. The final classifier is then trained on the best performing segment using all trials from the original training set.

**Table 1.** ANOVA results for classification performance. The factors *Selection*, *Features* and *Session* are abbreviated as  $f_1$ ,  $f_2$ , and  $f_3$ , respectively.  $F$  is the value of the  $f$ -statistic, with degrees of freedom DF<sub>n</sub> and DF<sub>d</sub>.

Effect	DF <sub>n</sub>	DF <sub>d</sub>	$F$	$p$	Sig
$f_1$	11	143	2.321	0.012	*
$f_2$	11	143	28.588	0.000	**
$f_3$	1	13	5.640	0.034	*
$f_1:f_2$	121	1573	1.418	0.003	**
$f_1:f_3$	11	143	0.632	0.799	
$f_2:f_3$	11	143	0.678	0.758	
$f_1:f_2:f_3$	121	1573	0.731	0.986	

**2.5.3. Single-trial connectivity classification.** Single-trial analysis is performed on the testing set. The testing set was not used during initialization, thus this analysis is performed on completely unseen data. First, the pruned unmixing matrix obtained during initialization is used to extract selected sources from the testing set EEG. Connectivity measures are obtained from a sliding window of length 1.5 s, and selected frequency bands are extracted as features. Subsequently, the features are classified by the classifier trained during initialization.

We measure classification performance with Cohen’s kappa  $\kappa$ . To obtain a simple and robust measure of performance, we estimate  $\kappa(t)$  for each time segment between 1 s and 4 s after the cue, and report the median of  $\kappa(t)$  from these segments as classification performance.

### 2.6. Data analysis

Each connectivity measure was independently applied to source channel selection and classification. We analyzed classification performance across subjects and factors with repeated measures analysis of variance (ANOVA). The independent variable was  $\kappa$ , and the three factors were  $f_1$  (*Selection*, 11 levels),  $f_2$  (*Features*, 11 levels), and  $f_3$  (*Session*, 2 levels). Significant factors were further analyzed with Holm–Bonferroni corrected paired  $t$ -tests.

## 3. Results

Table 1 shows the results of the ANOVA for classification performance. There are highly significant ( $p < 0.01$ ) effects for  $f_2$  (*Features*) and the interaction between  $f_1$  (*Selection*) and  $f_2$  (*Features*). The factors  $f_1$  (*Selection*) and  $f_3$  (*Session*) were significant ( $p < 0.05$ ).

Post tests were performed for significant effects. Post tests of the interaction between  $f_1$  (*Selection*) and  $f_2$  (*Features*) led to similar results as analyzing the main effects; we could not identify an interpretable pattern. Thus, only the main effects are presented for improved clarity. Post tests found no significant differences in  $f_1$  (*Selection*) (see figure 4). The results of post tests on factor  $f_2$  (*Features*) are shown in figure 5. BP performed best for classification. However, it was not significantly better than S, ffDTF and dDTF. All other measures performed significantly worse. Factor  $f_3$  (*Session*) is shown in figure 6. Classification accuracy in the second session was significantly better than in the first session.

## Appendix B. Primary Publications

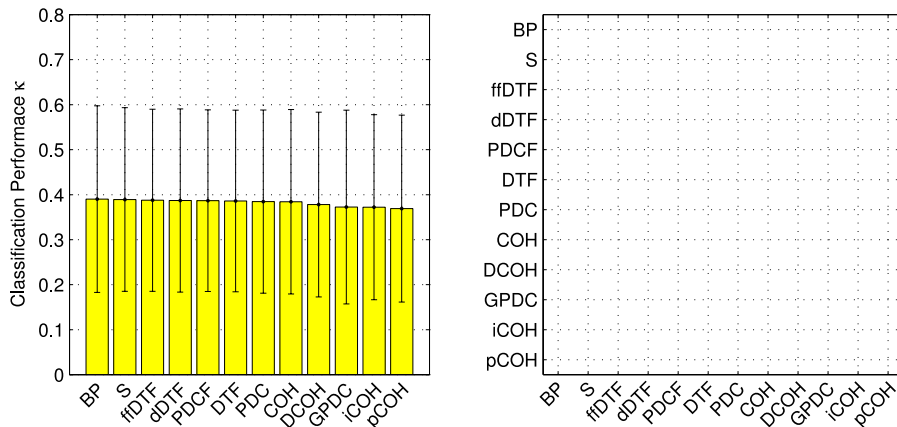


**Figure 4.** Factor  $f_1$  (Selection). Left: classification performance  $\kappa$  (mean and standard deviation) for each measure used for source channel selection. Right: significant (gray) and highly significant (black) differences between measures. *Note.* Since there are no significant differences, the plot is white and does not contain gray or black boxes.

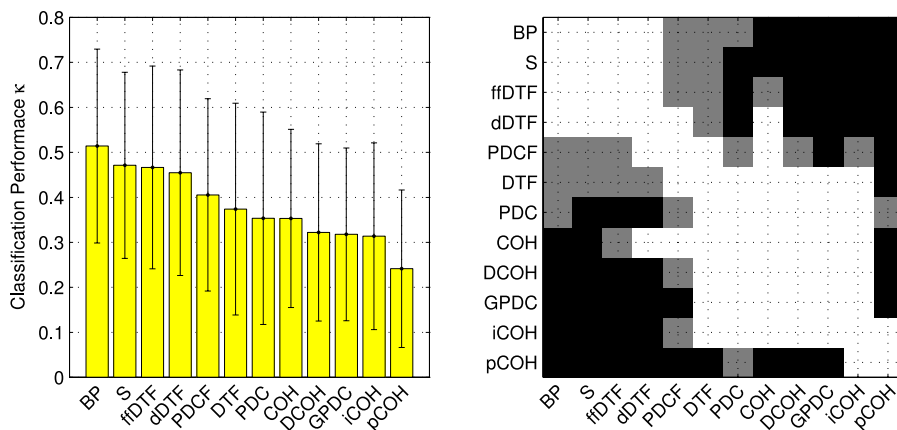


**Figure 5.** Factor  $f_2$  (Features). Left: classification performance  $\kappa$  (mean and standard deviation) for each measure used as feature for classification. Right: significant (gray) and highly significant (black) differences between measures.

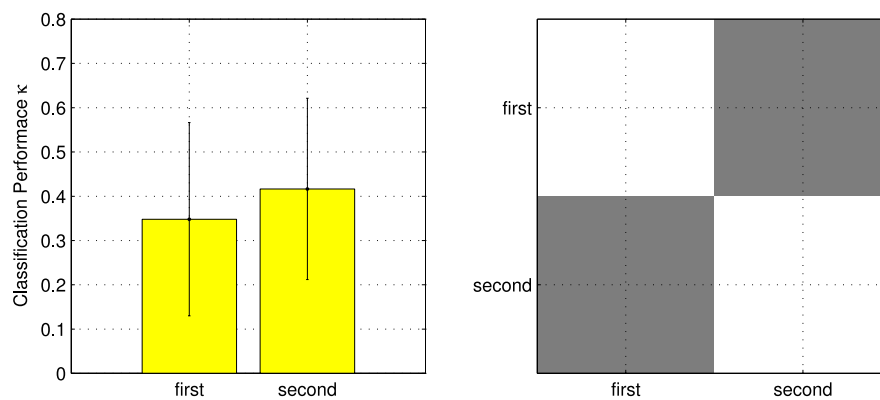


**Figure 6.** Factor  $f_3$  (Session). Left: classification performance (mean and standard deviation) for each session. Right: significant (gray) differences between sessions.

The optimal VAR model order, which depends on the data, was different every time the VAR model was fitted. Table 2 shows the relative amount of selected model orders. For 45

sources, a model order of  $p = 2$  was chosen most frequently. For the reduced set of eight sources, a model order of  $p = 4$  was selected in the majority of cases.

## Appendix B. Primary Publications

**Table 2.** Optimal model orders determined by Akaike’s FPE for VAR models fitted to 45 and 8 sources, respectively.  $p$  is the model order, and fraction is the total percentage of each model order being selected.

45 sources		8 sources	
$p$	Fraction	$p$	Fraction
1	22%	4	86%
2	77%	5	8%
3	1%	6	3%
4	<1%	7	2%
		8	1%

### 4. Discussion

We proposed a procedure for an offline simulation of single-trial connectivity BCIs. This procedure can be easily applied in an online BCI. Currently, we are working toward implementing an online version of that approach. There is no outer cross-validation in an online setting. Instead, the training set is replaced by pre-recorded screening data, and the testing set is replaced by the online data stream as it is recorded.

We selected the optimal time to train the classifier based on estimates of classification performance obtained with the inner cross-validation loop. Ideally, the feature selection would also utilize classification performance as a ranking criterion. However, this would require even more cross-validation runs, thus increasing the initialization time dramatically. With an online BCI application in mind, we chose the computationally much less demanding feature selection based on correlation.

We validated the procedure by obtaining BP classification performance similar to other studies (e.g. [37, 16]). Also, the finding that classification performance improved in the second session is plausible, especially since only naive subjects participated in our measurements.

In a recent study, S, COH, and phase coupling were shown to yield similar results in terms of classification performance [16]. The authors concluded that this was caused by a bias toward zero phase between EEG channels. Indeed, our results support this conclusion. With ICA preprocessing, we effectively reduced zero-phase bias, leading to significantly worse classification with COH features. Thus, it is reasonable to assume that the COH between sources includes less task-relevant information than spectral power measures such as BP. In contrast, COH between EEG channels contains similar information as spectral power measures due to highly correlated EEG channels.

Our results indicate that features derived from univariate BP perform at least as well as any connectivity measure. Clearly, measures such as COH as well as the unmodified DTF are not suitable for a BCI application. However, S, dDTF, and ffDTF perform similarly to BP. For S, this is not surprising, since the cross-spectral density is a generalization of the spectral density, the basis of BP.

The dDTF is similar to the ffDTF, but only characterizes direct connections [38]. The fact that they perform equally well indicates that this difference might not be relevant for discriminating MI tasks.

ICA is ambiguous in terms of component order and scale. VAR models are invariant to permutations of the signals, but signal scale has a direct impact on the relative scaling of the VAR coefficients. This might introduce an error in the magnitude of connectivity measures. However, this error can be mitigated by using scale invariant connectivity measures such as GPDC or DCOH. We use both scale dependent and scale invariant measures, which allows us to determine the practical relevance of scale ambiguity for MI classification.

GPDC and DCOH are similar generalizations of the PDC and the DTF, respectively. This generalization makes the GPDC and the DCOH invariant to the scaling of the signals. However, the generalized measures do not outperform the unmodified measures in terms of classification performance. This indicates that MI classification is unaffected by the scale ambiguity of ICA sources.

Resolution of the proposed measures is limited due to the single-trial estimation constraint. However, a possible solution could be provided by employing regularization or sparse methods for VAR model fitting [39, 40]. By setting unimportant AR coefficients to zero, fewer free parameters need to be estimated. This, in turn, would permit higher model orders, more channels, or shorter estimation windows. Better time resolution would allow the BCI to react faster to the user’s input, and better frequency or spatial resolution might improve classification as more information about the underlying structures and processes is resolved. Furthermore, the implicit coefficient selection of sparse model fitting might remove the need for our procedure’s source selection pass.

### 5. Conclusions

Although there is potential for further improvement, we were able to show that reliable classification of MI tasks is possible with single-trial estimation of the effective connectivity measures ffDTF and dDTF.

The procedure we proposed in this paper can be used to consistently evaluate connectivity measures for BCI use. Thus, it may provide the basis for further research in the direction of connectivity-based BCIs.

To validate our findings in an online BCI system, the described methods can be easily adapted to an online system, since no major changes in the signal processing work flow are required.

### Acknowledgments

This work was supported by the FWF Project ‘Coupling Measures for BCIs’ (P20848-N15).

### References

- [1] Wolpaw J R, Birbaumer N, McFarland D J, Pfurtscheller G and Vaughan T M 2002 Brain–computer interfaces for communication and control *Clin. Neurophysiol.* **113** 767–91
- [2] Ramoser H, Müller-Gerking J and Pfurtscheller G 2000 Optimal spatial filtering of single trial EEG during imagined hand movement *IEEE Trans. Rehabil. Eng.* **8** 441–6

## Appendix B. Primary Publications

- [3] Mason S G, Bashashati A, Fatourechhi M, Navarro K F and Birch G E 2007 A comprehensive survey of brain interface technology designs *Ann. Biomed. Eng.* **35** 137–69
- [4] Friston K J 1994 Functional and effective connectivity in neuroimaging: a synthesis *Hum. Brain Mapp.* **2** 56–78
- [5] Friston K J 2011 Functional and effective connectivity: a review *Brain Connectivity* **1** 13–36
- [6] Baccalá L A and Sameshima K 2001 Partial directed coherence: a new concept in neural structure determination *Biol. Cybern.* **84** 463–74
- [7] Kamiński M J and Blinowska K J 1991 A new method of the description of the information flow in the brain structures *Biol. Cybern.* **65** 203–10
- [8] Schlögl A and Supp G 2006 Analyzing event-related EEG data with multivariate autoregressive parameters *Event-Related Dynamics of Brain Oscillations* ed C Neuper and W Klimesch (Amsterdam: Elsevier) pp 135–47
- [9] Faes L, Erla S and Nollo G 2012 Measuring connectivity in linear multivariate processes: definitions, interpretation, and practical analysis *Comput. Math. Methods Med.* **2012** 1–18
- [10] Gysels E, Renevey P and Celka P 2005 SVM-based recursive feature elimination to compare phase synchronization computed from broadband and narrowband EEG signals in brain–computer interfaces *Signal Process.* **85** 2178–89
- [11] Shoker L, Sanei S and Sumich A 2005 Distinguishing between left and right finger movement from EEG using SVM *Conf. IEEE Eng. Med. Biol. Soc.* **2005** pp 5420–5423
- [12] Brunner C, Scherer R, Graimann B, Supp G and Pfurtscheller G 2006 Online control of a brain–computer interface using phase synchronization *IEEE Trans. Biomed. Eng.* **53** 2501–6
- [13] Wang Y, Wang R, Gao X, Hong B and Gao S 2006 A practical VEP-based brain–computer interface *IEEE Trans. Neural Syst. Rehabil. Eng.* **14** 234–40
- [14] Wei Q, Wang Y, Gao X and Gao S 2007 Amplitude and phase coupling measures for feature extraction in an EEG-based brain–computer interface *J. Neural Eng.* **4** 120–9
- [15] Hamner B, Leeb R, Tavella M and del R Millán J 2011 Phase-based features for motor imagery brain–computer interfaces *Conf. IEEE Eng. Med. Biol. Soc.* **2011** pp 2578–81
- [16] Krusienski D J, McFarland D J and Wolpaw J R 2012 Value of amplitude, phase, and coherence features for a sensorimotor rhythm-based brain–computer interface *Brain Res. Bull.* **87** 130–4
- [17] Lim J H, Hwang H J, Jung Y J and Im C H 2011 Feature extraction for brain–computer interface (BCI) based on the functional causality analysis of brain signals *Proc. 5th Int. Brain–Computer Interface Conf.* pp 36–8
- [18] Daly I, Nasuto S J and Warwick K 2012 Brain–computer interface control via functional connectivity dynamics *Pattern Recognit.* **45** 2123–36
- [19] Haufe S, Nikulin V V, Müller K R and Nolte G 2013 A critical assessment of connectivity measures for EEG data: a simulation study *NeuroImage* **64** 120–33
- [20] Nolte G, Bai O, Wheaton L, Mari Z, Vorbach S and Hallett M 2004 Identifying true brain interaction from EEG data using the imaginary part of coherency *Clin. Neurophysiol.* **115** 2292–307
- [21] Nolte G *et al* 2008 Robustly estimating the flow direction of information in complex physical systems *Phys. Rev. Lett.* **100** 234101
- [22] Omidvarnia A H, Azemi G, Boashash B, Toole J M O, Colditz P and Vanhatalo S 2012 Orthogonalized partial directed coherence for functional connectivity analysis of newborn EEG *Neural Information Processing (Lecture Notes in Computer Science vol 7664)* ed T Huang, Z Zeng, C Li and C Leung (Berlin: Springer) pp 683–91
- [23] Erla S, Faes L, Tranquillini E, Orrico D and Nollo G 2009 Multivariate autoregressive model with instantaneous effects to improve brain connectivity estimation *Int. J. Bioelectromagn.* **11** 74–79
- [24] Faes L and Nollo G 2010 Extended causal modeling to assess Partial Directed Coherence in multiple time series with significant instantaneous interactions *Biol. Cybern.* **103** 387–400
- [25] Hyvärinen A, Zhang K, Shimizu S, Hoyer P O and Dayan P 2010 Estimation of a structural vector autoregression model using non-Gaussianity *J. Mach. Learn. Res.* **11** 1709–31
- [26] Gomez-Herrero G, Atienza M, Egiazarian K and Cantero J L 2008 Measuring directional coupling between EEG sources *NeuroImage* **43** 497–508
- [27] Delorme A *et al* 2011 EEGLAB, SIFT, NFT, BCILAB, and ERICA: new tools for advanced EEG processing *Comput. Intell. Neurosci.* **2011** 1–12
- [28] Makeig S, Bell A J, Jung T P and Sejnowski T J 1996 Independent component analysis of electroencephalographic data *Advances in Neural Information Processing Systems* (Cambridge, MA: MIT Press) pp 145–51
- [29] Bell A J and Sejnowski T J 1995 An information-maximization approach to blind separation and blind deconvolution *Neural Comput.* **7** 1129–59
- [30] Ding M, Bressler S L, Yang W and Liang H 2000 Short-window spectral analysis of cortical event-related potentials by adaptive multivariate autoregressive modeling: data preprocessing, model validation, and variability assessment *Biol. Cybern.* **83** 35–45
- [31] Schlögl A, Keinrath C, Zimmermann D, Scherer R, Leeb R and Pfurtscheller G 2007 A fully automated correction method of EOG artifacts in EEG recordings *Clin. Neurophysiol.* **118** 98–104
- [32] Pfurtscheller G and Neuper C 2001 Motor imagery and direct brain–computer communication *Proc. IEEE* **89** 1123–34
- [33] Akaike H 1969 Fitting autoregressive models for prediction *Ann. Ins. Stat. Math.* **21** 243–7
- [34] Billinger M *et al* 2013 Is it significant? Guidelines for reporting BCI performance *Towards Practical Brain–Computer Interfaces. Biological and Medical Physics, Biomedical Engineering* (Berlin: Springer) pp 333–54
- [35] Storey J D 2002 A direct approach to false discovery rates *J. R. Stat. Soc. B* **64** 479–98
- [36] Blankertz B, Lemm S, Treder M, Haufe S and Müller K R 2011 Single-trial analysis and classification of ERP components—a tutorial *NeuroImage* **56** 814–25
- [37] Scherer R, Pfurtscheller G and Neuper C 2008 Motor imagery induced changes in oscillatory EEG components: speed versus accuracy *Proc. 4th Int. Brain–Computer Interface Workshop and Training Course* pp 186–90
- [38] Korzeniewska A, Mańczak M, Kamiński M, Blinowska K J and Kasicki S 2003 Determination of information flow direction among brain structures by a modified directed transfer function (dDTF) method *J. Neurosci. Methods* **125** 195–207
- [39] Haufe S, Nolte G, Müller K R and Kraemer N 2008 Sparse causal discovery in multivariate time series *JMLR Workshop and Conf. Proc., Causality: Objectives and Assessment (NIPS)* vol 6 pp 97–106
- [40] Zou H and Hastie T 2005 Regularization and variable selection via the elastic net *J. R. Stat. Soc. B* **67** 301–20



# SCoT: a Python toolbox for EEG source connectivity

Martin Billinger, Clemens Brunner\* and Gernot R. Müller-Putz

Institute for Knowledge Discovery, Graz University of Technology, Graz, Austria

## Edited by:

Yaroslav O. Halchenko, Dartmouth College, USA

## Reviewed by:

Thorsten O. Zander, Berlin Institute of Technology, Germany

Timothy Mullen, University of California, San Diego, USA

Nick N. Oosterhof, University of Trento, Italy

## \*Correspondence:

Clemens Brunner, Institute for Knowledge Discovery, Graz University of Technology, Inffeldgasse 13/IV, Graz 8010, Austria  
e-mail: clemens.brunner@tugraz.at

Analysis of brain connectivity has become an important research tool in neuroscience. Connectivity can be estimated between cortical sources reconstructed from the electroencephalogram (EEG). Such analysis often relies on trial averaging to obtain reliable results. However, some applications such as brain-computer interfaces (BCIs) require single-trial estimation methods. In this paper, we present SCoT—a source connectivity toolbox for Python. This toolbox implements routines for blind source decomposition and connectivity estimation with the MVARICA approach. Additionally, a novel extension called CSPVARICA is available for labeled data. SCoT estimates connectivity from various spectral measures relying on vector autoregressive (VAR) models. Optionally, these VAR models can be regularized to facilitate ill posed applications such as single-trial fitting. We demonstrate basic usage of SCoT on motor imagery (MI) data. Furthermore, we show simulation results of utilizing SCoT for feature extraction in a BCI application. These results indicate that CSPVARICA and correct regularization can significantly improve MI classification. While SCoT was mainly designed for application in BCIs, it contains useful tools for other areas of neuroscience. SCoT is a software package that (1) brings combined source decomposition and connectivity estimation to the open Python platform, and (2) offers tools for single-trial connectivity estimation. The source code is released under the MIT license and is available online at [github.com/SCoT-dev/SCoT](https://github.com/SCoT-dev/SCoT).

**Keywords:** electroencephalogram, connectivity, Python, single-trial, brain-computer interface

## 1. INTRODUCTION

Quantifying interactions between brain areas is an important and useful tool in neuroscience (Michel and Murray, 2012). Spatially separated brain areas form dynamic large-scale networks that are described by functional and effective connectivity (Schnitzler and Gross, 2005; Siegel et al., 2012). While functional connectivity measures synchronous activation, effective connectivity explains causal relations between areas (Friston, 1994, 2011). We will use the term connectivity for both functional and effective connectivity throughout this manuscript.

Estimates of connectivity can be deduced from the multi-channel EEG by employing a VAR model. However, fitting such a model requires a large amount of data. In particular, the required number of time samples is proportional to the number of channels and the model order. A common approach to generate enough data is to use repeated trials of the same task. However, the EEG also contains task-related activity that varies from trial to trial, which would disappear when averaging over trials. Such activity can only be studied at the single-trial level (Michel and Murray, 2012). A framework for performing single-trial time-varying system identification and visualization was published recently (Mullen et al., 2013). An important use case for single-trial analysis are BCIs, which extract control signals from ongoing brain activity (Millán et al., 2010). Connectivity measures have already been used in several BCI-related studies (Gysels et al., 2005; Shoker et al., 2005; Brunner et al., 2006; Wei et al., 2007; Hamner et al., 2011; Lim et al., 2011; Daly et al., 2012; Billinger et al., 2013a).

Measuring connectivity from the EEG entails methodological challenges such as volume conduction and multiple comparison problems (Siegel et al., 2012). Due to volume conduction, electrical signals originating from one source in the brain are detected by multiple EEG electrodes. Conversely, each electrode measures a superposition of activity from multiple sources. Thus, interpreting connectivity between EEG channels is of limited usefulness. This can be overcome by transforming the problem from the electrode domain to the source domain. Common approaches to estimate source activities include source localization techniques and independent component analysis (ICA). Source localization attempts to map the scalp potential distribution to current source densities on the cortex. However, this approach requires accurate models of head anatomy and electrical properties, as well as accurate electrode locations (Baillet et al., 2001). In contrast, ICA performs a blind decomposition of EEG channels without having to rely on a head model. Additionally, source signals obtained from ICA can be interpreted as originating from cortical dipoles (Makeig et al., 1996). When measuring connectivity between ICA sources, the seemingly contradictory assumptions of dependence for connectivity estimation and independence for ICA must be carefully taken into account. We give a detailed discussion of this issue in section 2.

Our source connectivity toolbox (short SCoT) is a software package for Python that contains tools for estimating connectivity between cortical sources. While various implementations of connectivity are available on other platforms, source connectivity toolbox (SCoT) is the first Python package dedicated to

**Table 1 | VAR-derived measures included in SCoT.**

Measure	Description
A	Spectral representation of the VAR coefficients
H	Transfer function that transforms the innovation process into the VAR process
S	Cross spectral density
G	Inverse cross-spectral density
PHI	Phase angle
COH	Coherence Nunez et al., 1997
pCOH	Partial coherence Franaszczuk et al., 1985
PDC	Partial directed coherence Baccalá and Sameshima, 2001
ffPDC	Full frequency partial directed coherence
PDCF	PDC factor Baccalá and Sameshima, 2001
GPDC	Generalized partial directed coherence Faes et al., 2012
DTF	Directed transfer function Kamiński and Blinowska, 1991
ffDTF	Full frequency directed transfer function Korzeniewska et al., 2003
dDTF	Direct directed transfer function Korzeniewska et al., 2003
GDTF	Generalized directed transfer function (known as directed coherence) Faes et al., 2012

connectivity estimation. Apart from common multi-trial analysis techniques, SCoT also supports single-trial connectivity. The toolbox contains separate modules for ICA, VAR model fitting, and spectral connectivity measure estimation (supported measures are listed in Table 1). While the tools were originally designed for single-trial BCI feature extraction, they equally work with multiple trials and are useful for functional and effective connectivity analysis of EEG signals. SCoT implements the MVARICA approach (Gómez-Herrero et al., 2008), which combines VAR models and ICA for jointly estimating sources and connectivity. Furthermore, we implemented a novel supervised variant of MVARICA specifically tailored toward classification of BCI data, which we named CSPVARICA. The toolbox contains built-in routines for data processing, but can be configured to use the machine learning package scikit-learn (Pedregosa et al., 2011) or custom routines as backends. Unit tests assure correct functionality of the core routines.

The aim of this article is twofold. First, we want to introduce SCoT to researchers along with code snippets that show basic usage examples. Second, we give a technical overview of the methods we implemented and present our new CSPVARICA.

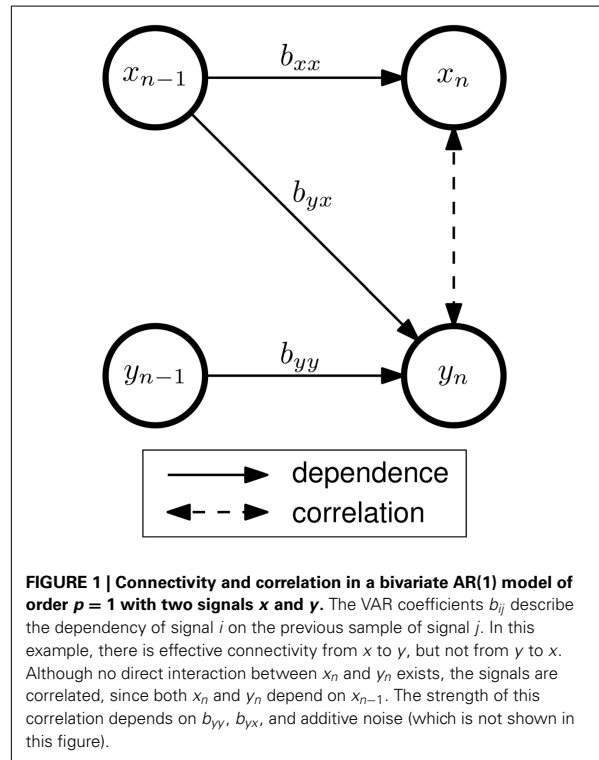
## 2. MATERIALS AND METHODS

### 2.1. SOURCE ESTIMATION AND VAR MODEL FITTING

The EEG is commonly modeled as a linear mixture of underlying cortical source activations (1). These source activations are modeled as VAR processes (2), which contain information about connectivity (Gómez-Herrero et al., 2008).

$$\mathbf{x}_n = \mathbf{M}\mathbf{s}_n \quad (1)$$

$$\mathbf{s}_n = \sum_{k=1}^p \mathbf{B}^{(k)} \mathbf{s}_{n-k} + \mathbf{e}_n \quad (2)$$



The mixing matrix  $\mathbf{M}$  transforms every sample  $n$  of the source activations  $\mathbf{s}_n$  into the observable EEG, which is denoted as  $\mathbf{x}_n$ . VAR model coefficient matrices  $\mathbf{B}^{(k)}$  and innovation process  $\mathbf{e}_n$  form the VAR model of order  $p$  that describes the source activations;  $\mathbf{e}_n$  is assumed to be a vector of independent non-Gaussian white noise processes.

The most naive approach to connectivity estimation is to ignore the mixing of cortical sources and assume that each EEG sensor corresponds to a unique cortical source. However, volume conduction between EEG sensors is not correctly captured by VAR models and therefore severely limits the usefulness of connectivity at the sensor level (Siegel et al., 2012).

More sophisticated approaches obtain source activations by constructing an unmixing matrix  $\mathbf{U}$  that mathematically reverses the mixing process so that  $\mathbf{s}_n = \mathbf{U}\mathbf{x}_n$  (with  $\mathbf{U}\mathbf{M}$  equal to the identity matrix  $\mathbf{I}$ ). ICA performs such a decomposition by attempting to find spatial EEG components with minimal instantaneous cross-dependencies between each other. These components can be interpreted as cortical source activations that are not affected by volume conduction. However, connectivity between sources can also cause instantaneous cross-dependencies (Figure 1). ICA assumes no temporal dependence structure within the data, but connectivity between sources violates this assumption. Thus, ICA treats the signals as though instantaneous cross-dependencies were exclusively caused by the mixing process. This might decrease the reliability of subsequent connectivity estimates, as was demonstrated by Haufe et al. (2010).

We provide an implementation of ICA source decomposition in SCoT. However, limitations and conflicting assumptions of VAR and ICA should be carefully considered before applying this approach. Therefore, we recommend more sophisticated techniques such as MVARICA or our novel CSPVARICA.

### 2.2. MVARICA

SCoT implements the MVARICA approach, which performs joint source decomposition and VAR model fitting while respecting their respective assumptions about dependencies (Gómez-Herrero et al., 2008). MVARICA works in three steps (see Figure 2). First, the EEG is transformed by applying principal component analysis (PCA) as follows:

$$y_n = Cx_n = CMs_n \quad (3)$$

The signals in  $y_n$  contain the PCA-transformed EEG. The PCA transformation matrix  $C$  is pruned to remove components that contribute least to the total EEG variance. This step reduces the dimensionality for subsequent processing and limits the number of sources found by MVARICA. Second, a VAR model with coefficients  $A^{(k)}$  and residual processes  $r_n$  is fitted to  $y_n$ :

$$y_n = \sum_{k=1}^p A^{(k)} y_{n-k} + r_n \quad (4)$$

By combining (2–4) we can relate the VAR model fitted to  $y_n$  with the VAR model that describes the source activations:

$$A^{(k)} = (CM)B^{(k)}(CM)^{-1} \quad (5)$$

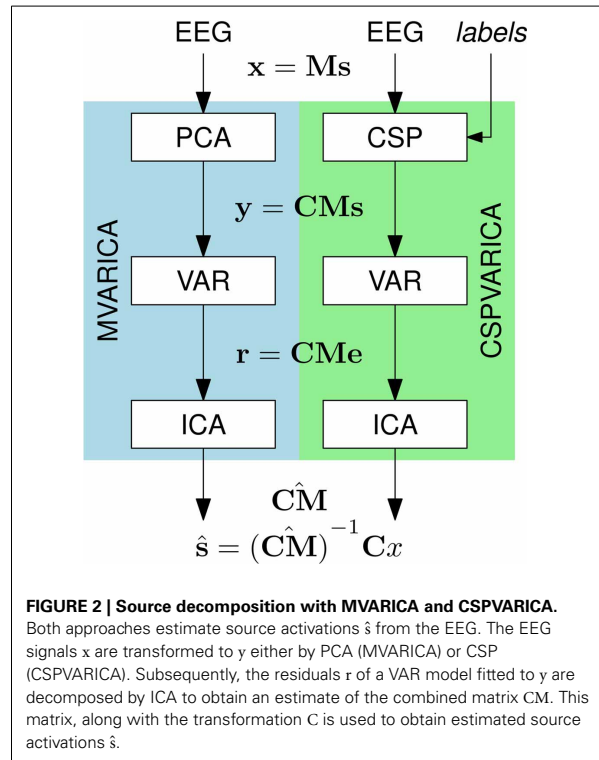
$$r_n = (CM)e_n \quad (6)$$

The residuals  $r$  contain cross-dependencies that cannot be explained by the VAR model. According to (6), all cross-dependencies remaining in the residuals are due to the transformation  $CM$ . In the third step, the residuals are decomposed by ICA in order to obtain an estimate of the transformation  $\hat{CM}$ . Finally, an estimated unmixing matrix  $\hat{U}$  is obtained as  $\hat{U} = (\hat{CM})^{-1}C$  so that

$$\hat{s}_n = \hat{U}x_n. \quad (7)$$

Typically, estimates of the VAR coefficients at the source level are obtained by inserting estimates  $\hat{A}$  and  $\hat{CM}$  in (5) and solving for  $\hat{B}$ . However, if sources are spatially stationary (constant  $M$ ), the unmixing estimate  $\hat{U}$  can be reused on other data sets to obtain source activations and fit VAR models directly to these activations according to (2). This allows us to determine the unmixing matrix from a set of training data, and subsequently perform connectivity estimation between the same sources on new data.

In general, MVARICA is applied to multi-trial data. Different strategies to obtain the VAR residuals  $r$  can be employed, depending on which stationarity assumptions hold on the data. If stationarity can be assumed across all trials, a single VAR model may be fitted to all trials. If stationarity can be assumed only across



trials from the same condition, a different VAR model may be fitted for each condition. Finally, if stationarity cannot be assumed across trials, a different VAR model may be fitted for each individual trial. The last approach requires single-trial VAR model fitting, which we will discuss in section 2.6.

### 2.3. CSPVARICA

MVARICA reduces the input dimensionality by discarding the principal components that contribute least to the total EEG variance. However, EEG components of interest often have a low signal-to-noise ratio. Thus, PCA might remove such components while retaining noise with higher variance. We propose to use common spatial patterns (CSP) instead of PCA. While PCA finds components according to their contribution to the total variance, CSP finds components that explain the differences (in variance) between two conditions (Koles et al., 1990). Thus, we expect CSP to be superior to PCA whenever differences between two conditions (e.g., baseline/task, task/task, etc.) are analyzed. CSPVARICA is implemented in SCoT as a supervised alternative to MVARICA (see Figure 2). CSPVARICA is similar to MVARICA except for the first step, where we replaced PCA with CSP. Equations (3–7) are equally valid for CSPVARICA; only the transformation matrix  $C$  is different because it represents the CSP transform instead of the PCA transform.

### 2.4. MODEL VALIDATION

MVARICA and CSPVARICA apply ICA to the residuals of VAR models. ICA assumes no temporal structure in the data. Thus, it

is important that the VAR models adequately describe the data so that the residuals are serially uncorrelated.

SCoT implements a multivariate portmanteau test to test for whiteness in the residuals (Hosking, 1980). The test compares the multivariate Li-McLeod statistic  $Q$  against the null hypothesis that the residuals are white (Lütkepohl, 2005). When the residuals are normally distributed,  $Q$  follows a chi-squared distribution. However, we explicitly assume non-Gaussian residuals. Thus, we estimate the distribution of  $Q_0$  under the null hypothesis from surrogate residuals. Temporal structure in the residuals is destroyed by randomly permuting the residuals along the time axis. We repeatedly calculate  $Q_0$  from different permutations and calculate the probability of observing a  $Q_0$  larger than  $Q$ . A probability of less than 0.05 indicates significantly non-white residuals.

### 2.5. CONNECTIVITY

Once source estimates are available, numerous connectivity measures can be extracted from VAR models. **Table 1** lists all measures currently implemented in SCoT. Some of the most commonly used measures are summarized in Schlögl and Supp (2006). All these measures may be extracted directly from the VAR coefficients returned by MVARICA or CSPVARICA.

In addition to well known measures, SCoT implements the full frequency partial directed coherence (ffPDC). The ffPDC is obtained by normalizing the partial directed coherence (PDC) over all frequencies instead of each frequency individually:

$$\text{ffPDC}_{ij}(z) = \frac{|A_{ij}(z)|}{\sqrt{\sum_z A_{ij}^H(z) A_{ij}(z)}} \quad (8)$$

Here,  $i$  and  $j$  correspond to the indices of the sink and the source signals, respectively.  $\mathbf{A}$  is the inverse of the VAR transfer function.

In general, repeatedly applying MVARICA or CSPVARICA to different data segments yields components in different order. This makes tracking of connectivity patterns difficult. However, it is possible to overcome this issue by re-using the unmixing matrix obtained from one decomposition. Applying this unmixing matrix to new portions of data results in varying activations of the same sources, which facilitates three important use cases: single-trial estimation, time-varying analysis, and comparing different conditions.

### 2.6. SINGLE-TRIAL ESTIMATION

VAR model fitting typically requires a large amount of data. To obtain a sufficient amount of data, a model can be fitted to multiple trials, assuming stationarity across trials (i.e., each trial is a realization of the same process). However, this is not feasible in applications such as MI BCIs, where trial duration is several seconds or continuous control is required. Instead, connectivity estimates need to be obtained from a single window of data. In SCoT, we perform single-trial connectivity estimation on short windows of source activations, but use a training set of multiple trials to obtain sources that are assumed to be spatially stationary.

One procedure for single-trial connectivity estimation is described in our previous work (Billinger et al., 2013a), where various connectivity measures were estimated on selected ICA sources. This procedure can be improved by replacing ICA and

source selection with MVARICA or CSPVARICA. Importantly, single-trial VAR model fitting is prone to overfitting due to the limited amount of data available in a single trial. However, this problem can be alleviated by regularization. Therefore, SCoT supports ridge regression for fitting VAR models to individual and multiple time windows. The scikit-learn backend provides additional model fitting routines including Lasso, Elastic Net, and generalized cross-validation (GCV) for determining the ridge parameter.

The degrees of freedom when fitting a VAR model depends on the model order. Typically, the order of VAR models is determined with cross-validation or selection criteria such as Akaike information criterion (AIC) or Bayesian information criterion (BIC). Regularization effectively limits the degrees of freedom, so both model order and regularization penalty can be optimized. For simplicity, we manually set the model order to a reasonably high value and optimize only the regularization penalty.

### 2.7. STATISTICS

So far, we have only discussed point estimates of connectivity. However, scientists will usually want to make statistical inferences about connectivity to either determine if there really is connectivity from one source to another, or to determine if there is a difference in connectivity between two conditions.

In SCoT, presence of connectivity is deduced using the method of surrogate data generated by phase randomization. While removing connectivity from each signal pair individually may give better results (Faes et al., 2009), we took a simpler approach, where connectivity is destroyed between all signals simultaneously. We obtain the distribution of connectivity under the null hypothesis of no connectivity by repeatedly estimating connectivity on surrogates. Connectivity estimated from actual data can be compared against this distribution to test if it is significantly non-zero.

Statistical difference in connectivity is obtained by performing bootstrap resampling. Bootstrap samples are drawn at the trial level, thus this method only works for multi-trial data sets. The distribution of difference in connectivity is obtained by bootstrapping both conditions. The difference is significantly different from zero if the confidence interval does not contain 0.

Typically, such tests are performed for each frequency bin and channel pair, which requires correction for multiple testing. However, individual tests are likely to be positively correlated. Thus, controlling for the family-wise error rate is likely to be overly conservative. Instead, controlling for the false discovery rate (Benjamini and Hochberg, 1995) is implemented in SCoT.

### 2.8. SOURCE CONNECTIVITY WORKFLOW

SCoT implements routines for estimating connectivity between EEG sources. Two estimation approaches are possible in SCoT. Too many Ps in approach is to estimate sources and connectivity jointly on the same data set using MVARICA or CSPVARICA. Alternatively, a two-step approach is supported, where sources and connectivity are estimated on different data sets. Both approaches impose strong spatial stationarity assumptions on the sources. However, in the latter approach source activity may vary over time.

Joint estimation is performed by applying MVARICA or CSPVARICA to a data set where sources are spatially and temporally stationary. Two-step estimation consists of separately performing source decomposition and VAR model fitting, possibly on different data sets. MVARICA or CSPVARICA can be employed in the source decomposition step by discarding their VAR estimates. In the second step, the unmixing matrix is used to obtain source activations on a different data set. Connectivity measures are estimated from VAR models fitted to these source activations.

The two-step approach is useful whenever connectivity is expected to vary between spatially stationary sources. Possible applications include comparing different conditions, analyzing time-varying connectivity, and estimating single-trial connectivity.

It is often useful to estimate time-varying connectivity. This can be done on a multi-trial or a single-trial basis, whichever is appropriate for the data and the research question. Time-varying multi-trial connectivity estimation facilitates analysis of cue-locked connectivity dynamics. Here, we estimate connectivity on the first time segment of multiple trials, then for the second (possibly overlapping) segment, and so on. This results in an average time-course of connectivity related to the trial start. Time-varying single-trial connectivity estimation may be employed when connectivity dynamics are not cue locked, or no cues are available such as in continuous BCIs. Here, we estimate connectivity on short (possibly overlapping) windows, resulting in a time course of instantaneous connectivity.

### 3. IMPLEMENTATION

#### 3.1. OVERVIEW

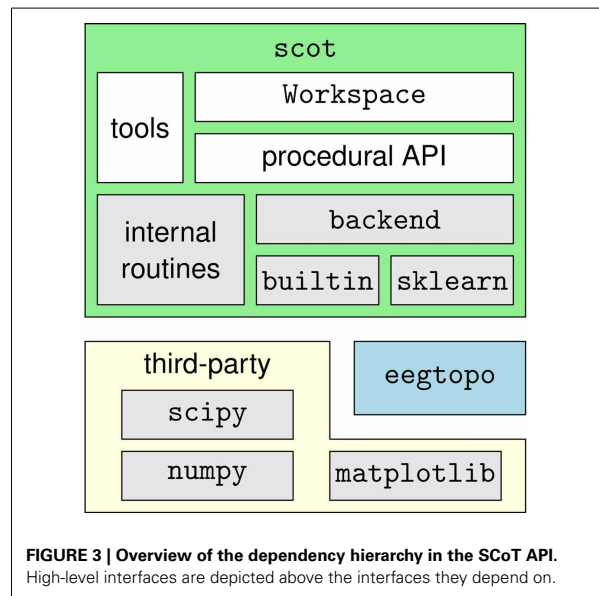
SCoT is distributed as a Python package named `scot`. The package contains several modules that implement the toolbox's functionality and the two sub-packages `scot.backend` and `scot.builtin`. The former contains backend modules that allow SCoT to use different implementations of low-level routines such as PCA, ICA, or model fitting. The other package implements built-in versions of these routines. See **Figure 3** for an overview of the package structure.

SCoT depends on NumPy, SciPy (Oliphant, 2007), and optionally on scikit-learn (Pedregosa et al., 2011). Matplotlib is required for visualization only. Furthermore, SCoT contains the complementary `eegtopo` package, which is used for EEG topography plots based on spherical spline interpolation (Perrin et al., 1989).

Development is test-driven, with unit tests covering core functionality as far as the stochastic nature of the implemented algorithms allows. The source code is released under the open source MIT license and is available online at [github.com/SCoT-dev/SCoT](https://github.com/SCoT-dev/SCoT).

#### 3.2. BACKEND MECHANISM

A design goal of SCoT is to keep external dependencies at a minimum. The backend mechanism provides a common interface that allows SCoT to optionally utilize routines from third-party software without introducing unnecessary dependencies. A backend consists of targets that represent thin



wrapper functions, class implementations or even modules. These are stored in a global dictionary, where they can be accessed from within SCoT. The dictionary is updated when including a backend module. Thus, the user can easily select a backend by simply importing the module. SCoT comes with two backends: `scot.backend.builtin`, which provides basic implementations of backend functionality and `scot.backend.sklearn`, which provides wrappers for routines implemented in the external scikit-learn package.

The built-in ICA backend calls BINICA to perform Infomax ICA (Makeig et al., 1996). BINICA is an external binary, which is either shipped with EEGLAB (Delorme and Makeig, 2004), or separately available online<sup>1</sup> and is downloaded on demand.

Currently, the following backend targets are used by SCoT: ICA (ICA function), PCA (PCA function), VAR (VAR model fitting class), and `utils` (miscellaneous helper routines). The backend mechanism relies on duck-typing, which allows users to easily create custom backends by simply putting their own functions in the global backend dictionary.

#### 3.3. WORKSPACE

The `scot.oopapi` module exposes the class `Workspace`, which provides convenient access to SCoT from interactive Python sessions. This class also serves as an example for usage of the more flexible low-level application programming interface (API), which is described in detail later. An instance of the `Workspace` class is optionally initialized with sampling rate, desired dimensionality reduction, number of fast Fourier transform (FFT) bins and/or electrode locations. This alleviates the user of the burden to pass these parameters to each individual function call. The `Workspace` class can perform source decomposition on EEG data, estimate connectivity on the same or a

<sup>1</sup><http://sccn.ucsd.edu/eeglab/binica/>

different data set, conduct statistical analysis, and visualize the results.

### 3.4. PACKAGE STRUCTURE

Here, we provide a summary of the modules that form the SCoT package. Please refer to the API reference in the SCoT documentation for a more detailed description. A summary of the modules is listed in **Table 2**.

#### 3.4.1. Internal modules

These are modules mainly intended for internal use in SCoT.

`builtin` is actually a sub-package. It contains SCoT's own implementations of PCA, CSP, VAR, and a wrapper to the BINICA binary.

The `config` module defines global variables for configuring SCoT. Currently, it contains only the backend dictionary. This dictionary is populated when importing a backend. Functions like `mvarica` query this variable to determine which implementations of PCA, ICA, etc., to use.

Internal utility functions are defined in the `utils` module. These include among others a function for calculating autocovariance matrices and the `memoize` decorator that caches function return values.

#### 3.4.2. User facing modules

These are modules that users of SCoT will often work with.

`backend` is actually a sub-package. It contains a separate module for each backend currently available in SCoT. At the moment these are `builtin` and `sklearn`.

The `connectivity` module provides a class for extracting connectivity measures from VAR model coefficients (see **Table 1** for a list of available connectivity measures). Some connectivity measures are calculated from other measures (e.g., the dDTF). To avoid unnecessary recalculations of repeatedly used measures, this class makes use of the `memoize` decorator to quickly get the cached return values of member functions that have been called before.

Functions for statistical evaluation of connectivity are available in `connectivity_statistics`. These include surrogate estimation under the null-hypothesis of no connectivity, bootstrapping, statistical tests, and correction for multiple testing.

The `datatools` module contains functions for manipulating EEG data, such as cutting segments from continuous data or applying spatial filters to segmented data. The `matfiles` module allows loading and saving of MATLAB `.mat` files. This module converts the result of `scipy`'s `loadmat` to nested Python dictionaries.

The `ooapi` module provides the `Workspace` class, which is described in detail above.

ICA source decomposition is implemented in the `plainica` module. It performs optional dimensionality reduction with PCA and subsequent ICA source decomposition.

The `plotting` module contains visualization routines. This module depends on `matplotlib` to create plots similar to MATLAB. The dependency is optional and required only for visualization; if `matplotlib` is not available, the module can still be imported, but the functions cannot be called. The visualization

**Table 2 | Python modules that form the SCoT API.**

Module	Purpose
<code>backend</code>	(sub-package) Backend interfaces
<code>builtin</code>	(sub-package) Implementation of the builtin backend
<code>config</code>	Global configuration
<code>connectivity</code>	Connectivity analysis
<code>connectivity_statistics</code>	Statistical evaluation of connectivity
<code>datatools</code>	Basic data manipulation
<code>matfiles</code>	Routines for loading and saving MATLAB <code>.mat</code> files
<code>ooapi</code>	Object oriented API (Workspace)
<code>plainica</code>	Source decomposition with ICA
<code>plotting</code>	Visualization
<code>utils</code>	Utility functions
<code>VAR</code>	VAR model interface
<code>varica</code>	Joint source/VAR estimation
<code>xvschema</code>	Cross-validation strategies

routines rely on the `eegtopo` package to plot scalp projections of sources.

The `VAR` module contains the class `VARBase`, which is the VAR base class for VAR models in SCoT. This class implements routines common to all implementations of VAR models, such as prediction or model validation. However, model fitting routines are provided by the derived classes `scot.builtin.var.VAR` and `scot.backend.sklearn.VAR`.

The MVARICA and CSPVARICA procedures are implemented in the `varica` module. The module exposes one function for each procedure.

Cross-validation strategies are implemented in `xvschema`. This module contains functions that generate indices for testing and training sets for single-trial and multi-trial optimization. While multi-trial strategy is a normal leave-one-out cross-validation, the single-trial strategy creates training sets that contain only single trials.

## 4. RESULTS

### 4.1. USING SCoT

#### 4.1.1. Basic usage

Here, we will demonstrate how to use SCoT to estimate multi-trial connectivity from EEG data. More detailed examples are distributed with the source code.

First, the SCoT package must be made available to the Python interpreter. By default, SCoT uses the built-in routines for PCA and ICA. Alternatively, `scikit-learn` can be used by importing the `sklearn` backend.

```
import scot
import scot.backend.sklearn
```

SCoT works with three-dimensional NumPy arrays. The three dimensions of an EEG data set are time, signals, and trials. An example data set is available with SCoT. This data set contains a recording of 45 EEG channels from one subject performing hand

and foot MI. The subject was instructed to perform either MI task by a visual cue. Every 9.5–10.5 s such cues were presented 90 times for each class in randomized order.

```
from motorimagery import data
```

In the following code snippets we use the variables `raweeg`, `triggers`, `classes`, and `fs`. These variables are taken from the example data set and contain the continuous EEG data (samples  $\times$  channels), a list of trigger locations (sample indices) that mark individual trials, class labels (`'hand'`, `'foot'`) for each trial, and the sampling rate (Hz).

Convenience functions for basic data manipulation are available. The following example cuts segments of 1 s starting 3 s after each trigger from continuous EEG and arranges them in three dimensions as described above.

```
eeg =
    scot.datatools.cut_segments(
        raweeg, triggers, 3*fs, 4*fs)
```

The `Workspace` class provides a high-level interface to the toolbox. As the name suggests, an instance of this class provides a workspace on which SCoT routines operate. The workspace contains data, source and connectivity estimates, and settings.

```
ws = scot.Workspace(
    {'model_order': 40},
    reducedim=4,
    locations=locs)
```

This command initializes a new workspace with VAR model order 40, dimensionality reduction to four components, and EEG electrode locations described in the variable `locs`.

If `reducedim` was not set, it would default to retaining 99% of the EEG variance. Alternatively, PCA can be disabled by setting `reducedim` to `'no pca'`.

A dataset is passed to the workspace with the `set_data` method. The optional second argument may contain a list of labels that assigns a class label to each trial in the data. The method `do_mvarica` decomposes the EEG data into source activations and fits a VAR model in the process. It is important to test the VAR residuals for whiteness. A  $p$ -value of less than e.g., 0.05 returned by `VAR.test_whiteness` would indicate significantly non-white residuals, and the VAR settings would need to be tuned. To obtain separate VAR models for each class, we call `set_used_labels()` to specify which classes to use in subsequent operations. Once VAR models are fitted with the `fit_var` method, we can plot spectral connectivity measures with `get_connectivity`. Finally, `show_plots` displays the plots.

```
# perform source decomposition
# and plot source topos
ws.set_data(eeg, classes)
ws.do_mvarica()
p = ws.var_.test_whiteness(50)
print('Whiteness:', p)
fig = ws.plot_connectivity_topos()
```

```
# estimate and plot connectivity
ws.set_used_labels(['foot'])
ws.fit_var()
ws.get_connectivity('ffDTF', fig)

# estimate and plot connectivity
ws.set_used_labels(['hand'])
ws.fit_var()
ws.get_connectivity('ffDTF', fig)

ws.show_plots()
```

**Figure 4** (left) shows the result of applying these steps to the example data set. By replacing `do_mvarica` with `do_cspvarica`, we obtain different sources (**Figure 4**, right). The two frequency bands  $\mu$  (8–12 Hz) and  $\beta$  (16–24 Hz) are known to play a part in motor processing (Pfurtscheller, 1981). While MVARICA detects connectivity mostly in the  $\mu$  band, CSPVARICA reveals connectivity in the  $\mu$  and  $\beta$  bands. Furthermore, connectivity between the CSPVARICA sources varies more between classes. This difference between MVARICA and CSPVARICA is somewhat expected, because MVARICA selects sources that explain as much of the EEG variance as possible, while CSPVARICA prefers sources with maximally different activations between classes.

#### 4.1.2. Time-varying connectivity

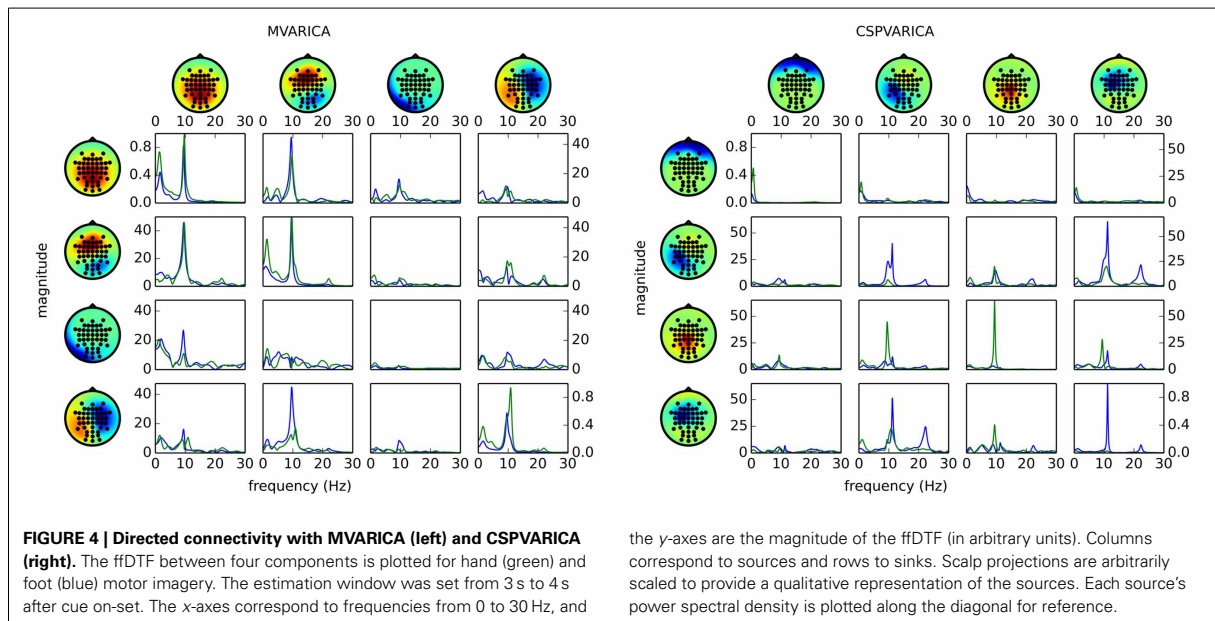
The plots in **Figure 4** only show a snapshot of connectivity in one time segment. In order to get an overview on how connectivity evolves over time, the estimation process is repeated for multiple time-shifted segments. However, source decomposition should not be performed for every time segment individually. Even if the same sources were detected in consecutive windows, their signs and order would change randomly. This in turn would make interpreting the results very difficult. Instead, it is reasonable to re-use the same sources (represented by the unmixing matrix) in each time segment.

In the following example, such time-frequency analysis is performed over the whole trial of the data set. The new data set is prepared by cutting 10 s long slices starting 2 s before each trigger from the continuous EEG.

```
eeg_long =
    scot.datatools.cut_segments(
        raweeg, triggers, -2*fs, 8*fs)
```

The source decomposition obtained before from the short time segments will be re-used by simply assigning the new data set to the workspace. Time-frequency analysis does not require the user to call `fit_var`. Instead, separate models are fitted internally for each time segment. The function `get_tf_connectivity` takes three mandatory arguments: the measure to use, window length, and step size.

```
fig = ws.plot_connectivity_topos()
ws.set_used_labels(['hand'])
ws.get_tf_connectivity('ffDTF',
    1*fs, fs/5, plot=fig)
ws.show_plots()
```



The code snippet above produces output similar to the right side of **Figure 5**. Here, it becomes clear that most of the differences between the classes are due to reduced connectivity during hand motor imagery.

#### 4.2. BCI SIMULATION

Using SCoT, we performed a BCI simulation study to demonstrate the efficacy of CSPVARICA and MVARICA on single trial classification on EEG recordings of MI data. Fourteen subjects participated in this study, all of them gave informed consent and were paid for their participation. Each participant took part in two sessions on separate days, with six recording runs of 30 trials in each session. The sessions comprised 90 right hand MI and 90 foot MI trials. Trial duration was 7 s with breaks of varying duration (2.5–3.5 s) between trials. EEG preprocessing included removing electrooculogram (EOG) artifacts (Schlögl et al., 2007) and downsampling to 100 Hz. A more detailed description of the data and preprocessing procedure can be found in Billinger et al. (2013a).

We performed cross-validation per subject and session, using each of the six runs for testing once and the remaining five runs for initializing the procedure. In each cross-validation step, we decomposed the raw EEG into 16 components with either CSPVARICA or MVARICA. Subsequently, we split the component activation signals into segments of 1.5 s length that overlapped by 0.2 s. The following two steps were applied to each segment individually. First, we determined the optimal regularization parameter  $\lambda$  for subsequent single-trial VAR model fitting. Second, we extracted full frequency directed transfer function (fDfTF), fPDC, and band power (BP) features in two frequency bands (7–13 Hz and 15–25 Hz). While fDfTF and fPDC were based on the VAR model, logarithmic BP was calculated directly from the time signals to serve as a baseline. Finally, we trained

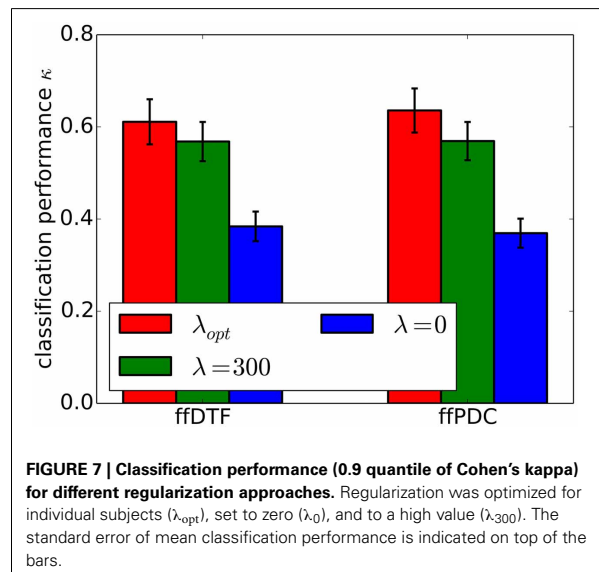
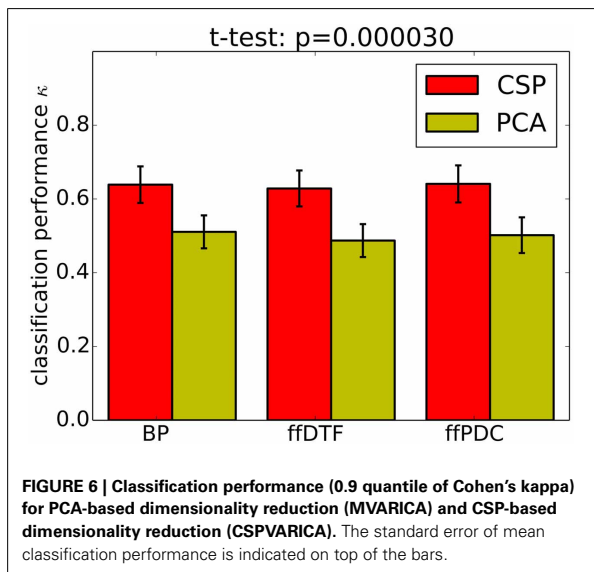
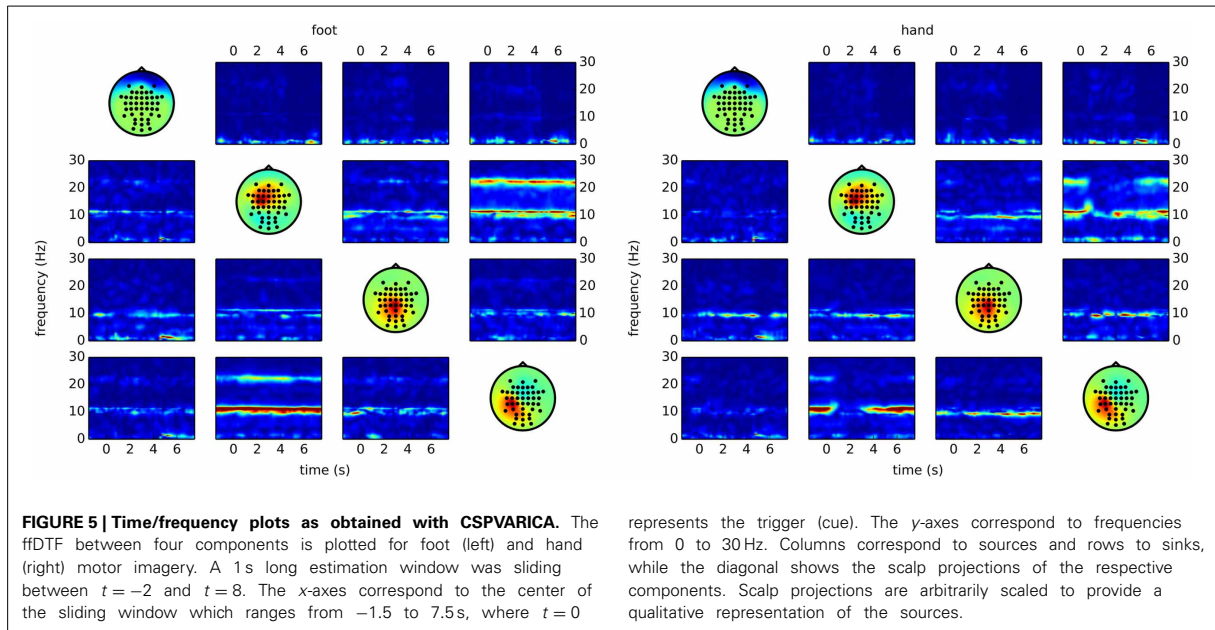
a shrinkage linear discriminant analysis (sLDA) classifier on the time segment where classes were best discriminated for each feature type.

We tested the procedure on the run that was previously withheld from initialization. First, we decomposed the EEG into the same components as in the initialization step by spatially filtering the test set with the unmixing matrix obtained during initialization. For each time segment, we subsequently fitted regularized VAR models individually on every trial, extracted the fDfTF, fPDC, and BP features, and applied the classifier. This resulted in a confusion matrix for each time segment. We calculated Cohen's kappa  $\kappa$  for each segment during the MI phase. The  $\kappa$  metric is preferable over classification accuracy because it takes class distribution into account (Billinger et al., 2013b). From all segments, we took the 0.9 quantile of  $\kappa$  as classification performance, which is less sensitive to outliers than peak performance. This measure of classification performance was obtained for each subject and session.

Classification performance is significantly higher with CSPVARICA than with MVARICA (**Figure 6**). Thus, CSPVARICA seems to be preferable over MVARICA for MI classification. It is also reasonable to assume that CSPVARICA is useful for studying connectivity under varying conditions or tasks.

Furthermore, we demonstrate the effects of regularization on classification performance. In **Figure 7**, we compare per-subject optimization of the regularization parameter with no regularization and with applying over-regularization by setting the parameter to a high value. Optimal regularization was determined in the initialization phase of the cross-validation for each time segment individually, resulting in  $\kappa = 0.62 \pm 0.18$ . Clearly, no regularization performs worst with  $\kappa = 0.38 \pm 0.11$ . For over-regularization, we chose  $\lambda$  roughly an order

## Appendix B. Primary Publications



of magnitude higher than the average optimal value, which slightly decreased classification performance to  $\kappa = 0.57 \pm 0.15$ . However, the impact of too much regularization is difficult to quantify.

### 5. DISCUSSION

In this article, we introduced SCoT, the Python toolbox for source connectivity estimation. It provides tools for ICA-based source decomposition, VAR model fitting, and extraction of connectivity measures.

Widely used neuroscience software packages<sup>2</sup> (Hanke and Halchenko, 2011) such as EEGLAB (Delorme and Makeig, 2004), Fieldtrip (Oostenveld et al., 2011), and Biosig (Schlögl and Brunner, 2008) support connectivity analysis. Particularly, the SIFT toolbox (Delorme et al., 2011) includes routines for adaptive and segmented VAR model fitting with various smooth and sparse regularization techniques. Furthermore, SIFT supports

<sup>2</sup><http://neuro.debian.net/survey/2011/results.html>

SCSA (Haufe et al., 2010) for jointly estimating sources and connectivity. These packages are released under open source licenses and are available for MATLAB<sup>3</sup>. In contrast, the MNE software package<sup>4</sup> supports model-based source reconstruction and exposes functionality for calculating several non-parametric connectivity measures in a Python API. With SCoT, we attempt to provide reusable and modular routines, which can help application developers avoid re-implementing the wheel in future projects based on Python.

For the first time, we presented our new CSPVARICA method and demonstrated that it is a useful source decomposition approach for data that contains different labeled conditions. Currently, our implementation supports only two conditions, but generalization to an arbitrary number of conditions is planned for a future release. Our BCI simulations showed that CSPVARICA outperforms MVARICA in terms of classification performance. This is not surprising since CSPVARICA favors sources that contain highly discriminative signals. However, MVARICA might be less susceptible to noise because it retains high-variance components. Whether or not one of these methods yields physiologically more meaningful results is an open question.

Although we conceived CSPVARICA mainly for application in BCIs, it is likely to be useful for other disciplines of neuroscience as well. Therefore, we encourage researchers to consider using CSPVARICA when analyzing differences between conditions.

SCoT relies on MVARICA or CSPVARICA for source decomposition. Alternative joint source/connectivity estimation techniques such as SCSA (Haufe et al., 2010) have not been implemented yet in SCoT. Furthermore, model-based source reconstruction is not included, because source localization is not within the scope of SCoT. However, SCoT can work with source decompositions obtained from such approaches by utilizing unmixing matrices obtained from other software packages.

VAR model fitting in SCoT is performed with regularized least squares optimization in general. Routines for ridge regression are built in, and other approaches such as Lasso, Elastic Net, LARS, or Bayesian regression are available through scikit-learn. Our simulations show an improvement in classification performance from  $\kappa = 0.38$  without regularization to  $\kappa = 0.62$  when applying ridge regression, which underscores the importance of regularization in single-trial connectivity. Support for more VAR fitting and regularization strategies is planned. A noteworthy approach is the group LASSO (Vidaurre et al., 2013), which promotes sparse connectivity. This could prove useful for the visualization of large networks, as it limits the number of non-zero connections.

Time-varying connectivity analysis is possible in SCoT by employing a sliding window. An alternative could be adaptive VAR models. However, adaptive models can be more difficult to handle due to their inherent exponential window. Furthermore, such models need to be updated for every single sample, while sliding windows can skip an arbitrary number of samples.

Our default implementation of ICA uses an external Linux binary to perform Infomax ICA. On other platforms, the FastICA implementation from scikit-learn may be used

instead. Furthermore, the flexible backend mechanism should make it easy to include other ICA implementations such as CUDAICA (Raimondo et al., 2012) or the ICAs shipped with MDP (Zito et al., 2009).

In summary, SCoT provides tools required for estimating connectivity on EEG data to the free and open Python platform. It is designed to tightly integrate with popular scientific computation and visualization modules in order to be accessible to researchers familiar with Python.

### ACKNOWLEDGMENTS

This work was supported by the FP7 Framework EU Research Project ABC (No. 287774) and the Austrian Science Foundation FWF Project ‘Coupling Measures for BCIs’ (P20848-N15).

### REFERENCES

- Baccalá, L. A., and Sameshima, K. (2001). Partial directed coherence: a new concept in neural structure determination. *Biol. Cybern.* 84, 463–474. doi: 10.1007/PL00007990
- Baillet, S., Mosher, J. C., and Leahy, R. M. (2001). Electromagnetic brain mapping. *IEEE Signal Process. Mag.* 18, 14–30. doi: 10.1109/79.962275
- Benjamini, Y., and Hochberg, Y. (1995). Controlling the false discovery rate: a practical and powerful approach to multiple testing. *J. R. Statist. Soc. B* 57, 289–300.
- Billinger, M., Brunner, C., and Müller-Putz, G. R. (2013a). Single-trial connectivity estimation for classification of motor imagery data. *J. Neural Eng.* 10, 046006. doi: 10.1088/1741-2560/10/4/046006
- Billinger, M., Daly, I., Kaiser, V., Jin, J., Allison, B. Z., Müller-Putz, G. R., et al. (2013b). “Is it significant? Guidelines for reporting BCI performance,” in *Towards Practical Brain-Computer Interfaces, Biological and Medical Physics, Biomedical Engineering*, eds B. Z. Allison, S. Dunne, R. Leeb, J. del R. Millán, and A. Nijholt (Berlin Heidelberg: Springer), 333–354.
- Brunner, C., Scherer, R., Graimann, B., Supp, G., and Pfurtscheller, G. (2006). Online control of a brain-computer interface using phase synchronization. *IEEE Trans. Biomed. Eng.* 53, 2501–2506. doi: 10.1109/TBME.2006.881775
- Daly, I., Nasuto, S. J., and Warwick, K. (2012). Brain computer interface control via functional connectivity dynamics. *Patt. Recogn.* 45, 2123–2136. doi: 10.1016/j.patcog.2011.04.034
- Delorme, A., and Makeig, S. (2004). EEGLAB: an open source toolbox for analysis of single-trial EEG dynamics including independent component analysis. *J. Neurosci. Methods* 134, 9–21. doi: 10.1016/j.jneumeth.2003.10.009
- Delorme, A., Mullen, T., Kothe, C., Akalin Acar, Z., Bigdely-Shamlo, N., Vankov, A., et al. (2011). EEGLAB, SIFT, NFT, BCLILAB and ERICA: new tools for advanced EEG processing. *Comput. Intell. Neurosci.* 2011:130714. doi: 10.1155/2011/130714
- Faes, L., Erla, S., and Nollo, G. (2012). Measuring connectivity in linear multivariate processes: definitions, interpretation, and practical analysis. *Comput. Math. Methods Med.* 2012, 1–18. doi: 10.1155/2012/140513
- Faes, L., Porta, A., and Nollo, G. (2009). Surrogate data approaches to assess the significance of directed coherence: application to eeg activity propagation. *Conf. Proc. IEEE Eng. Med. Biol. Soc.* 2009, 6280–6283. doi: 10.1109/IEMBS.2009.5332477
- Franaszczuk, P., Blinowska, K., and Kowalczyk, M. (1985). The application of parametric multichannel spectral estimates in the study of electrical brain activity. *Biol. Cybern.* 51, 239–247. doi: 10.1007/BF00337149
- Friston, K. J. (1994). Functional and effective connectivity in neuroimaging: a synthesis. *Hum. Brain Mapp.* 2, 56–78. doi: 10.1002/hbm.460020107
- Friston, K. J. (2011). Functional and effective connectivity: a review. *Brain Connect.* 1, 13–36. doi: 10.1089/brain.2011.0008
- Gómez-Herrero, G., Atienza, M., Egiuzarian, K., and Cantero, J. L. (2008). Measuring directional coupling between EEG sources. *Neuroimage* 43, 497–508. doi: 10.1016/j.neuroimage.2008.07.032
- Gysels, E., Renevey, P., and Celka, P. (2005). SVM-based recursive feature elimination to compare phase synchronization computed from broadband and narrow-band EEG signals in brain-computer interfaces. *Signal Process.* 85, 2178–2189. doi: 10.1016/j.sigpro.2005.07.008

<sup>3</sup><http://www.mathworks.com/products/matlab/>

<sup>4</sup><http://www.martinos.org/mne/>

## Appendix B. Primary Publications

- Hamner, B., Leeb, R., Tavella, M., and Millán, J. D. R. (2011). "Phase-based features for motor imagery brain-computer interfaces," in *Annual International Conference of the IEEE Engineering in Medicine and Biology Society (EMBC)* (Boston, MA), 2578–2581.
- Hanke, M., and Halchenko, Y. O. (2011). Neuroscience runs on gnu/linux. *Front. Neuroinform.* 5:8. doi: 10.3389/fninf.2011.00008
- Haufe, S., Tomioka, R., Nolte, G., Mäijller, K.-R., and Kawanabe, M. (2010). Modeling sparse connectivity between underlying brain sources for EEG/MEG. *IEEE Trans. Biomed. Eng.* 57, 1954–1963. doi: 10.1109/TBME.2010.2046325
- Hosking, J. (1980). The multivariate portmanteau statistic. *J. Am. Statist. Assoc.* 75, 602–608. doi: 10.1080/01621459.1980.10477520
- Kamiński, M. J., and Blinowska, K. J. (1991). A new method of the description of the information flow in the brain structures. *Biol. Cybern.* 65, 203–210. doi: 10.1007/BF00198091
- Koles, Z. J., Lazar, M. S., and Zhou, S. Z. (1990). Spatial patterns underlying population differences in the background EEG. *Brain Topogr.* 2, 275–284. doi: 10.1007/BF01129656
- Korzeniewska, A., Mańczak, M., Kamiński, M., Blinowska, K. J., and Kasicki, S. (2003). Determination of information flow direction among brain structures by a modified directed transfer function (dDTF) method. *J. Neurosci. Methods* 125, 195–207. doi: 10.1016/S0165-0270(03)00052-9
- Lim, J. H., Hwang, H. J., Jung, Y. J., and Im, C. H. (2011). "Feature extraction for brain-computer interface (BCI) based on the functional causality analysis of brain signals," in *Proceedings of the 5th International Brain-Computer Interface Conference* (Graz), 36–38.
- Lütkepohl, H. (2005). *New Introduction to Multiple Time Series Analysis*. Berlin Heidelberg: Springer. doi: 10.1007/978-3-540-27752-1
- Makeig, S., Bell, A. J., Jung, T.-P., and Sejnowski, T. J. (1996). "Independent component analysis of electroencephalographic data," in *Advances in Neural Information Processing Systems*, eds D. Touretzky, M. Moser, and M. Hasselmo (Cambridge, MA: MIT Press), 145–151.
- Michel, C. M., and Murray, M. M. (2012). Towards the utilization of EEG as a brain imaging tool. *Neuroimage* 61, 371–385. doi: 10.1016/j.neuroimage.2011.12.039
- Millán, J. D. R., Rupp, R., Müller-Putz, G., Murray-Smith, R., Giugliemma, C., Tangermann, M., et al. (2010). Combining brain-computer interfaces and assistive technologies: state-of-the-art and challenges. *Front. Neurosci.* 4:161. doi: 10.3389/fnins.2010.00161
- Mullen, T., Kothe, C., Chi, Y. M., Ojeda, A., Kerth, T., Makeig, S., et al. (2013). Real-time modeling and 3d visualization of source dynamics and connectivity using wearable EEG. *Conf. Proc. IEEE Eng. Med. Biol. Soc.* 35, 2184–2187. doi: 10.1109/EMBC.2013.6609968
- Nunez, P. L., Srinivasan, R., Westdorp, A. F., Wijesinghe, R. S., Tucker, D. M., Silberstein, R. B., et al. (1997). EEG coherency I: statistics, reference electrode, volume conduction, Laplacians, cortical imaging, and interpretation at multiple scales. *Electroencephalogr. Clin. Neurophysiol.* 103, 499–515. doi: 10.1016/S0013-4694(97)00066-7
- Oliphant, T. E. (2007). Python for scientific computing. *Comput. Sci. Eng.* 9, 10–20. doi: 10.1109/MCSE.2007.58
- Oostenveld, R., Fries, P., Maris, E., and Schoffelen, J. (2011). Fieldtrip: open source software for advanced analysis of MEG, EEG, and invasive electrophysiological data. *Comput. Intell. Neurosci.* 2011:156869. doi: 10.1155/2011/156869
- Pedregosa, F., Varoquaux, G., Gramfort, A., Michel, V., Thirion, B., Grisel, O., et al. (2011). Scikit-learn: machine learning in python. *J. Mach. Learn. Res.* 12, 2825–2830.
- Perrin, F., Pernier, J., Bertrand, O., and Echallier, J. F. (1989). Spherical splines for scalp potential and current density mapping. *Electroencephalogr. Clin. Neurophysiol.* 72, 184–187. doi: 10.1016/0013-4694(89)90180-6
- Pfurtscheller, G. (1981). Central beta rhythm during sensorimotor activities in man. *Electroencephalogr. Clin. Neurophysiol.* 51, 253–264. doi: 10.1016/0013-4694(81)90139-5
- Raimondo, F., Kamienkowski, J. E., Sigman, M., and Fernandez Slezak, D. (2012). CUDAICA: GPU optimization of infomax-ICA EEG analysis. *Comput. Intell. Neurosci.* 2012, 206972. doi: 10.1155/2012/206972
- Schlögl, A., and Brunner, C. (2008). Biosig: a free and open source software library for bci research. *Computer* 41, 44–50. doi: 10.1109/MC.2008.407
- Schlögl, A., Keirnath, C., Zimmermann, D., Scherer, R., Leeb, R., and Pfurtscheller, G. (2007). A fully automated correction method of EOG artifacts in EEG recordings. *Clin. Neurophysiol.* 118, 98–104. doi: 10.1016/j.clinph.2006.09.003
- Schlögl, A., and Supp, G. (2006). "Analyzing event-related EEG data with multivariate autoregressive parameters," in *Event-Related Dynamics of Brain Oscillations*, eds C. Neuper and W. Klimesch (Amsterdam: Elsevier), 135–147.
- Schnitzler, A., and Gross, J. (2005). Normal and pathological oscillatory communication in the brain. *Nat. Rev. Neurosci.* 6, 285–296. doi: 10.1038/nrn1650
- Shoker, L., Sanei, S., and Sumich, A. (2005). "Distinguishing between left and right finger movement from EEG using SVM," in *Engineering in Medicine and Biology Society, 2005. IEEE-EMBS 2005. 27th Annual International Conference* (Shanghai), 5420–5423.
- Siegel, M., Donner, T. H., and Engel, A. K. (2012). Spectral fingerprints of large-scale neuronal interactions. *Nat. Rev. Neurosci.* 13, 121–134. doi: 10.1038/nrn3137
- Vidaurre, D., Bielza, C., and Larrañaga, P. (2013). Classification of neural signals from sparse autoregressive features. *Neurocomputing* 111, 21–26. doi: 10.1016/j.neucom.2012.12.013
- Wei, Q., Wang, Y., Gao, X., and Gao, S. (2007). Amplitude and phase coupling measures for feature extraction in an EEG-based brain-computer interface. *J. Neural Eng.* 4, 120–129. doi: 10.1088/1741-2560/4/2/012
- Zito, T., Wilbert, N., Wiskott, L., and Berkes, P. (2009). Modular toolkit for data processing (MDP): a python data processing framework. *Front. Neuroinform.* 2:8. doi: 10.3389/neuro.11.008.2008

**Conflict of Interest Statement:** The authors declare that the research was conducted in the absence of any commercial or financial relationships that could be construed as a potential conflict of interest.

Received: 30 October 2013; accepted: 20 February 2014; published online: 11 March 2014.

Citation: Billinger M, Brunner C and Müller-Putz GR (2014) SCoT: a Python toolbox for EEG source connectivity. *Front. Neuroinform.* 8:22. doi: 10.3389/fninf.2014.00022 This article was submitted to the journal *Frontiers in Neuroinformatics*. Copyright © 2014 Billinger, Brunner and Müller-Putz. This is an open-access article distributed under the terms of the Creative Commons Attribution License (CC BY). The use, distribution or reproduction in other forums is permitted, provided the original author(s) or licensor are credited and that the original publication in this journal is cited, in accordance with accepted academic practice. No use, distribution or reproduction is permitted which does not comply with these terms.